Crustal Stresses and Seismicity in Intraplate Settings: Relationship to Geology and Driving Forces

by

William Alan Frank Baird

A thesis submitted to the Department of Geological Sciences & Geological Engineering in conformity with the requirements for the degree of Doctor of Philosophy

Queen's University

Kingston, Ontario, Canada

April, 2010

Abstract

This thesis explores the relationship between contemporary stresses, paleotectonic structure, and seismicity within continental interiors. This is achieved by combining a variety of geophysical and geological data coupled with numerical stress analysis to form seismotectonic models for local seismic zones in eastern North America.

The work focusses on two main areas: (1) Southern Ontario, a region with low to moderate earthquake activity, which is structurally dominated by the Grenville orogen. Numerical models are used to show that both increased seismicity and an identified perturbation in the local stress orientation could be explained by reactivation of basement faults. (2) The Charlevoix seismic zone, a region of comparatively high background seismicity and large historic events, which is structurally controlled by an Iapetan rift and a meteorite impact structure. Although the rift faults are poorly aligned for reactivation in the regional stress field, modelling indicates that if they are sufficiently weak, they may act as a conduit, channelling higher stresses into the interior of the fractured crater zone, triggering much of the background seismicity. Furthermore, interaction with the crater acts to enhance rift fault slip near their intersection points, matching the observed pattern of large events in the seismic zone. The results also highlight a potential structural bias inherent in intraplate focal mechanisms. The faulting style of large earthquakes is heavily influenced by the regional structural trends, while smaller events, which can take advantage of local complexity in fault orientation, produce mechanisms more indicative of local stress conditions.

Concepts developed with these studies as well as a comparison with the eastern Tennessee seismic zone are used to propose a regional model for eastern North American seismicity. Seismicity may be explained by a large deformation zone between the rigid North American craton and the Atlantic oceanic crust. Differential motion across the zone is accommodated by infrequent large earthquakes that localize on the major paleotectonic structures, which may produce a regional counterclockwise stress perturbation within the deformation zone. Stress orientations deduced from smaller magnitude events illustrate this regional perturbation.

Statement of co-authorship

This thesis incorporates three manuscripts for journal publication as Chapters 2, 3, and 4. My supervisors Stephen D. McKinnon and Laurent Godin contributed to the work through scientific discussion and editorial guidance.

Chapter 2, entitled "Linking stress field deflection to basement structures in southern Ontario: results from numerical modelling" is co-authored by Stephen D. McKinnon and was published in Tectonophysics in 2007.

Chapter 3, entitled "Stress channelling and partitioning of seismicity in the Charlevoix seismic zone, Québec, Canada" is co-authored by Stephen D. McKinnon and Laurent Godin and was published in Geophysical Journal International in 2009.

Chapter 4, entitled "Relationship between structures, stress and seismicity in the Charlevoix seismic zone revealed by 3-D geomechanical models: Implications for the seismotectonics of continental interiors" is co-authored by Stephen D. McKinnon and Laurent Godin and has been submitted to the Journal of Geophysical Research.

Acknowledgements

First I'd like to thank my supervisors Steve McKinnon and Laurent Godin for their guidance, advice and patience while writing my thesis. I've learned a great deal over the course of my research and I'm grateful for being given the opportunity to pursue it. I'd also like to acknowledge Colin Thomson who, while I was still toying with the idea of going to Graduate school, suggested that I might be interested in this project. It was a topic that I knew very little about at the time, but one which I've really grown to enjoy, thanks a lot.

The research was carried out as part of the Portable Observatories for Lithospheric Analysis and Research Investigating Seismicity (POLARIS) project. Financial support was provided by the Ontario Research and Development Challenge Fund, Natural Sciences and Engineering Research Council (NSERC) Discovery grants to Steve Mckinnon and Laurent Godin, as well as an Ontario Graduate Scholarship.

As I finish up my doctorate I can't help look back and reflect on my (long) time here at Queen's. I've grown a lot since I first started here as a teenager, fresh out of high school, starting my first year as an engineering student. I didn't really know what I was getting myself into at the time, and navigating my academic path over the years wasn't always easy, but it turned out to be well worth the trouble. I consider my years at Queen's as some of the best of my life, thanks in large part to the many friendships that have developed along the way. To all my friends at Queen's: Thank you for keeping me sane, you've made my stay here a truly enjoyable experience.

Finally I'd like to thank my family for all the love and encouragement they've provided to me over the years. And to my parents Bill Baird and Jane Pickersgill, who fostered my desire to learn at an early age, and provided me with the means to carry through with it: Thank you, I couldn't have done it without you.

Statement of originality

I hereby certify that the work embodied in this thesis is the result of my own research except where otherwise acknowledged.

Alan F. Baird

April, 2010

Contents

List of Figures

List of Tables

Chapter 1

Introduction

1.1 Background

On a global scale the distribution of earthquakes can easily be explained in the context of plate tectonics. The vast majority of earthquakes occur either along the plate boundaries, or in broad regions of actively deforming continental crust around plate boundaries (Figure 1.1A). Although these regions cover only 18% of the earth's surface, they account for ∼99.4% of the global seismic moment release (Johnston *et al.*, 1994). By comparison, the less than 0.5% contribution to moment release provided by the so called "stable continental regions" (SCRs), defined as regions of continental crust that have no significant Cenozoic tectonism or volcanism (Johnston *et al.*, 1994), is almost negligible (Figure 1.1B) (Célérier *et al.*, 2005). Nevertheless, large intraplate earthquakes do occur, and may pose significant societal risk. The largest intraplate earthquakes on historic record occurred during the winter of 1811–12, when three large (moment magnitude **M**∼8) earthquakes

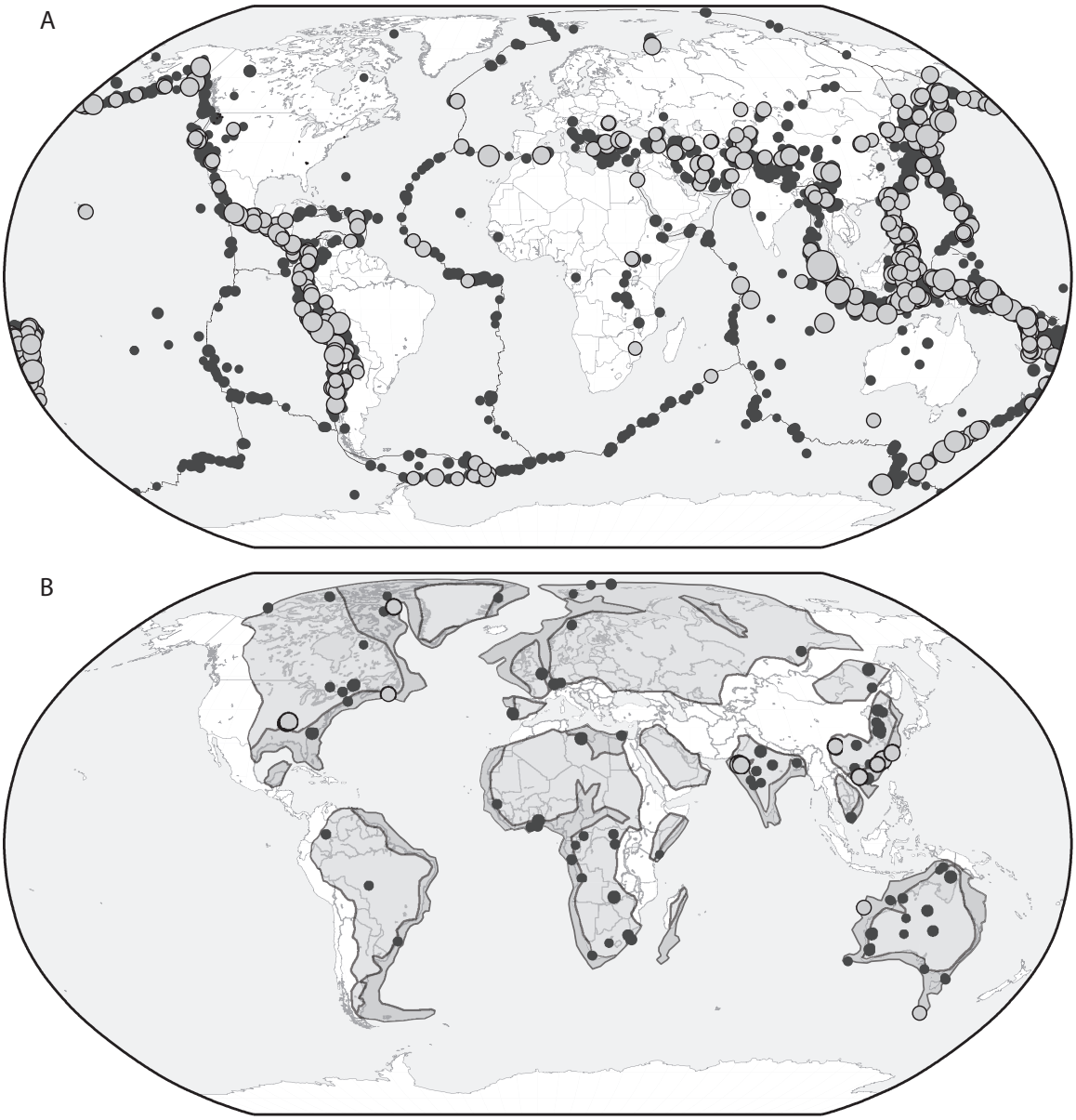

Figure 1.1: (A) Global seismicity map showing all events moment magnitude $\mathbf{M} > 6$ (black) and $\mathbf{M} > 7$ (grey) between 1973–2009 from the United States Geologic Survey catalogue. (B) The seismicity of stable continental regions (SCRs) showing all events $\mathbf{M} > 6$ on historic record (from the catalogue of Schulte & Mooney, 2005). Grey polygons indicate the extent of SCRs as defined by Johnston *et al.* (1994), dark grey regions indicate "extended crust" (rifted margins and aulacogens).

occurred in the Mississippi River Valley near New Madrid, Missouri in the Central United States (Johnston, 1996). While the effect to human structures was minimal, due to sparse population at the time, the population has largely increased since the earthquakes, and a similar event today could cause significant damage to the nearby cities of St. Louis and Memphis. By comparison, the M 7.7 Gujarat earthquake of 2001, which occurred near the city of Bhuj in Western India, resulted in the deaths of $\sim$20,000 and caused billions of US dollars in damage (Bendick *et al.*, 2001).

Our understanding of intraplate seismicity is limited. This is primarily because the infrequent occurrence of large events, combined with the short time period of instrument measurements has provided us with an incomplete record of long-term earthquake distribution. Secondly, we lack an adequate model to provide a framework in which to explain the occurrence of seismicity. Nevertheless, it has been recognized that earthquakes are not evenly distributed in the SCRs, but often cluster around pre-existing weak zones. Sykes (1978), in one of the earliest comprehensive assessments of global intraplate seismicity, found that most events occur within crust that was affected by the last major orogenesis before the opening of the present oceans. These were interpreted to be the result of reactivation of existing fault zones, suture zones, failed rifts, and other tectonic boundaries. The interiors of cratonic blocks, in contrast, rarely host intraplate earthquakes (Figure 1.1B). Worldwide, there is a strong link between large intraplate earthquakes and rifted crust with nearly all of the $\mathbf{M} > 7$ events occurring within them. The correlation is particularly strong in eastern North America where most events $\mathbf{M} > 6$ are localize within Atlantic or Iapetan rifted basins, margins and aulacogens (Figures 1.2 and

1.3).

Despite the correlation between seismicity and paleotectonic structures, the question remains: Why do some portions of these features experience intense activity, while others experience very little? Perhaps the clustering of seismicity into small zones is due to a local weakness in an otherwise strong lithosphere. Such a model has been proposed to explain earthquake concentration in the New Madrid area, possibly due to a locally hot geothermal gradient (e.g. Liu & Zoback, 1997). Alternatively, the localized seismic zones may simply be an artifact of limited time period of seismic data collection within a transient system ($\sim$100 years). Over time, seismicity may be evenly distributed along the paleotectonic features, but with only small portions active over short intervals (e.g. Swafford & Stein, 2007). The greatly reduced intraplate strain rate relative to plate boundary regions, however, makes this difficult to ascertain.

1.2 This study

This thesis explores the complex dynamics of intraplate regions through numerical modelling in order to learn about the fundamental linkages between regional geology, stress and seismicity. The work is part of the Ontario POLARIS (Portable Observatories for Lithospheric Analysis and Research Investigating Seismicity) project. The Ontario POLARIS project was developed in part to obtain information on seismicity and seismic hazard of the southern Ontario region. As a result the thesis is decidedly eastern Canada-centric in scope, however, the work deals with a number of concepts and approaches which are broadly applicable to other

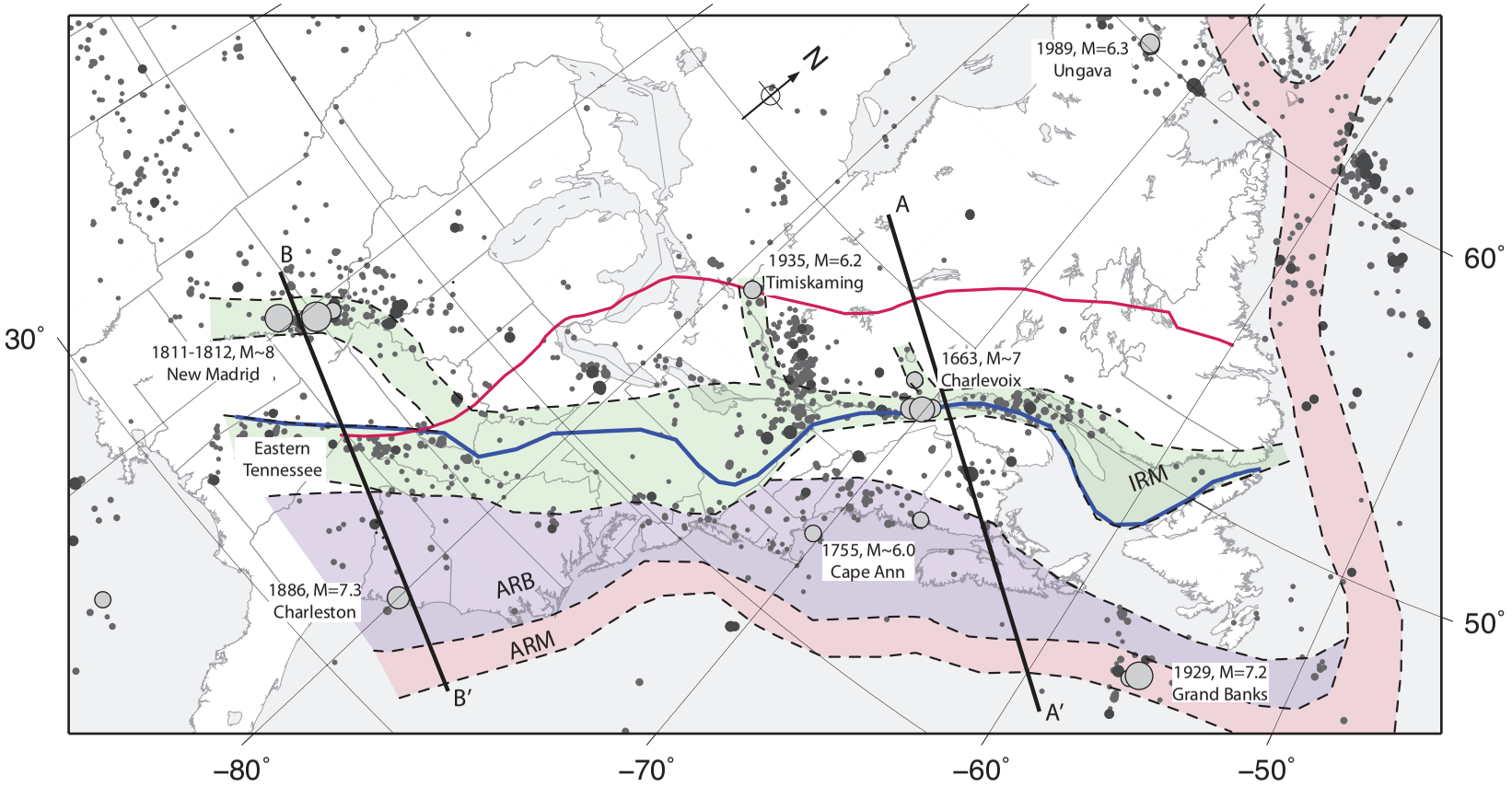

Figure 1.2: Seismicity and major paleotectonic features of eastern North America. Shaded regions indicate extent of rifted crust, IRM: Iapetan rifted margin, ARB: Atlantic rift basins, ARM: Atlantic rifted margin, Red line: Westward extent of deformation associated with the Grenville orogeny, Blue line: Westward limit of Appalachian thrust nappes. Background seismicity since 1973 is shown by dark grey ($M \geq 3$) and black ($M \geq 4.5$) circles. Historical large earthquakes (mostly $M \geq 6.0$) are shown by large grey circles. Thick black lines indicate the cross-sections of Figure 1.3. Seismicity data are from the Geological Survey of Canada and United States Geological Survey catalogues, historic Canadian events are from Lamontagne *et al.* (2007). Figure modified from Mazzotti (2007).

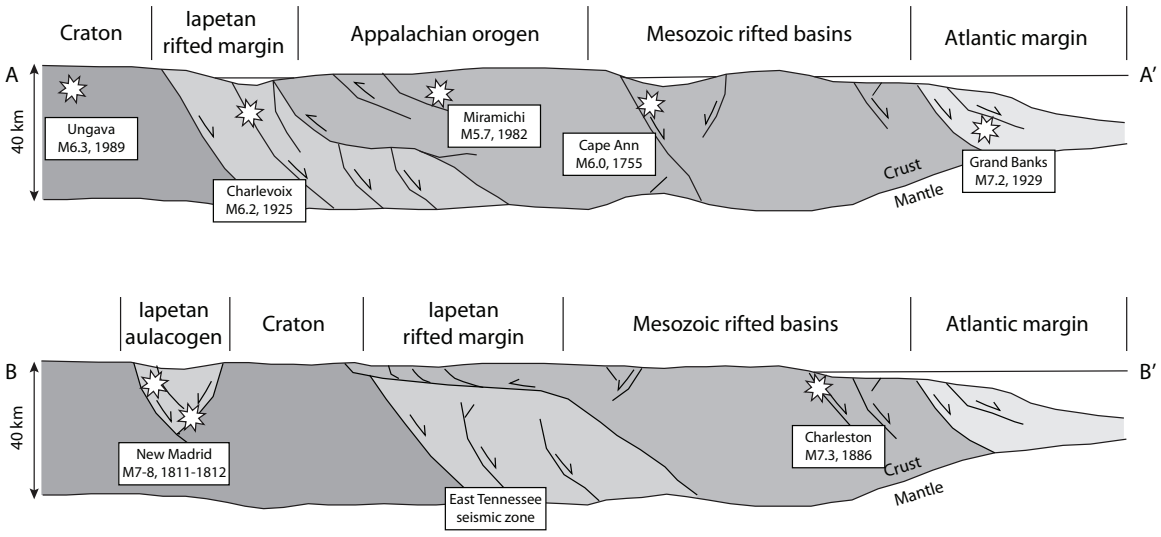

Figure 1.3: Schematic cross-section of eastern Canada and central eastern United States, showing large earthquakes and associated paleotectonic structures. See Figure 1.2 for locations. The black arrows indicate sense of fault displacement during their associated tectonic phases. Shades of grey refer to different crustal elements. Figure was modified from Adams *et al.* (1995) and Mazzotti (2007)

intraplate seismic zones throughout the world.

Because of the limited availability of long-term seismicity data, it is difficult to assess the potential for intraplate earthquakes. An alternative approach is to use other data, such as stress field measurements, geodetic displacements, and focal mechanism solutions, to infer fault stability. Simple conceptual models can be made to explain patterns of stress or GPS measured displacements; however, integrated models incorporating several different types of data would be far more valuable and informative.

The approach to the problem is to look for intraplate regions with unusual patterns of seismicity and stress that appear to be related to geological structures, then use geomechanical models to explore their interaction. Geomechanical modelling is selected here as the tool used to investigate the link between structural geol-

ogy and the stress field as a means of understanding the mechanics of neotectonic stress field modification in intraplate regions. It provides a way of validating the mechanical consistency of proposed geological models, and identifying regions of higher seismic hazard.

The models are built using the Itasca Consulting Group's suite of geomechanical software. The code is primarily used at the mining and engineering scale, but has been used for larger, tectonic-scale problems in the past (e.g. Homberg *et al.*, 1997; Pascal & Gabrielsen, 2001; Stevenson *et al.*, 2006). The codes allow the modelling of discontinuous media where joints and faults can be cut between continuum blocks and assigned frictional strength parameters. Classical finite difference techniques are used to compute stress and strain within the blocks. External boundary conditions can be applied to the assemblage while internal block boundary conditions are calculated from the interactions at their contacts. This allows pre-existing faults to be modelled explicitly, making it an ideal tool for modelling fault reactivation.

1.2.1 Sources of Data

A wide spectrum of data are required to determine adequate initial and boundary conditions for the geomechanical models. Additionally, data are needed to test the behaviour predicted in the models, and to assess whether or not they agree with observations. A selection of possible data sources are described below.

1.2.1.1 Geologic data

Since most intraplate seismicity appears to be related to the reactivation of paleotectonic structures, a good geologic model that reflects true geometry is an essential starting point. In particular, it is important to identify potentially seismogenic faults, or features that may indicate variations in rheology or strength. The assessment can be made from both surficial geology and mapped features, as well as from geophysical data that can provide details on the three dimensional architecture of the system and insight into features that may be obscured by cover rocks.

1.2.1.2 Seismicity

Precise locations of earthquake hypocentres are important for identifying potentially seismogenic features. By comparing earthquake locations with known structures, structural controls on the distribution of seismicity can be inferred, which can then be tested with the geomechanical models. Additionally, details on the magnitude of events can provide insight on the size of the active faults. Figure 1.4 shows a potential scaling relation between earthquake moment magnitude and rupture plane dimensions for intraplate seismicity. Low-magnitude seismicity ($\mathbf{M} \lesssim 3$) have rupture sizes on the 1-100 metre scale with slips of less than a few centimetres, and could conceivably occur along minor faults (Johnston, 1993). Larger magnitude events ($\mathbf{M} > 5$), on the other hand, have rupture dimensions at the kilometre to tens of kilometres scale, suggesting that they are likely occurring on major regional faults.

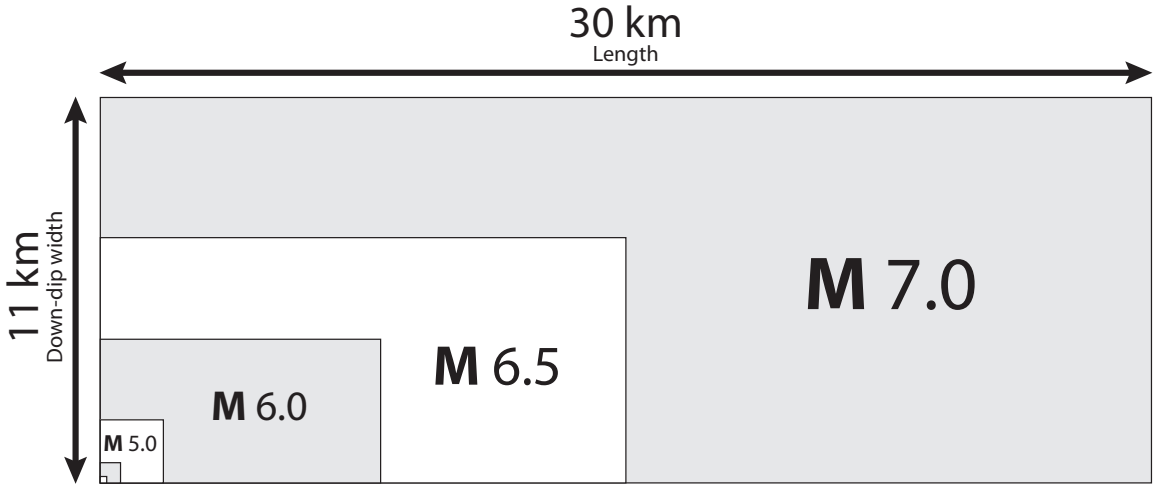

Figure 1.4: Approximate fault rupture dimensions for intraplate earthquakes at various moment magnitudes (**M**) based on the proposed scaling laws of Johnston (1993). Magnitudes indicated except for the smallest white and grey squares which represent **M** 3.0 and **M** 4.0 events, respectively.

1.2.1.3 Stress

Crustal stress is the driving mechanism behind seismicity, and thus forms an important component in the generation of seismicity models. The World Stress Map database (Heidbach *et al.*, 2008) is an online repository for crustal stress data from a variety of different sources including in-situ measurements, geological indicators, and earthquake focal mechanisms (see below). Investigations into stress patterns indicate that horizontal stress orientations and relative magnitudes are broadly uniform over large regions of the earth (e.g. Zoback & Zoback, 1989). The orientation of maximum horizontal compressive stress S_H correlates reasonably well with both absolute and relative plate motions on a global scale (Figure 1.5). This suggests that the main source of stress is derived from plate driving forces (e.g. Richardson & Reding, 1991). In addition to these broad first-order stress patterns,

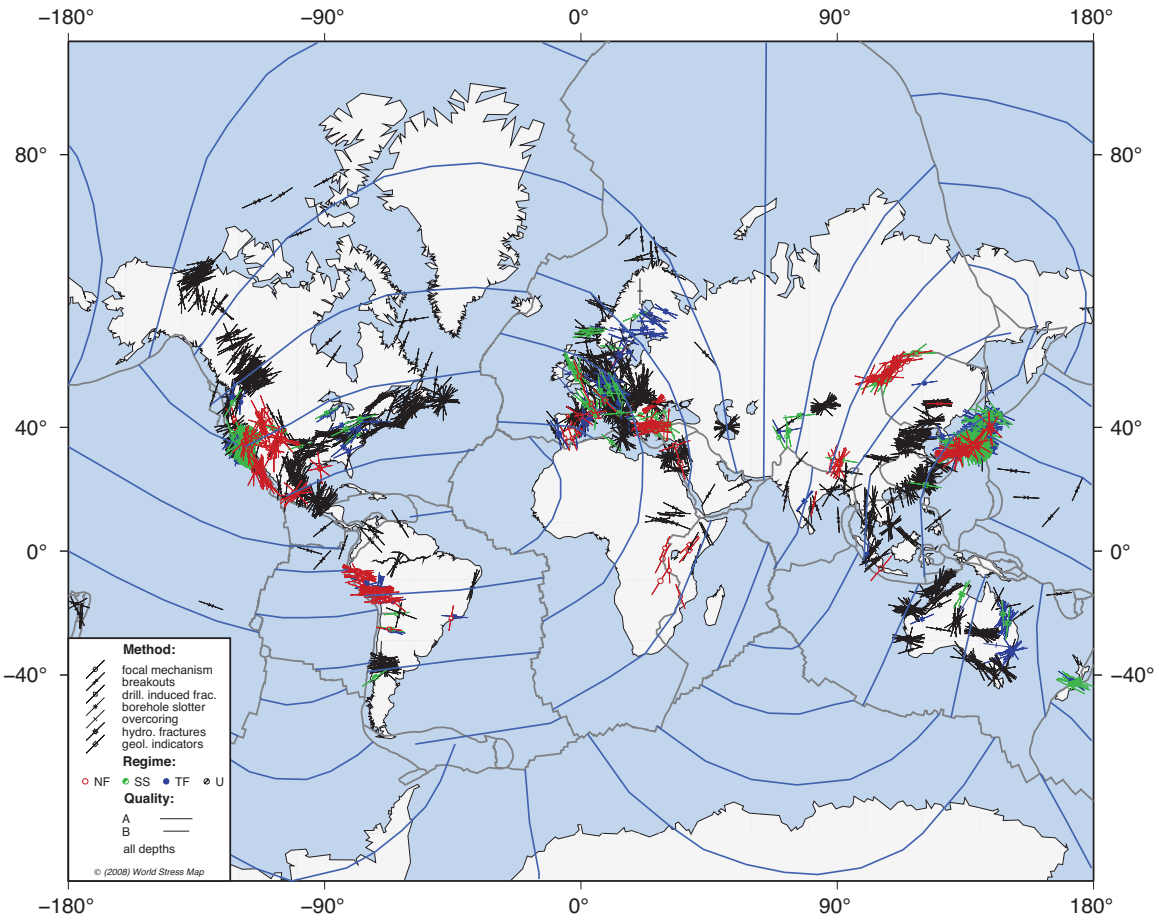

Figure 1.5: Stress map of the world, showing measurements of maximum horizontal compressive stress orientations (S_H), for data of quality A ($\pm 15°$) or B ($\pm 20°$) from the World Stress Map database (Heidbach *et al.*, 2008). Blue lines indicate trajectories of absolute plate motion (modified from Zoback *et al.*, 1989).

however, the data show some localized stress perturbations that may be related to specific geologic or tectonic features (Zoback, 1992b). Thus in geomechanical modelling, stress data can be valuable both as a source of boundary conditions, as well as a constraint on the influence of certain features to the modelled stress field.

1.2.1.4 Focal mechanisms

Earthquake focal mechanisms, also known as fault plane solutions, provide constraints on the geometry and kinematics of faults slip obtained from seismological data. The first motion of P-waves emanating from the earthquake source can vary from strongly compressional to strongly dilatational depending on the propagation direction relative to the fault plane and slip vector orientations (Figure 1.6A). This results in a distinctive radiation pattern which can be described by coupled forces with no-net torque (double couple; Figure 1.6B) (Stein & Wysession, 2003). The volume around the source can be split into quadrants of dilatational and compressional fields separated by two orthogonal nodal planes. One plane represents the fault plane and contains the slip vector, while the other plane, known as the auxiliary plane, has no structural significance but is oriented normal to the slip vector. Provided there is sufficient seismograph coverage of an event, the three dimensional radiation pattern of an event can be inferred and plotted on a lower hemisphere stereonet. Unfortunately, it is impossible to determine which nodal plane represents the fault from a single event with no other information. However, focal mechanisms do constrain the possible fault geometries, which can be compared with known geological structures as well as other nearby focal mechanisms to identify potential weak structures. This is particularly valuable in intraplate areas, where earthquakes rarely cause surface rupture, and fault planes cannot be readily identified.

In addition to the orientation of the nodal planes, a focal mechanism also describes the orthogonal set of pressure (P-), tension (T-) and null (B-) axes which cor-

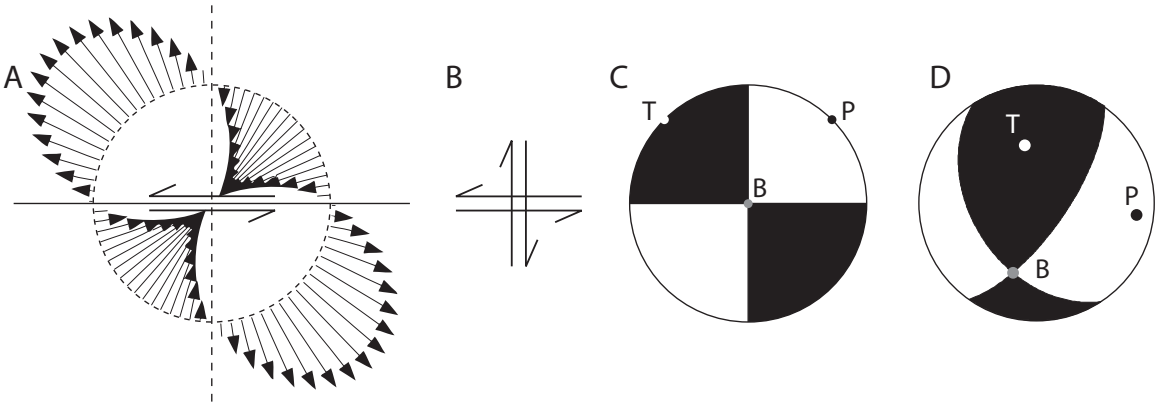

Figure 1.6: (A) Diagram showing the initial motion of P-waves surrounding the focus of an earthquake located along an E-W oriented sinistral strike-slip fault. (B) Paired force couples (double couple) which can describe the radiation pattern formed by the earthquake. (C) The resulting focal mechanism with black regions indicating compression and white regions dilatation. (D) A more generally oriented focal mechanism, this example illustrates an oblique reverse event with predominately E-W oriented compression. Modified from Stein & Wysession (2003).

respond to the maximum shortening direction, maximum extensional direction, and intermediate principal strain direction of the event, respectively. The B-axis lies along the intersection of the nodal planes, while the P- and T-axes lie perpendicular to the B-axis and bisect the dilatational and compressional quadrants, respectively, lying at 45° from both the fault and auxiliary planes (Figure 1.6C).

For individual mechanisms, the P-, B-, and T-axes are often used as crude estimates of the pricipal stress axes σ_1, σ_2, and σ_3, respectively. In reality, however, other orientations are possible or even more likely. Mohr Coulomb theory suggests that for an optimally oriented fault reactivation σ_1 would be at a lower angle from the fault plane than the 45° implied by the P-axis. However, ambiguity between the fault and auxiliary planes as well as the lack of prior knowledge of the frictional strength of the fault precludes a more appropriate estimate. Additionally, limited

availability of fault plane orientations and possible high pore-fluid pressures suggest that even non-optimally oriented faults may reactivate in certain situations. With all of these unknowns a wide variety of mechanisms are compatible with a single stress tensor; the only strict constraint is that the maximum principal stress must lie somewhere within the dilatational field (McKenzie, 1969). While a single mechanism can only be used as a crude stress indicator, a large number of mechanisms from a small, relatively homogeneous and isotropic volume can be used to provide a better stress estimate using a stress inversion technique (e.g. Gephart & Forsyth, 1984; Michael, 1984; Arnold & Townend, 2007)

1.2.1.5 Geodetic Measurements

With the proliferation of continuous Global Positioning System (GPS) stations over the past two decades, GPS derived velocities have been increasingly used for seismotectonic interpretation. While most of the velocity can be attributed to rigid motion of the tectonic plates, this can be subtracted leaving residual velocities which can be used to infer internal deformation. Unsurprisingly, the areas with the largest deviations from rigid plate motion are near the plate boundaries, which are characterized by deformation zones attributed to interaction with the adjacent plate (Stein & Sella, 2002). Within the plate interiors, however, the residual velocities are considerably more difficult to interpret. In North America the vertical velocity field is clearly dominated by the effects of glacial isostatic adjustment with uplift covering most of Canada and mostly subsidence in the United States (Sella *et al.*, 2007). Horizontal velocities, however, mostly have magnitudes smaller than their uncertainties at a 95% confidence level, making it difficult to reconcile

deformation patterns (Calais *et al.*, 2006). The use of GPS data to infer strain accumulation in the New Madrid seismic zone has proven to be very controversial (Smalley *et al.*, 2005a,b; Calais *et al.*, 2005), primarily due to the large level of uncertainty relative to the small signals. For this reason GPS velocities are not used as primary sources of data for constraining the models in this thesis. However, it is acknowledged that longer durations of continuous monitoring will eventually lead to greater accuracy and increased precision of measurements. Thus, high quality GPS velocities will increasingly be a valuable source of data for understanding intraplate seismotectonic systems, and may present a useful tool for validating or constraining the models presented in this thesis.

1.2.2 Outline of thesis

This thesis is structured in manuscript format, and fulfils the requirements of the Queen's University School of Graduate Studies. The main results of the thesis are presented as three stand-alone papers, which comprise Chapters 2, 3, and 4.

Chapter 2, which was published in Tectonophysics (Baird & McKinnon, 2007), focusses on the seismicity of southern Ontario, specifically the area of low-level activity in the western Lake Ontario region, which effects the most populous area of Canada as well as a number of nuclear power stations. The paper presents the results of 3-D discontinuum models that explore the relationship between variations of stress field orientation and basement features of the Grenville Province. The models outline a potential link between a subtle deflection in the tectonic stress field and the localization of seismicity through the reactivation of basement fea-

tures along a local segment of the Grenville Province which deviates from the regional strike of the orogen.

In Chapter 3, which was published in Geophysical Journal International (Baird, McKinnon, & Godin, 2009), the focus shifts to the Charlevoix seismic zone (CSZ) in the St. Lawrence valley of Québec. The CSZ is the most seismically active region of eastern Canada, with both a series of repeated large events ($\mathbf{M} > 6$) over the past 350 years, and continuous low-level activity. Because of the high amount of activity, the region is monitored with a relatively dense network of seismographs operated by the Geological Survey of Canada. The relative wealth of data, combined with complex geologic structure make the CSZ an ideal study location. The chapter presents the result of 2-D models which examine the influence that two main structural features in the region, the St. Lawrence rift faults and the $\sim$28 km wide Charlevoix impact structure, have on the flow of tectonic stress in the region. Results from the models suggest that the combined influence of both structures results in a localized region of increased stress within the weak crater, which corresponds to the observed patterns of background seismicity.

Chapter 4, which has been submitted to the Journal of Geophysical Research (Baird, McKinnon, & Godin, in review), expands on the results of the previous chapter by using 3-D models meant to better represent the true structural architecture of the Charlevoix seismic zone. In addition to corroborating the main findings of the 2-D models the results reproduce observed background seismicity patterns in greater detail. Additionally, the models address the localization of large magnitude events on the rift faults and provide some insight into unusual focal mechanisms observed in the CSZ, which has some major implications for intraplate seis-

micity in general.

While the three manuscripts all deal with site specific conditions, the results do have implications that can be applied elsewhere. Chapter 5 introduces another seismically active intraplate region, the Eastern Tennessee seismic zone (ETSZ). Many of the concepts and relationships explored in the previous chapters are used here to discuss possible structural controls on stress and seismicity patterns observed in the ETSZ. Following this, a generalized model of eastern North American seismicity is proposed.

Chapter 2

Linking stress field deflection to basement structures in southern Ontario: results from numerical modelling

This chapter was published with Stephen D. McKinnon as co-author in Tectonophysics (Baird & McKinnon, 2007).

2.1 Abstract

Analysis of stress measurement data from the near-surface to crustal depths in southern Ontario shows a misalignment between the direction of tectonic loading and the orientation of the major horizontal principal stress. The compressive stress field instead appears to be oriented sub-parallel to the major terrane boundaries such as the Grenville Front, the Central Metasedimentary Belt boundary zone and the Elzevir Frontenac boundary zone. This suggests that the stress field has been modified by these deep crustal scale deformation zones. In order to test this hypothesis, a geomechanical model was constructed using the three-dimensional discontinuum stress analysis code 3DEC. The model consists of a 45 km thick crust of southern Ontario in which the major crustal scale deformation zones are represented as discrete faults. Lateral velocity boundary conditions were applied to the sides of the model in the direction of tectonic loading in order to generate the horizontal compressive stress field. Modelling results show that for low strength (low friction angle and cohesion), fault slip causes the stress field to rotate toward the strike of the faults, consistent with the observed direction of misalignment with the tectonic loading direction. Observed distortions to the regional stress field may be explained by this relatively simple mechanism of slip on deep first-order structures in response to the neotectonic driving forces.

2.2 Introduction

Southern Ontario is one of the most populated regions of Canada, particularly in the eastern Great Lakes region. It is also a region of persistent low-level seismicity that is poorly understood. A focus of the POLARIS Ontario (POLO) project is to improve understanding of seismicity and seismic risk distribution in Ontario. A number of studies in the past 20 years have been focused on understanding seismic hazard in the eastern Great Lakes area. Many authors have made a connection between basement features and current seismicity (Mohajer, 1993; Seeber & Armbruster, 1993; Wallach *et al.*, 1998; Boyce & Morris, 2002). However these studies have been primarily qualitative in nature. There have been few quantitative links made between the hypothesis of basement reactivation and geophysical observations. To fully understand the system we need to form an integrated model incorporating many geological and geophysical constraints. Reactivation of faults requires optimally oriented driving forces, so understanding the source of the stress field and how it interacts with pre-existing structure could provide clues as to how to partition seismic hazard into structural domains.

Geomechanical modelling has been used by various authors in the past (e.g. Homberg *et al.*, 1997; Pascal & Gabrielsen, 2001) and is selected here as the tool used to investigate the link between structural geology and the stress field as a means of understanding the mechanics of neotectonic stress field genesis in the region. It provides the framework to validate the mechanical consistency of proposed geological models.

2.3 Geological and tectonic setting

In order to build a mechanical model we need to choose our model architecture and boundary conditions carefully, such that they effectively represent the real system. To do this we need to have a good understanding of the structural architecture of the region. We also need clues as to which structural features are most important so that we incorporate them in the model, for this we use geological evidence of fault reactivation as well as spatial association of seismicity with known features. Understanding of the stress field is important since it is the driving mechanism behind seismicity, and is necessary for choosing boundary conditions in the model. These data also allow us to test the effectiveness of our model by comparing model output to geophysical observations.

2.3.1 Regional geology

The crustal structure of southern Ontario is dominated by the northeast-trending, relatively shallow southeast-dipping thrust faults of the Grenville orogen (Easton, 1992). The Grenville Province in southern Ontario is composed of three main lithotectonic segments: Laurentia and its pre-Grenvillian margin, the Composite Arc Belt, and the Frontenac–Adirondack Belt (Carr *et al.*, 2000). The pre-Grenvillian Laurentian margin extends from the Grenville Front tectonic zone (GFtz) in the northwest to the Central Metasedimentary Belt boundary tectonic zone (CMBbtz) in the southeast (Figure 2.1). It is composed of reworked Archean crust and Paleo- and Mesoproterozoic rocks that were formed by Andean-type arcs (Carr *et al.*, 2000). The Composite Arc Belt extends from the CMBbtz in the northwest to the

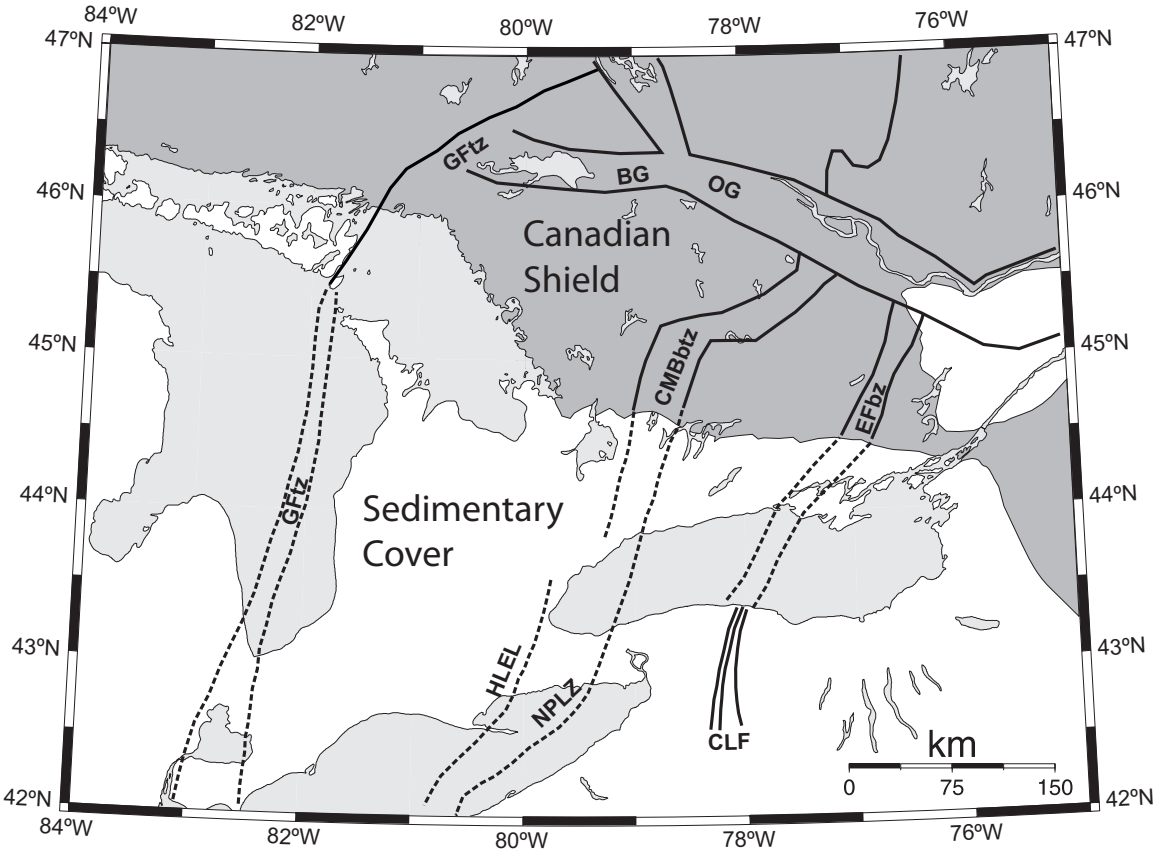

Figure 2.1: Simplified tectonic map of southern Ontario. GFtz–Grenville Front tectonic zone; CMBbtz–Central Metasedimentary Belt boundary tectonic zone; EFbz–Elzevir Frontenac boundary zone; HLEL–Hamilton-Lake Erie Lineament; NPLZ–Niagara Pickering Linear Zone; CLF–Clarendon-Linden fault; OG–Ottawa graben; BG–Bonnechère graben.

Elzevir Frontenac boundary zone (EFbz) in the southeast. It is a major Mesoproterozoic accumulation of carbonate, clastic, volcanic and plutonic rocks that experienced greenschist to granulite facies metamorphism (Easton, 1992; Carr *et al.*, 2000). Carr *et al.* (2000) interpret the Composite Arc Belt as a series of island arcs that were accreted and thrust onto Laurentia in a Himalayan style continent collision. To the southeast of the EFbz is a sequence of supracrustal marbles, quartzites, and quartzofeldspathic gneisses of the Frontenac–Adirondack Belt.

The boundary zones dividing the main tectonic segments of the Grenville province (the GFtz, CMBbtz, and EFbz) are major shear zones several kilometres wide (Easton, 1992). They are characterized by strongly deformed rocks with northeast trending, moderately to shallowly southwest-dipping tectonic layering, and southwest-plunging mineral lineation.

South of the exposed Grenville Province, rocks of the Grenville orogen underlie 500–375 Ma Lower Paleozoic shallow water sedimentary strata (Figure 2.1). The strata are essentially flat lying and laterally continuous, with a few exceptions (such as the Clarendon–Linden fault system, which is described later), suggesting that no substantial faulting occurred since deposition (Stepp *et al.*, 1995). Northeast-trending magnetic anomalies that are associated with the juxtaposition of contrasting rock types along the boundary zones of the Grenville basement (Boyce & Morris, 2002; Stepp *et al.*, 1995) extend southward beyond the edge of the Canadian shield. They provide a basis for projecting exposed Grenville structures beneath the Paleozoic cover rocks. The Niagara Pickering linear zone (NPLZ, Figure 2.1) is a well-defined linear magnetic anomaly that extends in a northeasterly direction from the Niagara Peninsula to Pickering, Ontario and northeast from

that point to the Precambrian–Paleozoic contact (Boyce & Morris, 2002). It is interpreted by some authors as a southward continuation of the CMBbtz (Forsyth *et al.*, 1994a), but others place the boundary farther to the west (O'Dowd *et al.*, 2004). Magnetic anomalies associated with the EFbz extend southwards and connect with the seismically active Clarendon-Linden fault (CLF) system in northern New York (Figure 2.1)(Hutchinson *et al.*, 1979).

Major structures of the Grenville orogen have been outlined in great detail by deep seismic reflection imagery from seismic surveys conducted by the Lithoprobe project (White *et al.*, 2000; Forsyth *et al.*, 1994a,b). A seismic-based cross-section through the southwest Grenville Province was interpreted by White *et al.* (2000)(Figure 2.5A). It shows that domains within the lithotectonic segments are separated by a series of northwest directed imbricate thrust sheets. Seismic sections of the orogen beneath the Great Lakes (Forsyth *et al.*, 1994a,b) and farther east in Québec (Martignole & Calvert, 1996) show a similar crustal architecture.

2.3.2 Reactivated structures

There is evidence that many of the structures of the Grenville orogen have been reactivated since their formation 1.3 billion years ago. Jacobi & Fountain (2002) provide evidence that the Clarendon-Linden fault (CLF, Figure 2.1) system was formed as a result of reactivation of basement structures associated with the EFbz after the deposition of the Lower Paleozoic rocks. From analysis of growth faults, Jacobi & Fountain (2002) concluded that the CLF has been active for much of the time that there is a rock record. It appears that the CLF failed each time a load

was applied from continental collisions or rifting associated with plate spreading. Hutchinson *et al.* (1979) used seismic data to locate a west facing bedrock ridge (the Scotch Bonnet sill) with 30 m relief that crosses lake Ontario along the projected strike of the CLF. The ridge coincides with linear magnetic and gravity anomalies associated with the EFbz. On the North side of Lake Ontario in Prince Edward county, the Picton and Salmon River faults are colinear with the CLF and Scotch Bonnet sill, and also have similar offsets (McFall, 1993) suggesting they are part of the same fault system caused by reactivation of the EFbz.

Sanford *et al.* (1985) showed that fault and fracture systems in the Paleozoic cover rocks of southwest Ontario have similar trends to the faults and lineaments on the exposed portion of the Grenville Province. Boyce & Morris (2002) noted a similarity in the trends of the major northeast-trending Paleozoic fracture sets with linear magnetic anomalies, and suggested that these boundaries are associated with reactivated basement faults. Dominant fracture patterns in the Paleozoic cover rock in the Balsam Lake area (Rutty & Cruden, 1993; Mitchell, 2007) above the CMBbtz lie parallel to the trend of basement structures, providing evidence of reactivation and upward extension into the cover rocks. Wallach *et al.* (1998) found evidence of at least two, if not three episodes of brittle faulting within the NPLZ near the northern edge of the Paleozoic cover. Fault orientations and displacements were found to be compatible with the current intraplate stress field, but their age was not known.

Eyles *et al.* (1993) used water well boreholes to map the bedrock topography in southwestern Ontario. They found that the CMBbtz/NPLZ coincides with valleys cut into the Paleozoic strata both on the north and south sides of Lake Ontario,

suggesting reactivation of the basement structures and their upward propagation through the Paleozoic and Pleistocene cover.

2.3.3 Seismicity

The most seismically active region in southern Ontario is along the Ottawa river (Figure 2.2). The seismicity in this area may be associated with normal faults along an arm of a failed rift (the Ottawa–Bonnechère graben) formed during the opening of the Iaptus Ocean (Adams & Basham, 1991; Adams *et al.*, 1995).

Outside of the Ottawa river area, seismicity occurs primarily in clusters around the region of western Lake Ontario and eastern Lake Erie (Figure 2.2). It is a region of low level, but persistent seismicity that is poorly understood. Seismicity in this area was described by Stevens (1994) as "intermittent scattered activity" with no preferred trends. Other authors, however, have put a greater emphasis on the apparent spatial correlation between seismicity and magnetic lineaments associated with major basement shear zones, suggesting causal links. Thomas *et al.* (1993) and Mohajer (1993) recognized two seismic zones that corresponded to the northeast trending NPLZ and the Hamilton-Lake Erie magnetic lineament (HLEL) (Figure 2.2). Clusters of seismicity have also been associated with the CLF and the Akron Magnetic boundary in Lake Erie (Jacobi & Fountain, 1993; Seeber & Armbruster, 1993). Wallach *et al.* (1998) interpreted the Akron Magnetic boundary as a southward extension of the NPLZ. Most of these studies have been primarily qualitative in nature, however Dineva *et al.* (2004) employed a statistical approach to attempt to test the hypothesis. They found that both seismicity and magnetic lin-

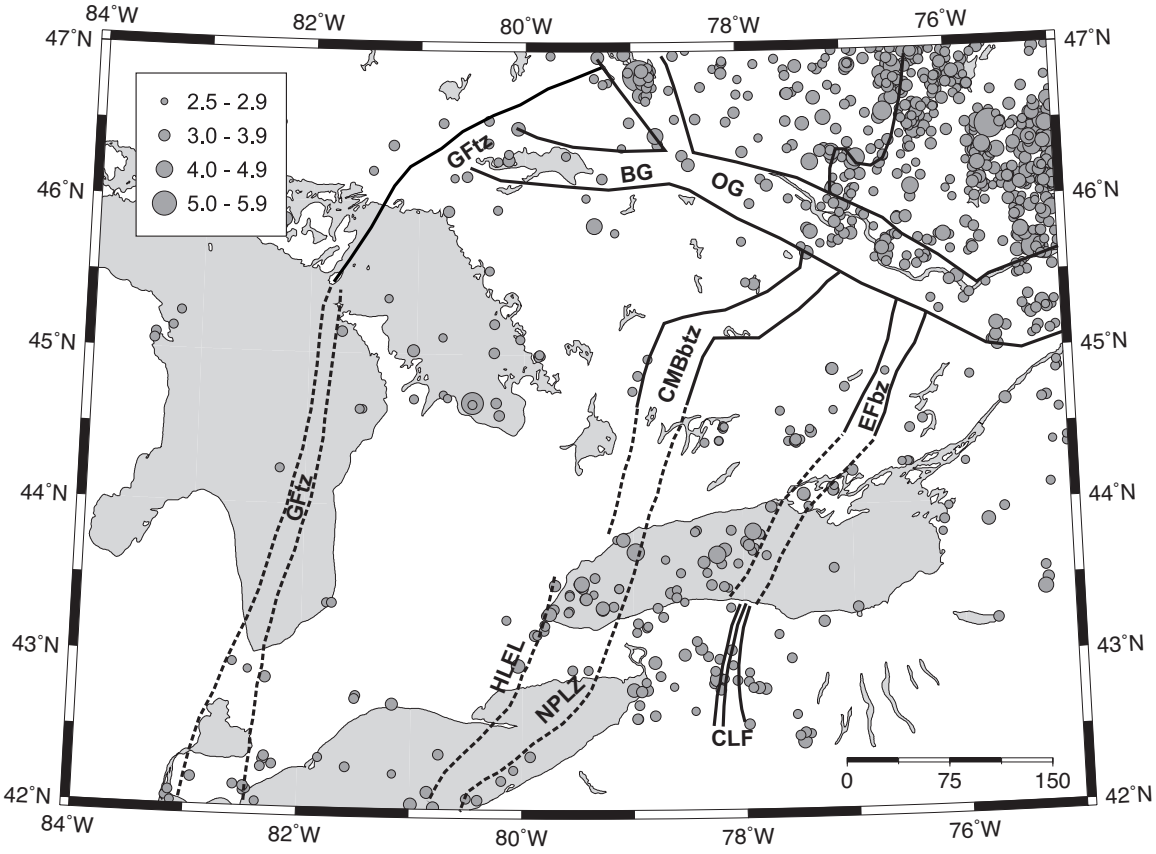

Figure 2.2: Earthquakes in southern Ontario (Seismicity data from the Geological Survey of Canada for the period 1985-2010).

eaments in Lake Ontario exhibit a statistically significant preferred orientation at N40°E–N45°E suggesting that basement structures influence the location of earthquakes in this region.

Analysis of focal mechanisms for several earthquakes in eastern North America shows a change from a strike-slip regime in the central eastern United States to a thrust regime in the southeastern Canada-U.S. border region (Zoback, 1992a; Du *et al.*, 2003). The earthquake hypocentres were also systematically deeper on the Canadian side (5–28 km vs. 2–8 km) (Du *et al.*, 2003). This transition occurs near

the former margin of the Laurentide ice sheet (Stewart *et al.*, 2000), prompting some authors to suggest that the seismicity in this area may be partially a result of stress perturbations induced by postglacial rebound (James & Bent, 1994; Zoback, 1992a).

2.3.4 Stress field

Southern Ontario lies within the Midplate stress province of eastern North America. This province dominates most of Canada, the central and eastern United States, and most of the western Atlantic (Zoback & Zoback, 1991). The orientation of maximum horizontal compressive stress (S_H) correlates reasonably well with both the absolute and relative plate motions (Zoback, 1992b; Zoback *et al.*, 1989). The source of the stress appears to be largely related to plate-driving forces (Richardson & Reding, 1991; Adams & Bell, 1991; Zoback & Zoback, 1991). However, the change in stress regime from thrust faulting in Canada to strike slip in the United States requires a laterally varying stress field that is not due to plate-driving forces (Zoback, 1992a; Ebel & Tuttle, 2002). Stresses induced by postglacial rebound have the correct orientation to cause the change in focal mechanism (Adams & Bell, 1991; Zoback, 1992a), however these stresses would be very small in magnitude and would not likely be capable of producing the observed stress regime changes (Zoback, 1992a).

Figure 2.3 shows a map of the stress field of southern Ontario, using data from the Canadian crustal stress database (Adams, 1995). The light grey inverted arrows show the orientation of measured values of S_H from the database, with the length of the vector proportional to its quality ranking (A, B, C, or D). The smoothing

algorithm of Müller *et al.* (2003) was used to smooth and interpolate the data using the assigned data quality weightings, in order to reveal the overall trend of the stress field. Smoothing parameters were chosen in order to accentuate local stress perturbations. The smoothed stress field is shown in Figure 2.3 as black vectors plotted on a regular grid. It should be noted that in the northern part of the study area there are very few stress data to constrain the smoothed map results. The absolute plate motion (APM) direction from the HS2-NUVEL 1 plate motion model of Argus & Gordon (1991) is also plotted on the map to show the approximate direction of tectonic loading.

Second-order stresses or local perturbations from the regional first-order stress field may be associated with specific geologic or tectonic features (Zoback, 1992b). In regions to the north of the study area (between 81°W–77°W and 45.5°N–47°N (Figure 2.3), there appears to be a large deviation in the direction of S_H from the expected direction parallel to APM. The deviation from the expected orientation may be due to perturbations associated with the Ottawa–Bonnechère Graben, however there are very few data in the region to constrain the stress field, so no conclusions can be made. Farther to the south, however, there appears to be another deviation from the expected stress field. Comparison of the smoothed stress field to the major tectonic features of the Grenville orogen (Figure 2.3) shows a local perturbation around the area of western Lake Ontario, where the stress field appears to deflect from the APM direction, to an orientation more parallel to the basement structures. Stress rotations due to lateral strength contrasts caused by faults have been observed elsewhere, the most notable example is the nearly fault-normal compression adjacent to the San Andreas fault (Zoback, 1992b). Because the San Andreas

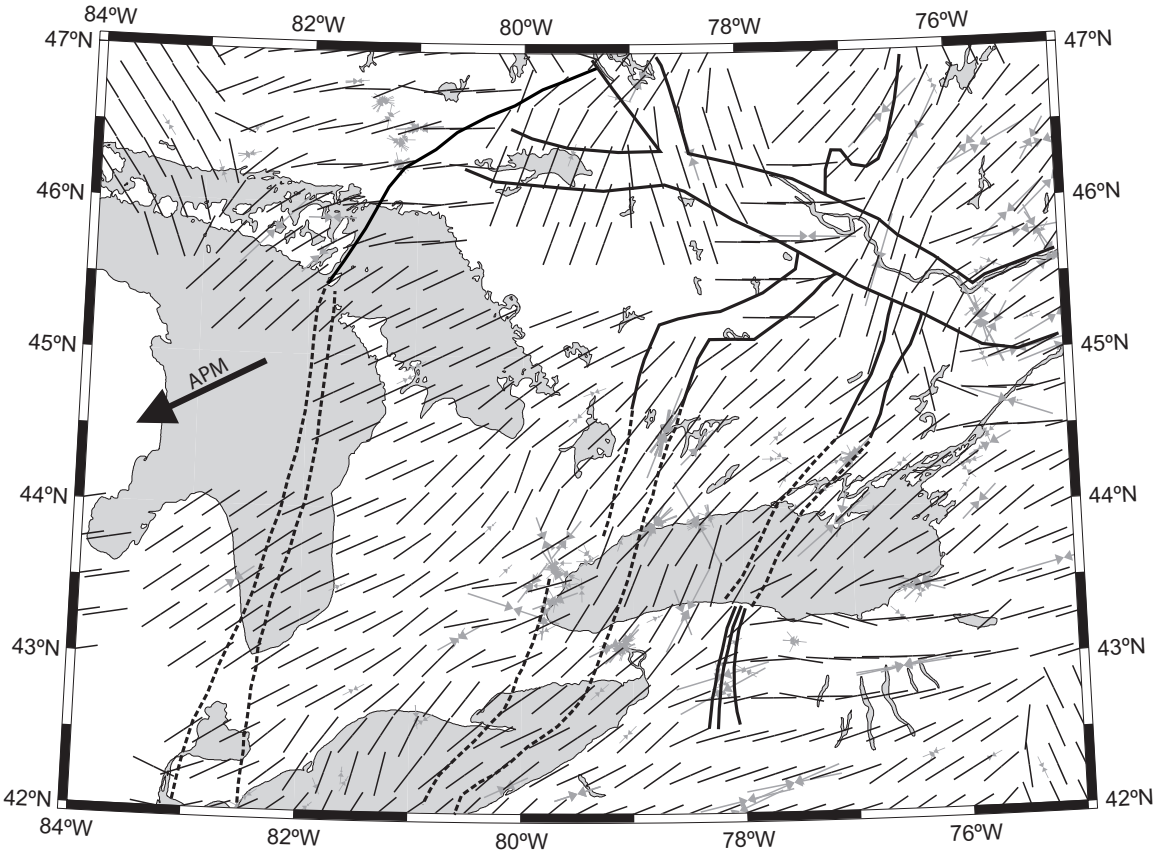

Figure 2.3: Smoothed stress map of southern Ontario, using data from the Canadian crustal stress database (Adams, 1995). Original data is shown in light grey. APM: Absolute plate motion direction (Argus & Gordon, 1991).

fault has a presumed low shear strength (Mount & Suppe, 1987), the stress field rotated so that the fault is nearly a principal stress plane, and the shear stress is minimized on the fault (Zoback, 1992b).

2.4 Numerical Representation

The geological evidence, including fault reactivation, fault slip displacement, and seismic activity, suggests that both the CMBbtz and the EFbz represent zones of mechanical weakness, and that deformation has occurred preferentially in these zones during previous tectonic events. Although there is no direct evidence for the GFtz acting in the same manner in Ontario, evidence of periodic reactivation in Ohio, to the south of our study area, has been reported (Onasch & Kahle, 1991). These three major shear zones, therefore, form the basis for constructing the structural representation of southern Ontario.

The way in which these shear zones are represented determines the type of numerical stress analysis code that can be used. Shear zones can be represented as weak bands of finite width, or as discrete faults. The finite width representation involves definition of more geometrical and material properties than discrete faults, many of which are unknown. Also, there are discretization issues involved in representing narrow zones in spatially extensive models. Since the main purpose of the study was to determine the effect of the shear zones on the regional stress field orientation and magnitude, as opposed to near-field stress effects close to the shear zones, the decision was made to represent the shear zones as discrete faults. By using this simpler representation, we are assuming that all displacement

is concentrated into the plane of the fault. The crust in between these faults was represented as a continuum.

2.4.1 Three-dimensional distinct element method

The distinct element method (DEM) was selected for our model as it enables stress and strain inside discontinuous media to be calculated. Due to the varying orientation of each shear zone, the model was developed using the three-dimensional code 3DEC (Itasca Consulting Group Inc., 2003). A detailed description of the method is provided by Cundall (1988) Hart *et al.* (1988) and Hart (1993).

Starting with a continuum block, the model is cut into a number of discrete blocks by faults or joints whose geometry is defined by piecewise planar segments. These segments are then assigned constitutive properties. Within the discrete blocks, classical continuum finite difference techniques are used to compute stress and strain. External boundary conditions can be applied to the assemblage while internal block boundary conditions are calculated from the interactions at their contacts. This allows pre-existing faults to be modelled explicitly, making the DEM ideal for modelling fault reactivation.

In order to compute the stress field in the model, 3DEC uses an explicit finite difference time marching scheme to solve damped equations of motion. These equations are applied in very small time steps to move gridpoints according to unbalanced force gradients and a new equilibrium is reached when unbalanced forces are reduced to zero. The time step is selected to maintain numerical stability during this process and does not correspond to an absolute time period. In con-

ventional static models, the equilibrium condition is reached using constant initial boundary conditions and this solution scheme is used to obtain the gridpoint displacements, and hence stress state. Since we wish to examine the state of stress when the faults are in a condition of marginal stability or slip, we use the solution scheme differently.

The initial stress condition for our models was chosen to be lithostatic, since this is a known stable condition for faults. Over many time steps, the internal stress field was modified through boundary displacements in a similar manner to far-field tectonic compression. Fault slip occurred when stresses resolved on fault segments exceeded fault strength. This pseudo-static equilibrium was maintained by adjusting the boundary gridpoint velocities to maintain the maximum gridpoint unbalanced forces within a low range. Although time-stepping and velocities were used, our model does not represent the evolution of fault displacement in absolute time. It has been developed to represent the current fault geometry and to show the potential for faults to influence the neotectonic stress regime.

The code is primarily used for engineering-scale problems such as mine design or slope stability, e.g. McKinnon & Garrido de la Barra (2003) used the code to investigate the influence of shear zones on the stress field in the El Teniente Mine, Chile. However the code has also been used for larger scale tectonic modelling. Pascal & Gabrielsen (2001) used the two-dimensional version of the code, UDEC, to investigate stress patterns in the mid-Norwegian margin and the North sea. Homberg *et al.* (1997) used the same code to investigate perturbations in the stress field near major faults.

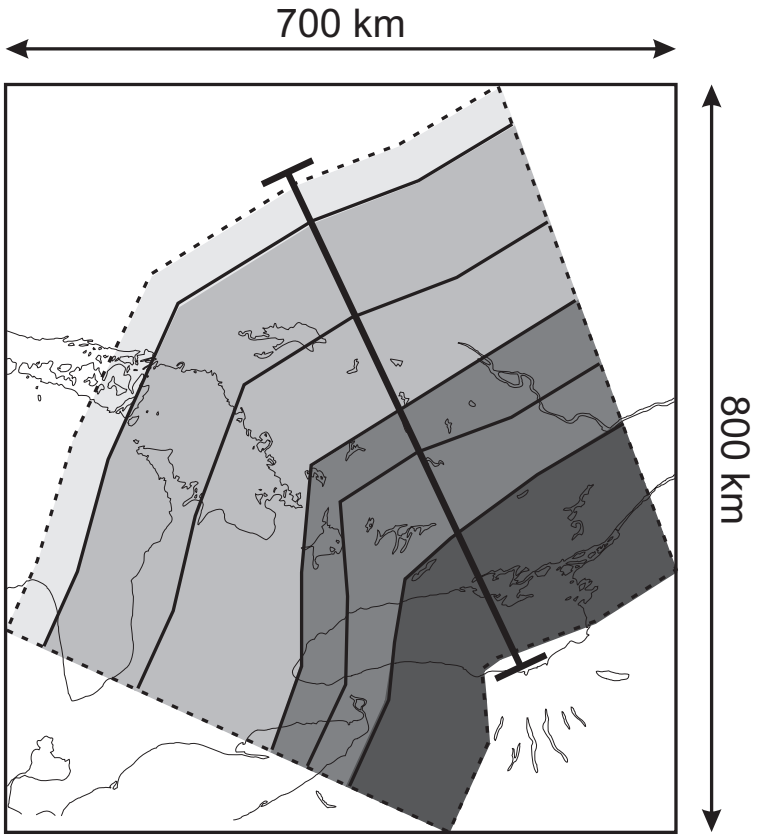

Figure 2.4: Plan view of model geometry. Fault traces are indicated by the solid lines, Dotted lines are locked contacts involved with the construction of the model. Cross-section indicated is shown in Figure 2.5.

2.4.2 Model strategy

The area considered in the model is located between approximately 85°W and 75°W longitude and between 42°N and 49°N latitude (approx. 700 km by 800 km). The model is 45 km thick, corresponding to the approximate thickness of the crust in southern Ontario as determined from Lithoprobe seismic studies (White *et al.*, 2000). Faults in the model are included to reflect the general tectonic architecture of the Grenville orogen (Figure 2.4). They are not meant to replicate detailed characteristics of tectonic features such as the CMBbtz or the EFbz. These struc-

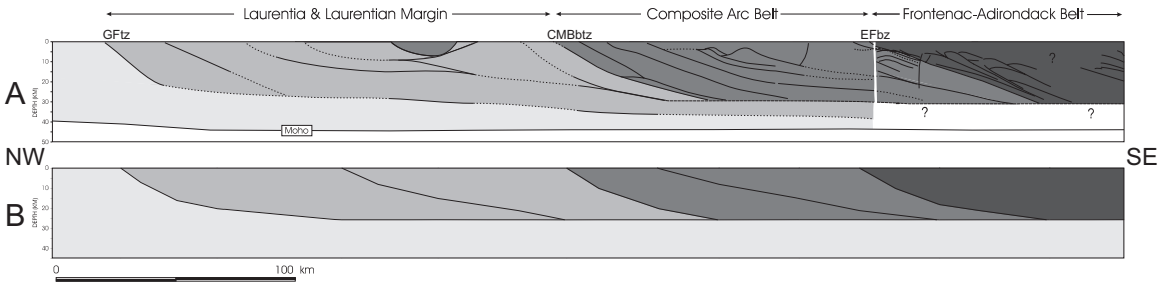

Figure 2.5: (A) Seismic based cross-section through the Grenville orogen (modified from White *et al.*, 2000). (B) Cross-section through the model, solid lines at contacts represent faults. Location of cross-section is shown in Figure 2.4.

tures are actually wide ductile shear zones, not brittle faults. However, given the correlation between seismicity and interpreted basement shear zones, as well as evidence that these features have been reactivated in the past, it seems likely that the geometry of seismically active faults is largely controlled by pre-existing structures, so representing the tectonic fabric as a series of discrete faults can be justified. Cross-sections showing a comparison of the model architecture to the actual tectonic features are shown in Figure 2.5.

2.4.3 Definition of model parameters

Parameter values for continuum and fault properties were specified as shown in Table 2.1. Linear elastic behaviour is assumed, with a Poisson's ratio ν of 0.25 and Young's modulus E of 40 GPa. An initial lithostatic stress field was set to ensure a stable fault configuration. Boundary velocities were then applied on the lateral faces in the direction of absolute plate motion (Figure 2.6), in order to build up a pre-slip stress field in this orientation, as is generally observed for regional crustal stresses (Zoback *et al.*, 1989). The velocity magnitudes were chosen in such a way

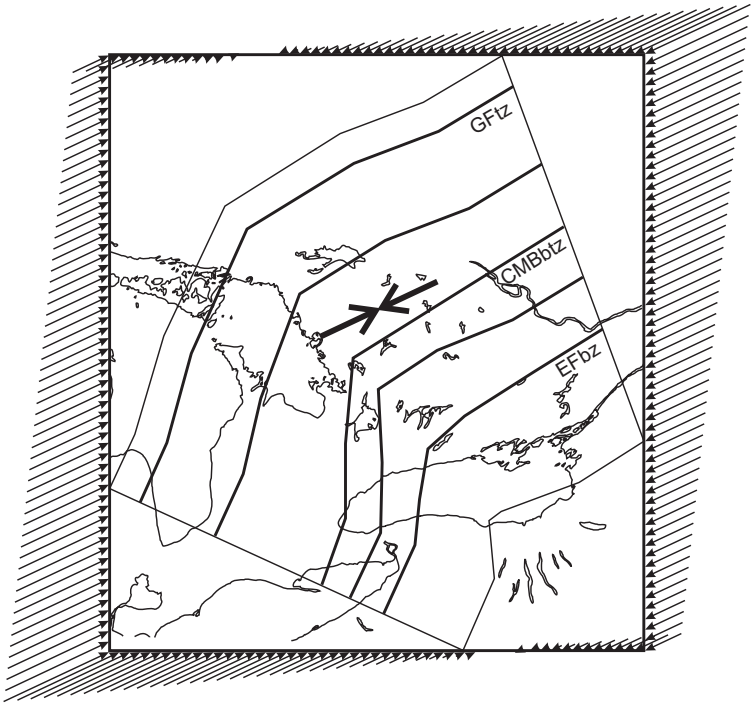

Figure 2.6: Pattern of boundary velocities applied to the later faces of the model. The relative magnitudes were chosen to generate an initial maximum compressive stress parallel to absolute plate motion with plane strain conditions perpendicular to the loading direction.

as to ensure plane strain conditions perpendicular to the loading direction, and the magnitudes were constantly adjusted to limit the maximum unbalanced gridpoint force to ensure model stability. By slowly building up the stress field from a stable fault configuration, we ensure that if fault slip occurs, stresses and displacements will evolve compatibly. The model was run with a variety of fault friction angles (Table 2.1).

Table 2.1: Model parameters

Block rheology	
Young's modulus	$E = 40$ GPa
Poisson's ratio	$\nu = 0.25$
Density	$\rho = 2750$ kg/m^3
Fault properties	
Friction angle	$\phi = 0^\circ, 5^\circ, 15^\circ, 30^\circ$
Cohesion	$C_0 = 0$
Normal and shear stiffness	$k_n = k_s = 5.5$ GPa/m

2.5 Results and analysis

The model was run until a pseudo-equilibrium state was achieved. The computed stress field tended to have S_H oriented sub-parallel to the loading direction (APM direction). However there were local perturbations in the stress field near the trace of the faults. Figure 2.7 shows contour plots of the rotation of S_H away from the loading direction at a depth of 2.5 km, which is comparable to the depth of much of the stress data. Regions in the northeast, where the faults trend nearly parallel to the loading direction, have very little perturbation in the stress field. In areas to the southwest, however, where the faults strike at an oblique angle from the loading direction, there is a significant amount of rotation to an orientation more parallel to the fault. The zones of high stress rotations tend to be localized on the down-dip (southeast) side of the faults, and their size depend both on the friction angle (ϕ) of the fault, and density of faults in the area.

The largest amount of fault displacement in the model occurs along the fault segments that are oblique to the loading direction in the southwest section of the model. The offset across the faults has a thrust dip-slip component and a right

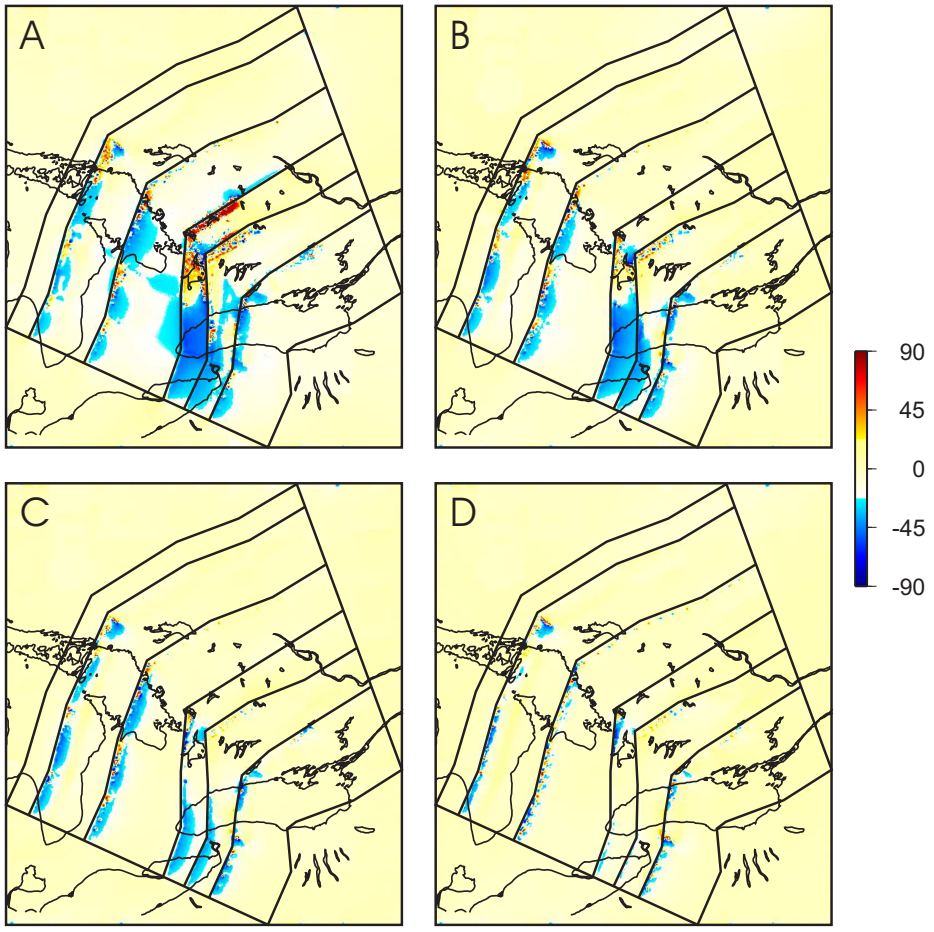

Figure 2.7: Contour plots of stress rotation away from loading direction at a depth of 2.5 km in degrees for friction angles of (A) 0°, (B) 5°, (C) 15°, and (D) 30°.

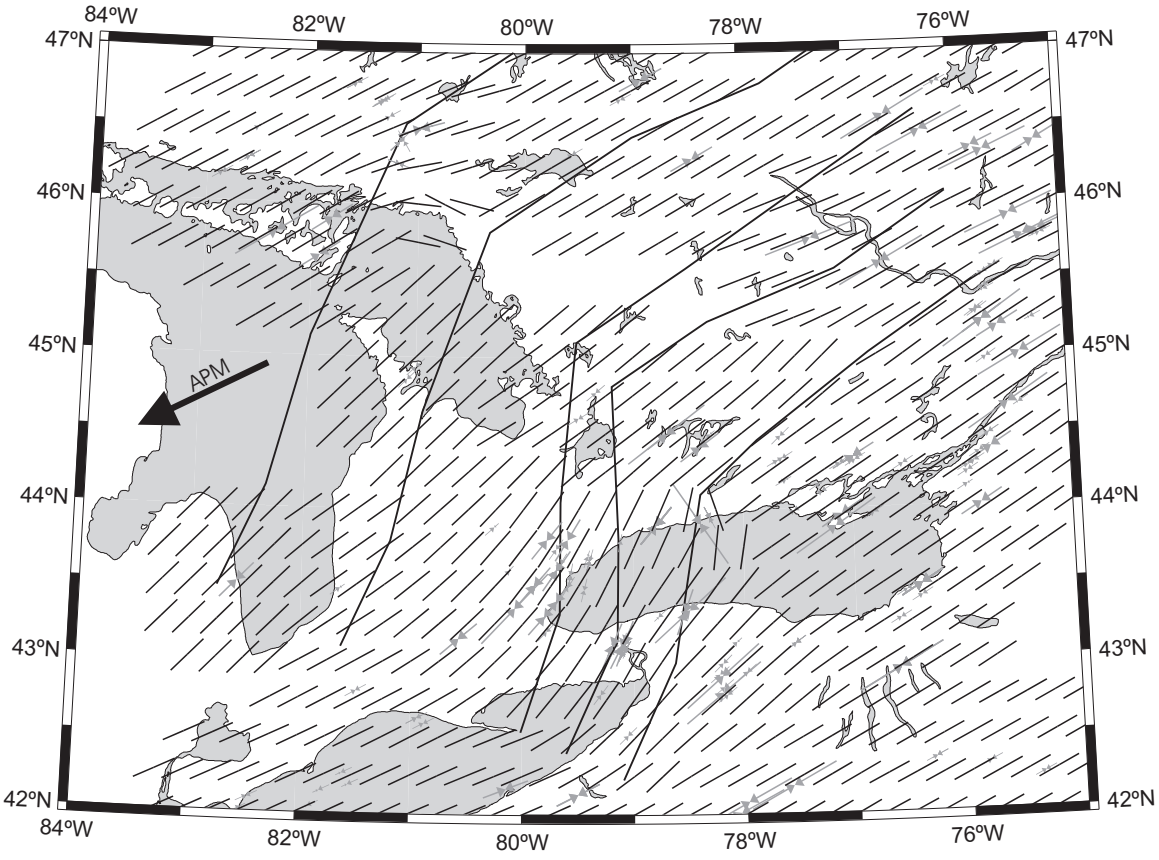

Figure 2.8: Smoothed stress map of model results using the algorithm of Müller *et al.* (2003). Black lines indicate location of model faults.

lateral strike-slip component.

The models were run with alternate Young's moduli of 60 and 80 GPa, and produced very similar results. This suggests that the effects are insensitive to the elastic properties chosen.

2.6 Discussion

2.6.1 Comparison of model with observed behaviour

A direct comparison of model results to the observed data is difficult, given the low density of data in the area. To allow a more meaningful comparison, the model coordinates were converted to geographic coordinates and stress information was sampled at the same locations as the data. The model data were then assigned the same quality values as the original data and then smoothed and interpolated using the smoothing algorithm of Müller *et al.* (2003). The resulting smoothed map for a friction angle of zero degrees is shown in Figure 2.8. Comparing this map to the original smoothed data (Figure 2.3) there appears to be a similar deflection of the stress field in the western Lake Ontario region. The smoothed plot does not pick up the stress rotation shown in Figure 2.7 associated with the faults in the western part of the study area (the GFtz). This is because there are very few stress measurements in this region, as a result very little insight into the stability of structures associated with the GFtz can be made from this model. Of the friction angles tested, the 0° case appears to fit best, although the 5° case also fits well.

The fault segments with the highest amount of slip occur on those that pass through Lake Ontario, as well as the region just to the north of the lake. The offset across the faults has a thrust dip-slip component and a right lateral strike-slip component, consistent with observed (possibly neotectonic) displacements across faults on the NPLZ (Wallach *et al.*, 1998). Fault slip in the western Lake Ontario area is consistent with the observations of continuous low level seismicity in that region (Wallach *et al.*, 1998; Mohajer, 1993; Seeber & Armbruster, 1993; Stepp *et al.*,

1995). The model also predicts significant slip along the fault segments just to the north of Lake Ontario, where there is much less observed seismicity (Figure 2.2). However, Wallach *et al.* (1998) noted an alignment of epicentres of four small earthquakes along the NPLZ in this area (near 45°N and 79°W, Figure 2.2). The lack of observed seismicity may be due to the short time window that seismicity has been recorded, or from a lack of coverage by seismographs. The new POLARIS seismograph array in southern Ontario may help resolve this issue.

2.6.2 Fault strength

The models with zero strength faults appear to match the observed stress rotation data best. While this strength does not correspond to the normal frictional strength of crustal faults, typically in the range of 30° to 40° (Sibson, 1994), it is not without precedence (Mount & Suppe, 1987). However, the major shear zones in the study area were represented in our models as discrete faults. Also, no effect of water pressure was included in the model. These model simplifications give rise to alternative interpretations to the physical significance of this low inferred fault strength.

The most likely reason that the low frictional strength models provided the best match to observations is the omission of pore water pressure. Based on the well-known concept of effective stress, the mechanical effect of fault friction angle or pore pressure is indistinguishable. By omitting pore pressure, the required friction angle to match observations must be lowered. This is particularly relevant to the region of the model close to Lake Ontario, where our models show high levels of

stress rotation and continuous low levels of seismicity are observed. It is likely in those regions that a realistic friction angle would be higher, as would fault pore pressure.

Another explanation stems from our models representation of shear zones as discrete faults. If the deformation occurring on the discrete faults in the model had been distributed over a more diffuse zone of closely spaced faults, the overall deformation could be matched to that of the single faults in our models. In this case, the strength of the smaller faults would be higher such that the smaller induced slip would cumulatively be similar to that of a single lower strength fault. Given the low density of data and uncertainty about the mechanical characteristics of the shear zones, we are currently unable to resolve this difference. Over time, the deployment of high resolution GPS sensors may resolve the issue of discrete vs. diffuse fault zone displacement.

It is also possible that over geological time the major regional structures creep, in which case their behaviour would be matched by low equivalent mechanical strength. This could be consistent with the paucity of observed seismicity correlating with the major shear zones, or simply too short a time window of observations. If this is the case, they may define stress/seismic sub-regions as they would act as weak boundary conditions for stronger (seismically active) interior megablocks. Future accumulated observations of lower level seismicity made possible by the POLO array should help to resolve this issue.

Despite these discrepancies, the overall correspondence between model results and data indicates that the mechanism of fault slip alone is sufficient to explain the observed stress rotations.

2.6.3 Model limitations

The model is limited in its use due to the poor density of data. Much of southern Ontario is not covered by the stress orientation dataset, so we can not use this to adequately refine our model. For instance, our model predicts a stress field deflection caused by structures associated with the GFtz. However the stress data in that area is too sparse to confirm whether or not there is a deflection.

As mentioned in the last section, the model is also limited in that all displacement must occur on our predefined faults. The faults in our model do not represent specific structures, rather they are meant to imitate the general tectonic fabric along which earthquakes are thought to nucleate. By confining all the slip to a few faults, we remove the possibility of distributed shear. Thus requiring unrealistically low strength structures to produce the observed large zones of stress rotation.

Our model also omits potentially important structures. These include the structures of the Ottawa–Bonnechère graben which are known to be associated with seismicity (Adams & Basham, 1991), as well as potentially seismogenic structures associated with the possible extension of the St. Lawrence rift through Lake Ontario (Wallach, 2002). These structures are not well understood, making them difficult to incorporate into the model.

2.7 Conclusions

Patterns of stress in southern Ontario appear to align with the structural grain of the Grenville basement rocks. Evidence of several reactivations of major tectonic subdivision fault zones of the Grenville Province, as well as present day seismicity

patterns suggest that these basement structures may be sources of weakness in the crust. A model of the crust of southern Ontario was constructed using the discontinuum code 3DEC. Several faults were included to replicate structurally controlled weaknesses along the Grenville orogenic belt. An applied stress field was oriented parallel to the absolute plate motion direction.

The model predicts a stress field reorientation resulting in the S_H direction rotating towards the strike of the faults, supporting hypotheses that the major basement features are weakness zones. However, the density of stress orientation data is too sparse to pick up any rotation in the northwest region of the study area, so no conclusions can be made for the possible reactivation of the GFtz. Predictions of relatively large fault slip correlate reasonable well with regions of persistent seismicity.

Due to a lack of data, our model was inconclusive as to whether fault slip is confined to large discrete low strength structures or whether the slip is accommodated by a series of smaller faults over a diffuse area. However, our model does succeed in showing that a relatively simple mechanism of slip on deep first order structures in response to the neotectonic driving forces is sufficient to explain the apparent stress deflection.

2.8 Aknowledgements

We are thankful for the helpful comments and suggestions of Catherine Homberg and one anonymous reviewer. Financial support for this research was provided through the Ontario Research and Development Challenge Fund.

Chapter 3

Stress channelling and partitioning of seismicity in the Charlevoix seismic zone, Québec, Canada

This chapter was published with Stephen D. McKinnon and Laurent Godin as co-authors in Geophysical Journal International (Baird *et al.*, 2009).

Abstract

The Charlevoix seismic zone (CSZ) in the St. Lawrence valley of Québec is historically the most active in eastern Canada. The structurally complex region comprises rift faults formed during the opening of the Iapetus Ocean, superimposed by a 350 Ma meteorite impact structure, resulting in a circular highly fractured zone. Although seismicity is localized along two steeply dipping planar rift-parallel zones, previous work indicates that most of the large-scale rift faults bound the low magnitude background seismicity rather than generate earthquakes themselves. In order to gain insight into the mechanics of the partitioning of this seismicity, a two-dimensional model of the CSZ was built using the stress analysis code FLAC. The rift faults are represented by frictional discontinuities. The heavily fractured impact structure is represented by an elastic continuum of reduced modulus. Boundary displacements are used to generate a regional stress field with the major horizontal component in the direction of tectonic loading. Given a high strength, the rift faults have little effect on the stress patterns. Stress trajectories naturally flow around the crater of reduced elastic modulus, leaving the fractured area with lower stresses than the background level. However, when the rift faults have low strength, they are unable to support stress trajectories inclined to them, due to the resolved shear stress exceeding their strength. This prevents trajectories from flowing out of the rift, effectively channelling higher magnitude stresses into the region of the impact structure between the faults. Low-strength bounding faults can thus explain the localization of seismicity into linear bands, rather than distributed seismicity throughout the impact structure. It also explains how the rift

faults act as boundaries to regions of low magnitude seismicity. These results indicate that the interplay between faults of varying strength and zones of differing elastic modulus can give rise to complicated stress patterns, and can explain many of the seismicity patterns observed in the CSZ. This has implications for other intraplate seismic zones, as it shows an example of how regional weak faults can modify stress conditions around local structures and drive seismicity. The results are particularly relevant for other regions located within rifted crust, such as the New Madrid seismic zone, which possibly display evidence of stress channelling.

3.1 Introduction

Large earthquakes in intraplate regions are relatively rare; they account for only about 5% of the global seismic moment release (Célérier *et al.*, 2005), however they have the potential to cause great damage and can pose significant societal risk. Our understanding of intraplate earthquakes is limited when compared to seismicity at the plate boundaries. The locations of earthquakes are not evenly distributed in continental interiors, rather they tend to cluster in smaller zones. Mazzotti (2007) outlined several end member geodynamic models to explain intraplate earthquake zones. These include the large-scale weak zone model in which crustal strain accumulates along weak paleotectonic structures, and the localized weak zone model, where earthquakes are confined to small areas of crustal weakness. The worldwide tendency of intraplate earthquakes to cluster around former rift zones (Sykes, 1978) fits well with the large-scale weak zone model, however, the localized weak zone model is often invoked to explain the existence of small clusters of conspicu-

ously high levels of seismicity such as the New Madrid seismic zone. This study examines one seismic zone that incorporates elements of both these models.

The Charlevoix seismic zone (CSZ) in the St. Lawrence valley of Québec, is historically the most active region in eastern Canada (Figure 3.1). Five earthquakes larger than magnitude 6 have been known to occur in 1663, 1791, 1860, 1870, and 1925 (Adams & Basham, 1991). The anomalously high level of seismicity in the CSZ, may be due in part to its unusual structural setting (Figure 3.2). The zone lies along a segment of an ancient rift that is superimposed by a meteorite impact structure.

3.1.1 Geological setting

The CSZ straddles the boundaries between three geological provinces (Figure 3.2), the Proterozoic Grenville Province to the northwest, the Cambro-Ordovician sedimentary rocks of the St. Lawrence Platform, which locally overlie the Grenville, and thrusted units of the Appalachian orogen to the southeast (Lemieux *et al.*, 2003). Normal faults, formed during the opening of the Iapetus Ocean (late Proterozoic to early Paleozoic), extend into the Grenville basement and are associated with the northeast trending St. Lawrence paleo-rift system. These faults include the Gouffre North-West and St. Laurent faults that parallel the St. Lawrence river along its north shore, the Charlevoix fault, which lies under the river, and the South Shore fault, which does not outcrop on surface but is inferred from gravity and magnetic data (Lamontagne, 1999) (Figure 3.2).

Extensive faulting due to a Devonian ($\sim$350 Ma) meteorite impact structure is

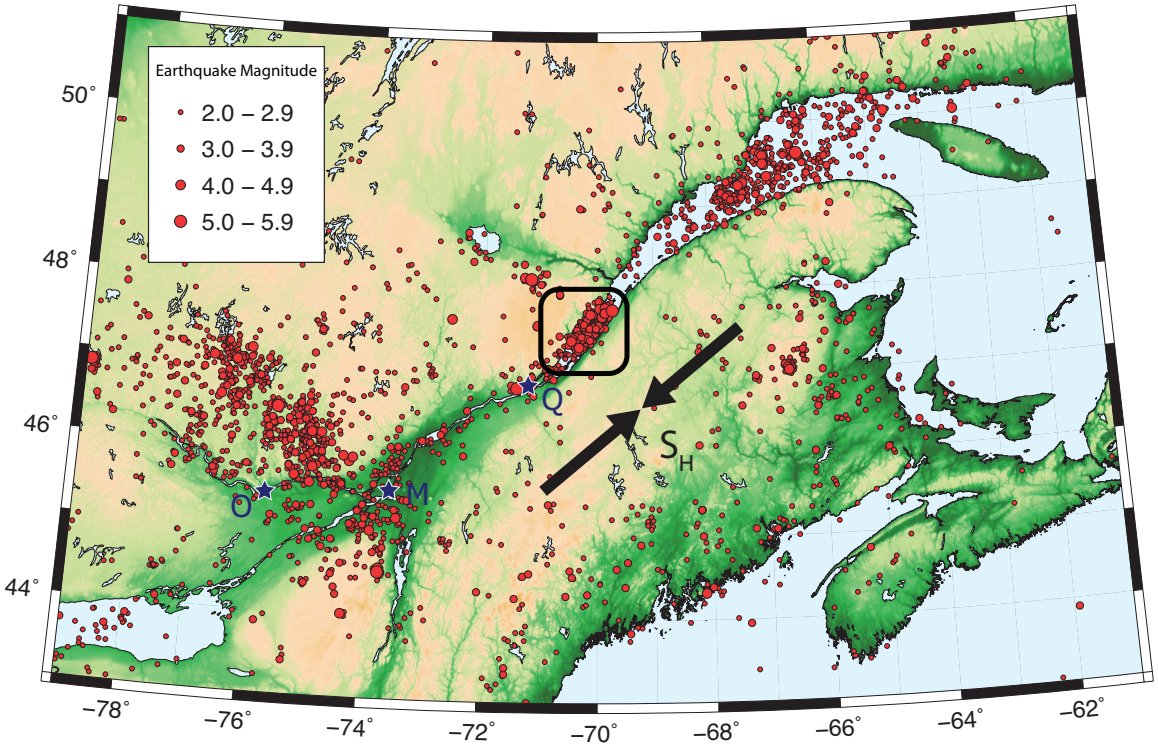

Figure 3.1: Seismicity map of eastern Canada, showing the location of the Charlevoix seismic zone (Earthquake data from the Geological Survey of Canada for the period 1985-2008). Inverted arrows show the dominant orientation of maximum compressive stress (S_H) (Zoback & Zoback, 1991). Abbreviations: *Q*: Québec City; *M*: Montréal; *O*: Ottawa.

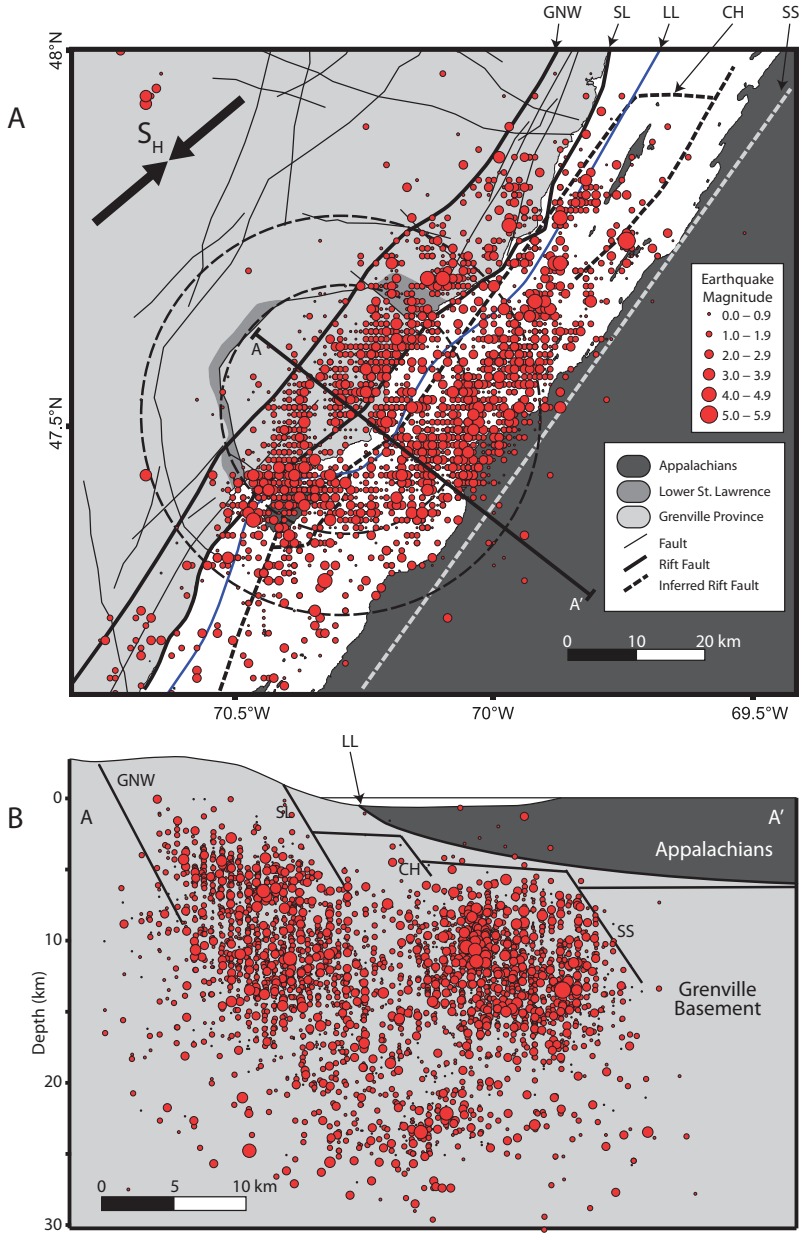

Figure 3.2: (A) Seismicity and structural geology of the Charlevoix seismic zone (modified from Vlahovic *et al.*, 2003). Abbreviations: *GNW*: Gouffre North-West fault; *SL*: Saint-Laurent fault; *CH*: Charlevoix fault; *SS*: South shore fault; *LL*: Logan's line (Appalachian deformation front), S_H: Maximum horizontal compressive stress orientation. (B) Schematic cross-section showing seismicity across the St. Lawrence river, with geology based on the work of Lamontagne (1999). Earthquake hypocentres group into two long clusters which appear to be bounded by faults associated with the St. Lawrence rift (Earthquake data from the Geological Survey of Canada for the period 1985-2008).

also preserved in addition to the rift related faulting (Rondot, 1971). The interior of the impact structure features much more varied fault orientations than the exterior. These include a polygonal set of normal faults around the centre of the impact that form graben and half-graben structures in which rocks of the St. Lawrence platform are locally preserved (Lemieux *et al.*, 2003) (Figure 3.2A). Faulting related to the impact is estimated to extend to a radius of 28 km laterally and approximately 11-12 km below the surface (Rondot, 1994). Major faults of the St. Lawrence rift system, such as the St. Laurent fault, cross the impact structure but are not significantly deflected by it, suggesting that they were reactivated post impact, possibly during the opening of the Atlantic ocean in the Mesozoic (Lemieux *et al.*, 2003).

The current regional stress field of the CSZ is dominated by the effect of ridge push at the Mid-Atlantic ridge, forming a fairly consistent NE-SW orientation of maximum compressive stress (S_H) throughout eastern North America (Zoback & Zoback, 1991)(Figures 3.1 and 3.2).

3.1.2 Seismicity

Earthquakes in the CSZ are primarily thrust or combination thrust / strike-slip events (Lamontagne, 1999). Hypocentres occur entirely within the Grenville basement rocks, concentrating mainly between depths of around 7 to 15 km but with some occurring as deep as 30 km (Leblanc & Buchbinder, 1977). They cluster into two elongate zones parallel to the St. Lawrence rift faults and extend beyond the boundaries of the impact structure, particularly in the NE region (Figure 3.2). A cross-sectional view reveals that the NW cluster is aligned along a steeply SE dip-

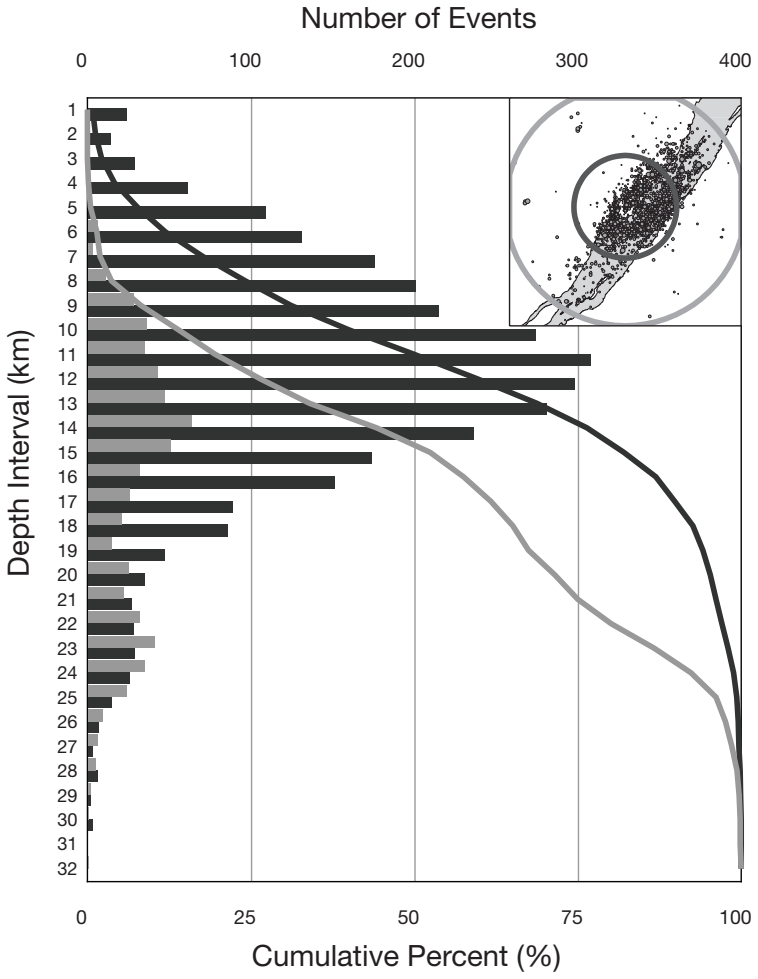

Figure 3.3: Earthquake depth distribution in two sub-zones of the Charlevoix seismic zone presented as number of events per 1 km interval (bars) and as cumulative percent (lines). The sub-zones are defined as epicentres within a 30 km radius from the centre of the impact structure (roughly the outer boundary of the crater, black) and from 30 km to 70 km from the centre (grey). Inset: Location map showing the two sub-zones. Shallow earthquakes are greatly enhanced in the inner zone relative to the outer zone (Earthquake data from the Geological Survey of Canada for the period 1985-2008).

ping plane ($\sim$70°, Figure 3.2B). The similarity of the location and orientation of these clusters with the St. Lawrence paleo-rift led Anglin (1984) to suggest that seismicity was caused by the reactivation of rift faults. This conclusion is in agreement with the global correlation of intraplate earthquake clusters with ancient rift and continental suture zones (Sykes, 1978). These features act as zones of weakness where earthquakes can be generated in the background regional stress field. However, this model is insufficient because it fails to explain the relative paucity of events in regions of the St. Lawrence just to the NW and SE of Charlevoix (See Figure 3.1). There is evidence from paleoseismic liquefaction studies that strong earthquakes have occurred within the CSZ area multiple times over the past 10,000 years, with no evidence of major earthquakes outside the zone (Ouellet, 1997; Tuttle & Dyer-Williams, 2009), suggesting that the seismicity is not simply migrating along the rift system over time. In addition, although focal mechanisms of larger events (e.g. 1925 **M** 6.2, and 1979 m_N 5.0) show SE dipping nodal planes consistent with slip along the rift faults (Bent, 1992; Lamontagne, 1999), detailed analysis of the smaller events reveals highly variable nodal plane orientations (Lamontagne, 1999). Events also cluster away from high P wave velocity structures located at the projected locations of the main rift faults at depth (Vlahovic *et al.*, 2003); thus the smaller events appear to form within a seismogenic volume bounded by the rift faults rather than being generated by them.

The Charlevoix impact crater is another structural feature which seems to play an important role in the seismicity of the region. Although most earthquakes larger than magnitude 4 occur outside or on the periphery of the impact zone, when smaller event locations are considered, there is a dramatic increase in activity in-

side the crater relative to the region surrounding it. Figure 3.3 shows an analysis of the depth distribution of earthquakes in the region directly below the crater relative to the area around it. Both regions show a bimodal distribution of earthquakes with a deep peak at $\sim$23 km. However, beneath the crater there is both a large increase in the total number of events, as well as a general shallowing of the events. Such a significant difference strongly suggests that the lower magnitude events are related to the impact structure.

In general, meteorite impact structures are not known to be associated with anomalously high levels of neotectonic seismicity (Solomon & Duxbury, 1987). Charlevoix and the Vredefort crater in South Africa are the only two large seismically active impact structures, and the Vredefort seismic events are almost entirely related to deep gold mine rock bursts (Solomon & Duxbury, 1987). However, the seismicity in Charlevoix is confined primarily to the region where the rift zone and impact structure overlap, suggesting that the two features together interact in such a way as to concentrate seismicity. Earthquakes occur along faults related to the impact structure, but only in those regions bounded by the larger rift faults.

The observed seismicity characteristics of the CSZ suggest that both the rift faults and the impact structure play an important role in the generated earthquake patterns. Large events appear to be related to slip along rift faults outside the boundaries of the crater; and small events primarily occur within or below the crater, but only in the region bounded by the rift faults. It appears that neither structural feature on its own would be sufficient to explain seismicity. However, the combined effect of both features is not clear. This study, through the use of numerical stress analysis, explores a possible mechanism by which the structural

features interact with far-field tectonic forces to produce local stress perturbations compatible with observed earthquake patterns.

3.2 Numerical approach

The intention of using numerical stress analysis models is not to replicate all observations, rather they are used to explore mechanisms by which major structures might interact with each other in a regional stress field. In light of this, a simplified model using the two-dimensional finite difference continuum code FLAC (Itasca Consulting Group Inc., 2005a) is used. Models can include a small number of discontinuities or interfaces that are given specific constitutive properties, allowing separate continuum zones to interact with each other.

The model geometry is shown in Figure 3.4. The crust is represented as a two dimensional elastic continuum, with a density of 2700 kg/m^3 and with a background bulk, and shear modulus (hereby denoted collectively as M_B) of 73 GPa and 44 GPa, respectively, following the physical parameters used by Assameur & Mareschal (1995). Next, a series of parallel linear discontinuities are introduced, which are assigned Mohr-Coulomb strength parameters (cohesion and friction) to represent the rift faults. The heavily fractured impact structure can be considered a "zone of weakness". Using the well-established concept of an equivalent continuum for fractured rock, the zone is represented by a continuum of reduced elastic modulus (e.g., Fossum, 1985). Although we do not know the equivalent modulus of the 30 km radius impact zone, it is tested with elastic moduli (both bulk and shear, denoted M_C) of $1/2$ and $3/4$ the value of the surrounding rock to determine

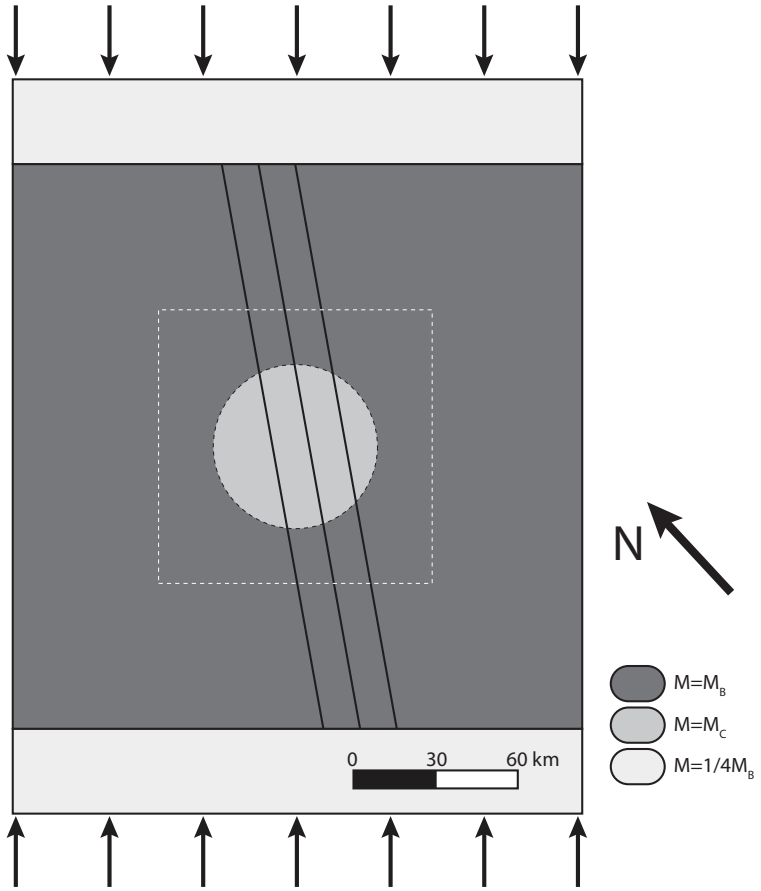

Figure 3.4: Model geometry of the Charlevoix seismic zone. The background moduli of the model (M_B) is given values of 73 GPa for bulk, and 44 GPa for shear modulus. The modulus of the crater (M_C) is varied from 50 to 100% of the background values. At the boundaries of the model soft zones with modulus 1/4 of the background values are added to reduce edge effects. The three black lines running through the crater represent the faults. The dashed square around the crater shows the boundaries of the contour plots of Figures 3.5 and 3.6. The two converging sets of arrows on the edges of the model represent the NE-SW oriented regional horizontal maximum compressive stress. North arrow indicates the relative orientation of the model with respect to the natural prototype.

the influence of this parameter in the overall mechanics of the system.

The internal stress field in the model is generated by applying displacements to boundary gridpoints over a series of timesteps (i.e., boundary velocities). These displacements are applied in the direction of tectonic loading, and boundary gridpoint velocities perpendicular to this are set to zero (Figure 3.4). Provided these velocities are small enough to maintain model stability, an internal stress field is generated in a similar manner to far-field tectonic compression. The orientation of the applied boundary velocities relative to the orientation of the faults was chosen based on a smoothed regional stress field map from the World Stress Map project (Heidbach *et al.*, 2008).

3.3 Model results and analysis

The models were run with a variety of values of elastic moduli and fault strength. Since the true values are not known, a range of values were used to explore the effect of reasonable changes in these parameters on model behaviour compared to observations. The elastic modulus of the impact crater was modified within the range of 50% to 100% of the background modulus values, which is within the limits of effective modulus due to randomly oriented fractures in two dimensions (Fossum, 1985). The friction angle of the faults was tested at values of 90° (locked), 15°, and 5° with no cohesion. The low values are meant to account for the effects of fault gouge and pore fluid pressure. Contour plots of computed magnitude of deviatoric stress and orientation of S_H are shown in Figures 3.5 and 3.6, respectively.

3.3.1 Effect of modulus

Column A of Figures 3.5 and 3.6 show the results of the models with fault friction set to 90°, which is equivalent to removing the faults from the model. By using this column as a reference, the effect of progressively lowering the modulus of the crater zone on the predicted deviatoric stress and orientation of S_H can be observed. With no modulus contrast (A1), a uniform stress field is generated, with S_H oriented parallel to the loading direction. As the impact zone modulus is decreased in rows 2 and 3, a partitioning of stress magnitude develops that intensifies as the modulus contrast increases. The behaviour follows that known for stress around soft inclusions. The magnitude of stress in the crater interior is lower than the background level because the lower modulus requires less stress for the same amount of strain (Figure 3.5). This lower stress magnitude is achieved by diverting stresses around the crater (Figure 3.6), which also results in high stress magnitudes concentrating in lobes on either side of the crater.

3.3.2 Effect of fault strength

The effect of fault strength on the state of stress in the model is shown in row 1 of Figures 3.5 and 3.6. Lowering the fault strength has very little impact on the magnitude of deviatoric stress (Figure 3.5), however, at very low friction angles (5°) the faults affect the orientation of S_H. If the faults are sufficiently weak they are unable to support the resolved shear stress of the applied stress field, in which case they slip and stresses rotate toward an orientation parallel to the faults (Figure 3.6, C1).

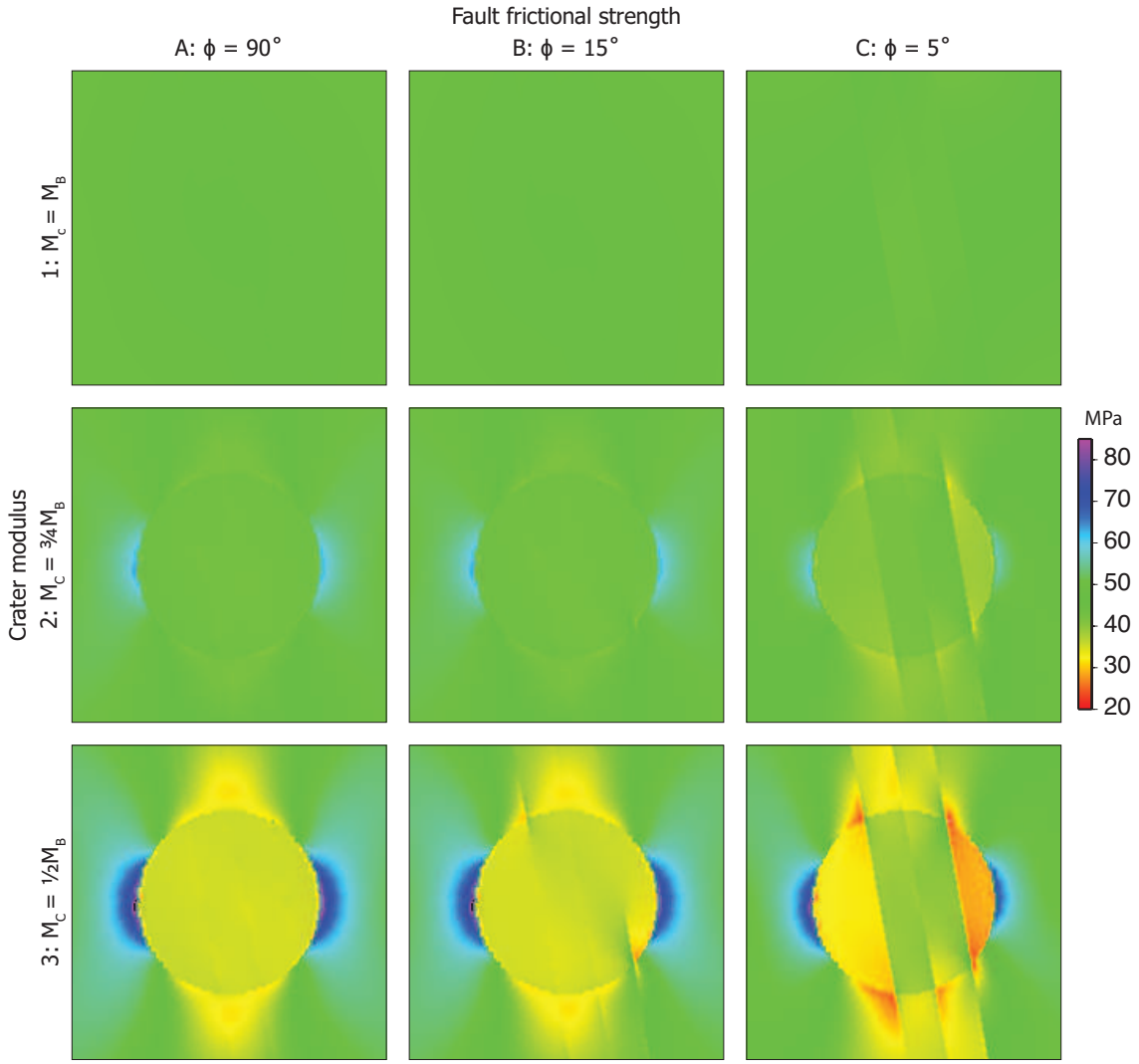

Figure 3.5: Contour plots of maximum deviatoric stress magnitude for varying values of Mohr-Coulomb fault friction angle (ϕ) and relative crater elastic moduli (M_C, both bulk and shear) compared to the surrounding rocks (M_B). A reduction in crater modulus results in a reduction of stress in the crater at the expense of stress concentration in two lobes on either side of the crater. In the absence of a large modulus contrast, a low fault strength has little effect on stress magnitude, however, when the two features are combined there is an added partitioning of stress magnitude in the interior of the crater.

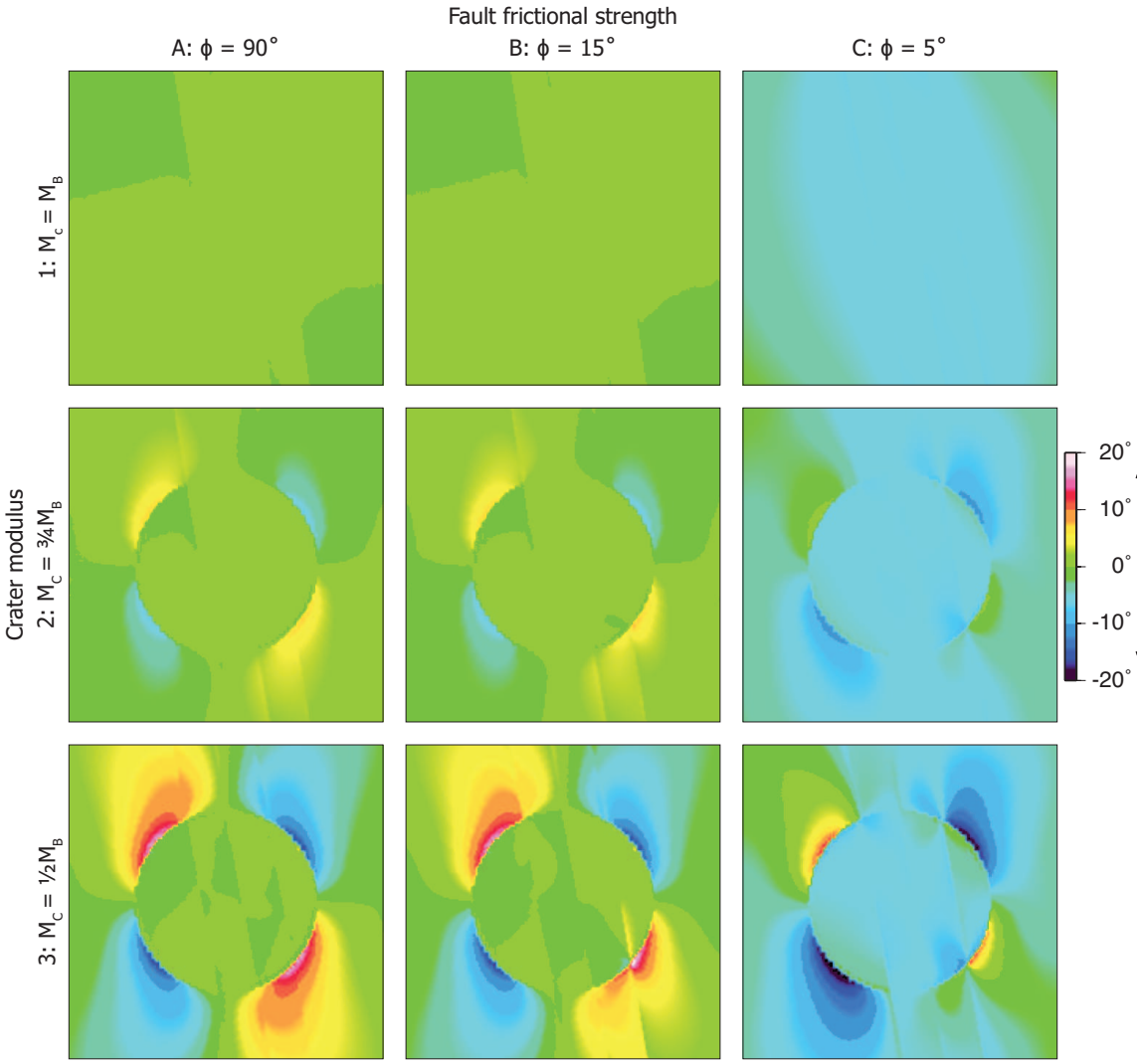

Figure 3.6: Contour plots of maximum compressive stress (S_H) orientation for varying values of Mohr-Coulomb fault friction angle (ϕ) and relative crater elastic moduli (M_C, both bulk and shear) compared to the surrounding rocks (M_B). Orientation is given relative to model loading direction, with clockwise rotation positive and counterclockwise negative. A reduction in crater modulus results in the stress field flowing around it, and a reduction in fault strength causes stress to flow parallel to them.

3.3.3 Combined effect of modulus and fault strength

When both fault strength and impact crater modulus are lowered (the diagonal of Figures 3.5 and 3.6), the two effects combine in a non-trivial manner. The most conspicuous effect is the partitioning of stress magnitude in the interior of the crater bounded by the faults (Figure 3.5, C3). Within the impact structure the region bounded by the faults is at a higher state of stress than the region outside the faults. The reason for this partitioning can be explained by examining the stress orientations (Figure 3.6, C3). Stress orientations well away from the faults are similar to the model with locked faults (A3), however, stress orientation closer to the faults is perturbed and tends to rotate parallel to the strike of the faults, similar to model C1. The result is that stress trajectories in regions between the faults are now forced to align parallel to the faults, which effectively channel higher magnitude stresses into the interior of the crater, as opposed to the periphery of the crater.

The partitioning of stress in the interior of the crater requires the presence of two or more weak faults. When a model is constructed with just one of the faults with low strength, there is no such partitioning of stress magnitude (Figure 3.7). In this single fault model there are still local perturbations of stress orientation in the vicinity of the fault. However, since there is no region bounded on both sides by faults, stresses can simply flow around to the other side of the crater. Channelling, resulting in a higher stress zone, does not occur.

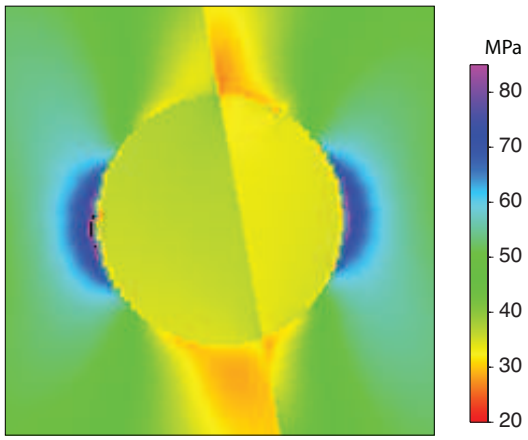

Figure 3.7: Contour plot of deviatoric stress showing the effect of only a single weak rift fault. The impact structure modulus is set to 50% of the background level and fault friction at 5°. In this case, since there is no region bounded on both sides by faults, stress simply flows around either side of the crater.

3.4 Discussion

The results of the modelling show that although the individual effects on the stress field are simple, the combined effect of a high contrast in elastic modulus as well as a series of weak parallel faults can result in complex stress partitioning. The presence of weak faults bounding both sides of the rift zone prevents stresses from flowing around the impact structure and effectively channels higher magnitude stresses into the interior. In order to relate this stress model to seismicity, further analysis is required. If the assumption is made that stress magnitudes correlate directly with seismicity potential, it is expected that most earthquakes would occur around the lobes of high stress at the sides of the impact crater. This does not agree with observations. However, there are other factors in addition to the state of stress that can affect seismicity, such as variations in the brittle strength of the rock, or the presence of pre-existing faults and fractures.

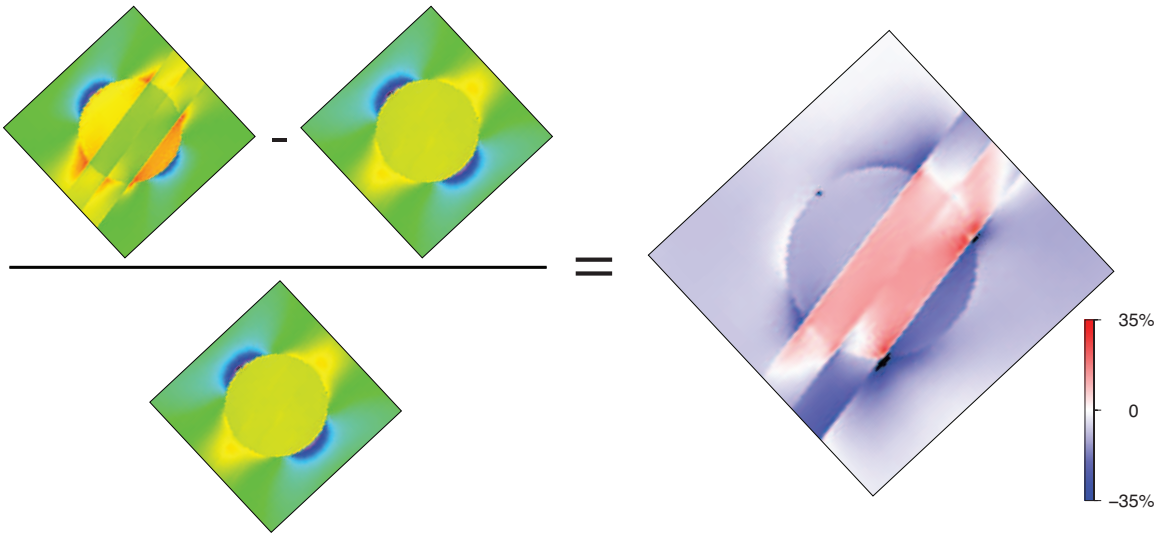

Figure 3.8: Grid algebra equation used to isolate the effect of weak rift faults and give a plot of change in deviatoric stress relative to the seismically stable locked rift model. The red area between the faults in the impact crater marks a region of increased deviatoric stress stress and can be considered a region of increased potential for earthquakes.

One approach to estimate where seismicity might occur is to compare the results to a similar structural model that is known to have very few seismic events. An obvious choice for this would be to compare it to other impact structures around the world, which are overwhelmingly aseismic (Solomon & Duxbury, 1987). What sets Charlevoix apart from these other impact structures is that it also has the rift faults running through the crater. Based on this information an assumption can be made that a model in which the rift faults are locked (i.e., model C1 of Figures 3.5 and 3.6) should produce a stress field that will not generate seismicity. A better indication of the potential for seismicity can be determined by examining the difference in the stress fields between a model with just the impact zone, and another with the weak faults included. This is achieved through the use of

"grid algebra" by subtracting the predicted values of deviatoric stress between the two models, which should highlight areas of stress magnitude change relative to a stable model. As Figure 3.8 shows, the combination of weak rift faults and a soft zone results in an increase in stress in the region of the impact zone between the rift faults, while the regions outside the faults result in little change or a reduction in stress levels. In these regions of increased deviatoric stress we expect a corresponding increase in the potential for earthquakes. The comparison of the red area of Figure 3.8 with a map of earthquakes in the Charlevoix area (Figure 3.2) reveals a good correlation with observed seismicity.

As discussed earlier, the difference in orientation of the rift faults relative to the applied stresses was chosen to be 10° based on the smoothed regional stress map (Heidbach *et al.*, 2008). However, due to uncertainty in this value, variations in the angle were tested to see if there was any noticeable effect of the regions of increased seismicity potential (Figure 3.9). The results show that although small changes in the orientation of the faults do affect the magnitudes of stress change, the main effect of increased deviatoric stress between the faults relative to regions outside still remains. This test also highlights the subtle effect of asymmetry in the system caused by the rift not running straight through the centre of the impact crater, but offset to one side. This asymmetry results in extension of the zone of increased seismicity potential along the rift to the north of the crater at the expense of the region to the south. The effect is observed in all the models, but is most clearly shown by the model at 5° to the applied stress (Figure 3.9). This may partially explain the higher concentration of events to the northeast of the crater relative to the region to the southwest (Figure 3.2A).

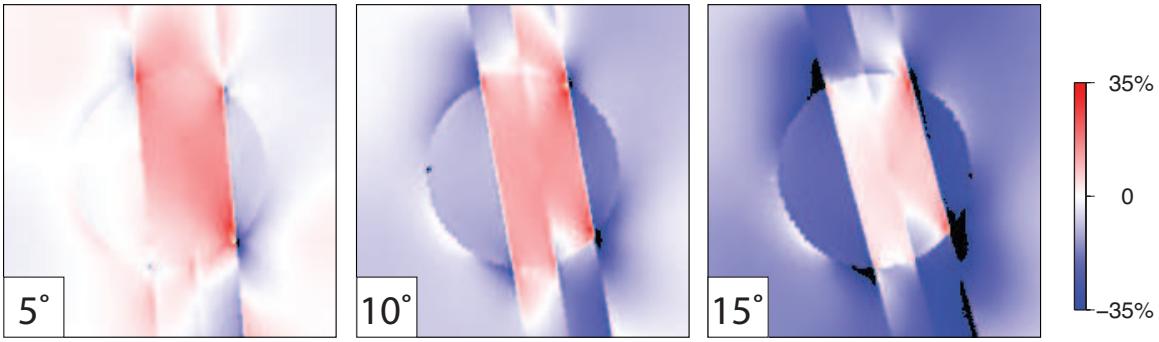

Figure 3.9: Contour plot of increased earthquake potential (as defined in Figure 3.8) for varied orientations of faults relative to the applied boundary stress. Note the extension of the zone of increased earthquake potential along the rift to the north of the crater, most apparent in the 5° model, which may explain the increased concentration of earthquakes compared to the southern region (see Figure 3.2A).

Pre-existing zones of weakness are often used to explain regions of persistent intraplate seismicity. These weak zones can either have a large extent, or be very localized (Mazzotti, 2007). Both of these end-member models have been used to explain the seismicity in the CSZ. Leblanc *et al.* (1973) proposed that the seismic activity may be due to the impact structure becoming active under postglacial uplift strain. Adams & Basham (1991), noting the absence of earthquakes at other meteorite craters in Canada, attributed the seismicity primarily to the St. Lawrence rift system. Many others, however, associated the earthquakes with a combined effect of the rift faults and impact structure, either by the reduction of the rift fault strength caused by the meteorite impact (Anglin, 1984; Lamontagne, 1987) or by increased fluid pressure brought into the impact crater via the rift faults (Lamontagne, 1999). This study's models similarly incorporate both features, however they differ in that the seismicity is a result of a stress concentration caused by their interaction rather than by local weakening of the structures. The impact structure

is a localized weak zone which concentrates most of the low-level continuous seismicity, however, the large-scale weak rift faults act as the locus for most of the larger, but less frequent events, and are required in order to act as a conduit to concentrate stresses into the interior of the crater.

3.4.1 Limitations of model

The simplification of the model to two dimensions raises a number of issues that must be addressed in order to justify the modelling approach. Perhaps the most significant limitation is that because we are confined to two dimensions we are unable to represent the true three dimensional shape of the crater. In three dimensions the crater would have a bowl shape, with limited depth extent. By treating it as a two dimensional problem we are effectively modelling the crater as a column of weak material. The two lobes of high stress observed in the model on the sides of the crater are largely an artifact formed as a consequence of this simplification (Figure 3.5). In two dimensions, stress flowing around the crater is confined to the horizontal plane, and must therefore concentrate around the perimeter of the crater. In three dimensions stress would also be able to flow beneath the crater, spreading out and reducing the concentration effect. In our analysis, this problem is minimized by observing the differences in stress between two models rather than the total stress field. The bowl shape of the crater also presents a problem for explaining the presence of earthquakes below the crater. The maximum depth of faulting related to the Charlevoix impact is estimated to be approximately 12 km (Rondot, 1994). Analysis of the depth distribution of earthquakes indicates that although a

large number of events occur within this depth, a significant portion extend below the crater (Figure 3.3). This cluster of seismicity can still be explained under the framework of the stress channelling model by considering the behaviour of stress in the slab of rock between the rift faults. In this situation the stress channelling effect should restrict most of the flow of stress within the plane of the dipping slab. Stress can still flow down below the crater, however, only within the boundaries of the faults. This effectively reduces the problem to a two dimensional geometry, where we would expect a lobe of high stress below the crater. If the bounding faults are sufficiently strong, however, stress flowing around the crater will be able to cross faults and benefit from the geometric spreading effect, reducing the possibility of large concentrations, and therefore, seismicity.

Although many of the events in the CSZ indicate NE–SW compressive stress direction, some indicate orientations at high angle to this with NW–SE oriented compression (Mazzotti *et al.*, 2006). Within the crater the discrepancy between the modelled orientation of S_H and the inferred compressive direction from individual focal mechanisms may be partially due to the omission of the fine detail of the complex faulting brought out by using the more simplified equivalent continuum representation. The presence of several pre-existing faults can result in complex perturbations in the stress field orientation and magnitude, however, the average stress field throughout the zone should be relatively consistent with the regional field (e.g., McKinnon, 2006).

Another limitation of the model is its inability to explain the larger magnitude earthquakes ($\mathbf{M} > 4$) , which tend to occur within the rift zone but just outside the impact structure (Stevens, 1980; Lamontagne, 1999). These large earthquakes

have focal mechanisms that are consistent with reverse sense reactivation of the major rift faults. This is not possible in our model due to the simplification of the problem to two dimensions; displacement on the rift faults is confined to strike slip. The localization of the large earthquakes outside the crater rather than in its interior may be due to the availability of large continuous rupture surfaces, which may not exist within the heavily fractured impact zone. The local clockwise rotation in the orientation of S_H to the NE and SW of the impact structure, caused by the flow of stress around the crater (Figure 3.6), would increase the resolved shear stress on the faults in these areas. This provides some indication of the process of generating large events just outside the crater as opposed to farther along the rift away from the crater, however, because non-strike slip is not represented in the model the result would need to be examined using 3-D models. The focal mechanisms of these large events tend to have the inferred compressive direction oriented NW-SE, which is at high angles to the regional stress field. This orientation is consistent with modelled displacements associated with glacial rebound (e.g., Wu & Mazzotti, 2007), and with GPS measured displacements indicating convergence across the St. Lawrence river (Mazzotti *et al.*, 2005). However, our models omit this source of strain and focus only on the far-field tectonic stresses. Despite these limitations, the stress channelling model provides a mechanism to explain much of the low-magnitude continuous seismicity.

3.4.2 Implications

Despite the unusual structural setting of the CSZ the results of these models are relevant for other intraplate areas. The models show how different scales of structures, both local and regional, can interact with each other when loaded tectonically, producing complicated stress patterns. The results are particularly relevant for regions associated with rifted crust, which account for over half of intraplate earthquakes (Schulte & Mooney, 2005). The models indicate that weak parallel faults can act as conduits to channel stresses onto intersecting structures. This same mechanism could be invoked to help explain some of the concentrations of seismicity found in other ancient rifts.

One major difference that sets Charlevoix apart from other intraplate seismic zones is that the active structures involved are not simply a small number of discrete faults. Rather the CSZ comprises a distributed damaged volume resulting from a meteorite impact. It is this difference that makes it an ideal location to illustrate the effect of stress channelling by parallel rift faults. In the early stages of a seismic zone study, the initial focus of the investigation is often to determine which structures are "active". In Charlevoix because the structures generating seismicity are distributed throughout the crater, the investigation shifts to explain why only part of the crater is active (Figure 3.10A). This draws attention to the rift faults which, although possibly not currently active themselves, clearly have an important role in partitioning seismicity. In an alternative scenario the active structures could be a small number of discrete faults rather than an impact crater (Figure 3.10B). In this situation linear trends of seismicity clearly define

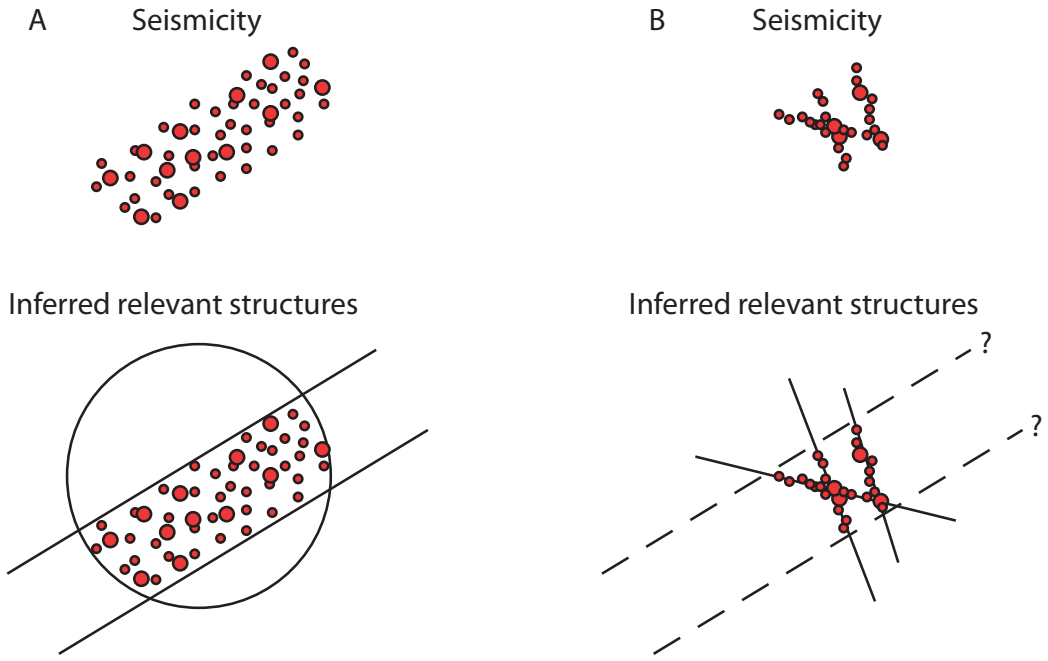

Figure 3.10: Cartoon showing the seismicity and relevant structures in two scenarios involving stress channelling within rift zones. (A) Stress channelling into an impact structure producing a volume of seismicity with clearly defined boundaries at the rift boundaries, indicating their significance. (B) Stress channelling resulting in partial reactivation of intersecting faults, in this example the rift faults are significant yet it is not clearly evident from the seismicity data.

which structures are seismically active. Seismicity could still be truncated by the rift faults, however, if they are aseismic or only periodically active and not in the seismic record, then their role is more subtle and could easily be missed, leading to an incomplete model.

The Charlevoix models show that some apparently aseismic structures can have a major role in partitioning stress in a rift environment. Evidence for similar processes may be found in the New Madrid seismic zone (NMSZ) in the eastern United States (Figure 3.11). The NMSZ is the site of the largest intraplate earthquakes on historic record in 1811-1812 (Grana & Richardson, 1996), and is a region with continued seismic activity. The earthquakes are contained within the NE-SW trending Reelfoot rift which formed during the opening of the Iapetus Ocean, the same event which created the St. Lawrence rift. The active structures are interpreted as two rift-parallel right-lateral strike-slip faults with the northeastern arm forming the northwest boundary of the rift and the southeastern arm trending along the centre of the rift (Cox *et al.*, 2006). These two strike-slip faults are connected by a left stepping reverse slip fault called the Reelfoot thrust. Seismicity along the Reelfoot thrust extends beyond the southeastern arm and is truncated by the southern margin of the rift, which experiences much less seismic activity (Figure 3.11)(Cox *et al.*, 2001). Although the trend of the rift is oblique to the average regional orientation of S_H (approx. 80°, Ellis, 1994), many stress orientations inferred from focal mechanism data within the seismic zone lie subparallel to the strike of the rift (e.g. Ellis, 1994; Horton *et al.*, 2005). The truncation of seismicity by the relatively aseismic rift margin is similar to the behaviour at the CSZ. Combined with evidence of stress rotation within the Reelfoot rift, this provides compelling

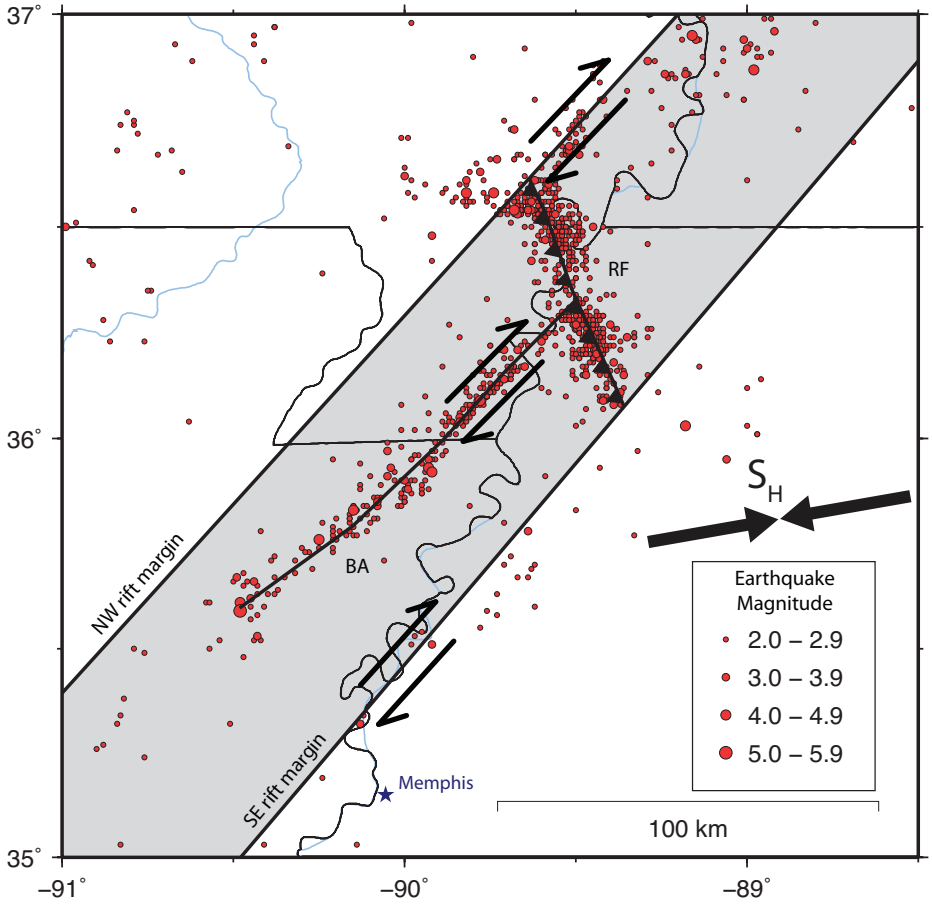

Figure 3.11: Earthquakes epicentres of the New Madrid seismic zone (1974–2008) with interpretation based on Cox *et al.* (2001). Abbreviations: *RF*: Reelfoot thrust fault; BA: Blytheville Arch; S_H: Maximum horizontal compressive stress orientation for the NMSZ area (Ellis, 1994). Note that earthquakes along the Reelfoot thrust fault are truncated by the southeast margin of the Reelfoot rift. Proposed stress channel between the NE and SW rift margins is shown in grey. Seismicity data from the catalogue of Center for Earthquake Research and Information, University of Memphis.

evidence that stress channelling is active in the NMSZ, and may be a contributing factor in the continued seismicity there.

3.5 Conclusions

Mazzotti (2007) describes a number of models to explain intraplate earthquakes in North America including the localized weak zone model, where earthquakes are confined to small areas of crustal weakness, and the large-scale weak zone model, where crustal strain is concentrated on major paleotectonic structures. Our model of the CSZ shares components of both of these models: the large-scale weak zone represented by the Iapetan rift structures interacting with the stress perturbation associated with the localized impact structure weak zone. The rift faults act as a conduit to concentrate higher stresses into the weak impact crater. Both components are required to generate the observed pattern of low-level seismicity.

Despite some of the limitations of the stress channelling model, such as its failure to explain the largest earthquakes of the CSZ, it provides a potential mechanism for much of the low level continuous events frequently observed in the area. Using a very simple model incorporating only a few faults of varying strength and zones of differing elastic properties we are able to produce stress patterns that can explain many of the observed seismicity characteristics of the CSZ. These include why the earthquakes are localized into linear bands, rather than distributed throughout the impact structure, and how the rift faults act as boundaries to the seismicity.

The CSZ's unique structural setting makes it an ideal location to show the role

of weak bounding faults on altering the stability of intersecting structures. These large-scale weak faults can not only form the locus of intraplate seismicity but can act as natural boundaries for local stress volumes, and can form conduits for concentrating stress. Similar models involving stress channelling between rift faults could be invoked to explain earthquake concentrations on the Reelfoot thrust fault of the New Madrid seismic zone, on which seismic activity is truncated by the margins of the Reelfoot rift. Given that more than half of intraplate earthquakes occur within rifted crust, it is likely that this mechanism can be invoked elsewhere.

3.6 Aknowledgements

Financial support for this work was provided by the Ontario Research and Development Challenge Fund, Natural Sciences and Engineering Research Council of Canada Discovery Grants to Steve McKinnon and Laurent Godin, and by an Ontario Graduate Scholarship in Science and Technology to Alan Baird. We are thankful for the helpful comments and suggestions of two anonymous reviewers and Editor Xiaofei Chen.

Chapter 4

Relationship between structures, stress and seismicity in the Charlevoix seismic zone revealed by 3-D geomechanical models: Implications for the seismotectonics of continental interiors

This chapter has been submitted with Stephen D. McKinnon and Laurent Godin as co-authors to the Journal of Geophysical Research (Baird *et al.*, in review).

Abstract

The Charlevoix seismic zone in the St. Lawrence valley of Québec is the most active in eastern Canada. The structurally complex region comprises a series of subparallel steeply dipping Iapetan rift faults, superimposed by a 350 Ma meteorite impact structure, resulting in a heavily faulted volume. The elongate seismic zone runs through the crater parallel to the rift. Most large events localize outside the crater and are consistent with slip along the rift faults, whereas background seismicity primarily occurs within the volume of rock bounded by the rift faults within and beneath the crater. The interaction between rift and crater faults is explored using the three-dimensional stress analysis code FLAC3D. The rift faults are represented by frictional discontinuities and the crater by a bowl-shaped elastic volume of reduced modulus. Deviatoric stresses are slowly built-up from boundary displacements similar to tectonic loading. Results indicate that weakening the rift faults produces a stress increase in the region of the crater bounded by the faults. This causes a decrease of stability of optimally oriented faults, and may explain the localization of low-level seismicity. Additionally, slip distribution along the rift faults shows that large events localize at the perimeter of the crater and produce focal mechanisms with P-axes oblique to the applied stress field, consistent with historic large earthquakes. It is speculated that similar systematic rotation of focal mechanisms P-axes may be expected along other intraplate rift zones, raising a potential caveat for the use of focal mechanisms in stress estimation in continental interiors.

4.1 Introduction

The Charlevoix seismic zone (CSZ) in the St. Lawrence valley of Québec is the most seismically active region in eastern Canada (Figure 4.1). It has been the site of several large historic events (five moment magnitude $\mathbf{M} > 6$ events since 1663) (Adams & Basham, 1991) as well as continuous low-level activity. Like most intraplate earthquake zones, the cause of the focus of seismic activity is not well understood. On a broad scale, intraplate seismicity is often associated with preexisting weak structures such as ancient rift zones and aulacogens (e.g. Sykes, 1978), however, small areas of intense activity are often attributed to local effects. The CSZ lies at the intersection of two potential sources of weakness; the Cambro-Ordovician St. Lawrence rift, which strikes NE-SW along the river, and the Charlevoix Impact structure, which is a large bowl shaped damage zone formed as a result of a meteorite impact $\sim$300 Ma (Rondot, 1971).

The relative importance of the two structures in the distribution of seismicity has been debated. Leblanc *et al.* (1973), noting several small events coinciding with the location of large past events and a meteorite crater, proposed that weakened crust caused by the impact could yield more easily to postglacial strain. Extensive microseismic monitoring further delineated the extent of the seismic zone, and revealed that there were in fact two clusters of seismicity running along the length of the St. Lawrence, which coincide with the interpreted location of rift faults (Anglin, 1984). This information, combined with an absence of seismicity at other Canadian meteorite craters, led Adams & Basham (1991) to attribute the earthquakes to the reactivation of rift faults, possibly weakened by the crater. Improvements in

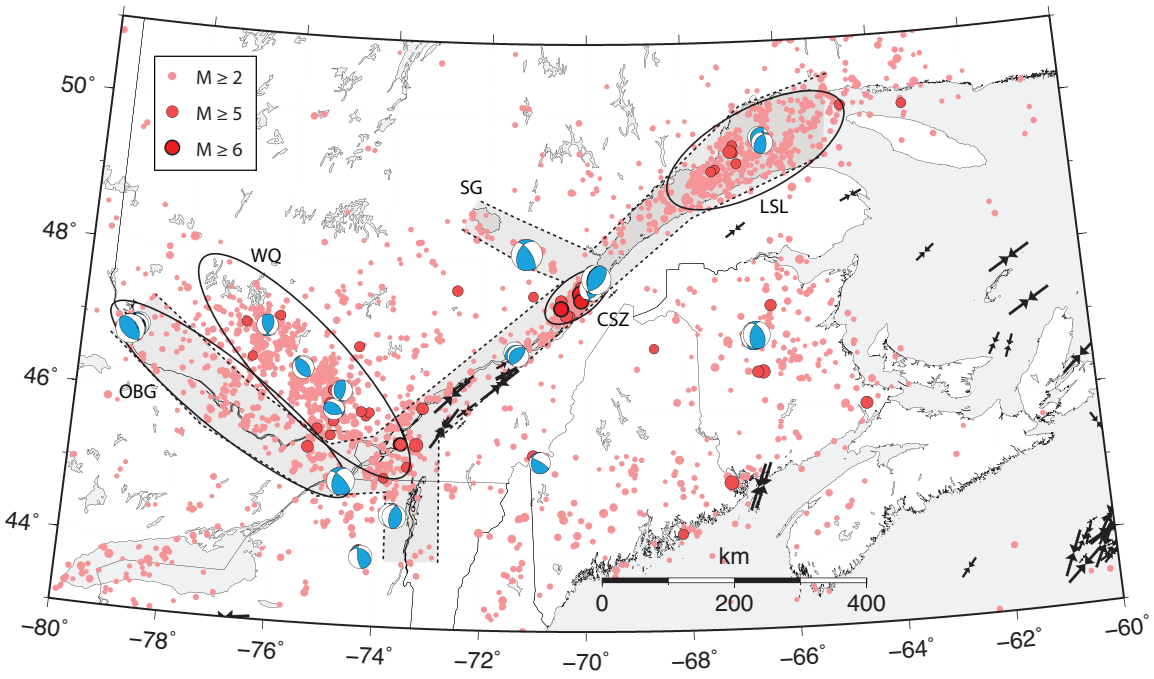

Figure 4.1: Seismicity and seismic zones in southeastern Canada. Background seismicity (Nuttli magnitude, m_N, $\geq$ 2 since 1985) from the Geological Survey of Canada, supplemented by large historic events (mostly moment magnitude, **M**, $\geq$ 5) since 1663 from Lamontagne *et al.* (2007). Selected focal mechanisms of moderate to large earthquakes (**M** $\geq$ 4.3) from the compilation of Mazzotti & Townend (2010). Inverted black arrows indicate the orientation of S_H inferred from borehole breakouts (Heidbach *et al.*, 2008). Shaded grey area indicates the extent of Iapetan rifting (Adams & Halchuk, 2003). Abbreviations: CSZ, Charlevoix Seismic zone; LSL, Lower St. Lawrence; OBG, Ottawa-Bonnechère graben; WQ, Western Québec seismic zone; SG, Saguenay graben.

hypocentre location and analysis of microseismicity focal mechanisms in the 1990's however, has revealed that much of the seismicity clusters are not occurring along planar structures, but appear to be located in fractured volumes of rock bounded by the major rift faults (Lamontagne, 1999). Thus both the impact structure and the rift faults appear to play an important role in the distribution of seismicity in the CSZ.

While much has been published describing the seismicity in the CSZ, little work has been done to explain the mechanics behind the partitioning of seismicity. Baird *et al.* (2009), addressing this with simple 2-D stress models, showed that a series of parallel weak faults intersecting a 'soft zone' can act as a stress conduit, channelling background stresses into the interior of the weak zone, which would otherwise simply flow around it. The models were able to illustrate this concept as a way to explain much of the background seismicity patterns observed in the CSZ. The models, however, had a number of limitations, primarily brought on by the restriction to two dimensions. The current study builds on the results of Baird *et al.* (2009) by extending the models to three dimensions in order to better represent the true 3-D architecture of the system. In addition to corroborating the results of the 2-D models, the 3-D models explain the extension of earthquakes below the crater, address slip along the rift faults themselves, which appear to form the locus of the less frequent large events, and provide evidence for a misfit between focal mechanism P-axes and the orientation of maximum horizontal compressive stress S_H.

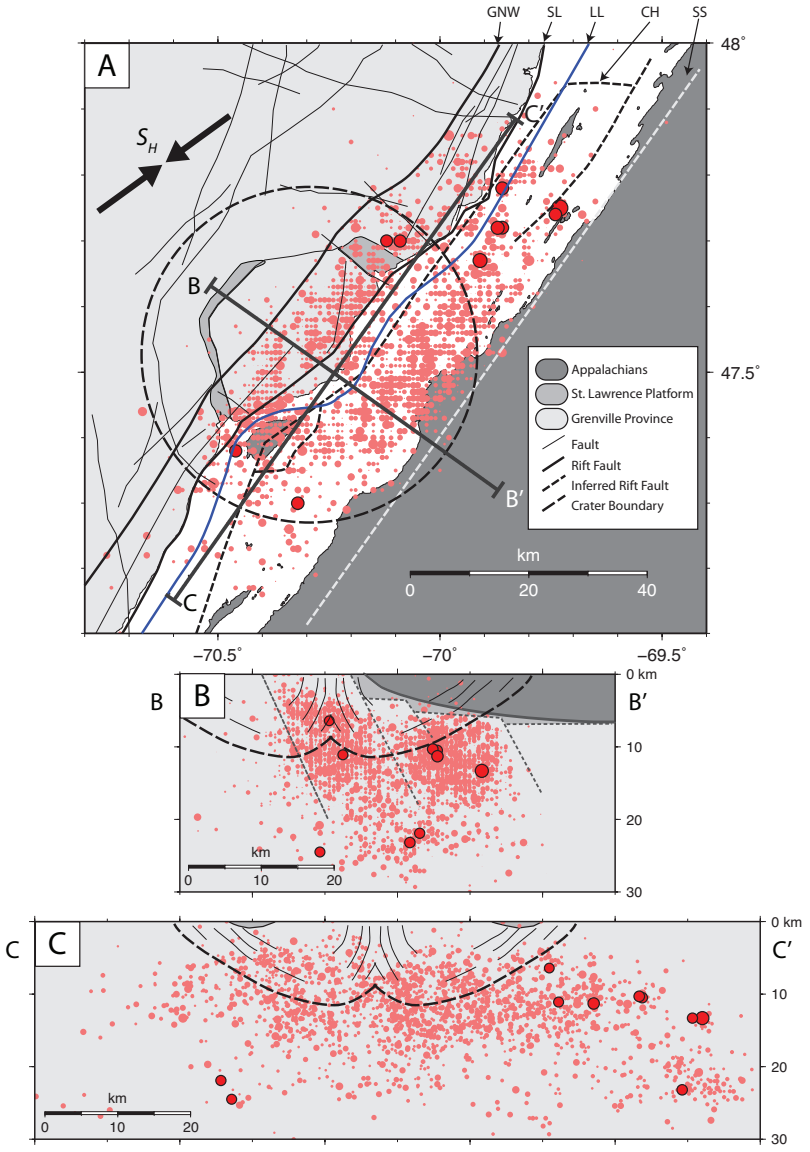

Figure 4.2: (A) Seismicity and structural geology of the Charlevoix seismic zone. Pink and red circles represent earthquakes with Nuttli magnitudes (m_N) of less than 4.0 or greater than 4.0, respectively. Abbreviations: GNW, Gouffre North-West fault; SL, Saint-Laurent fault; CH, Charlevoix fault; SS, South shore fault; LL, Logan's line (Appalachian deformation front); S_H, Maximum horizontal compressive stress orientation. Lines B–B′ and C–C′ refer to cross-sections in (B) and (C) (Earthquake data from the Geological Survey of Canada for the period 1985–2009). Cross-sectional view of the Charlevoix seismic zone (B) across strike and (C) along strike of the St. Lawrence rift. Geological structure and crater boundary based on the work of Lamontagne (1999) and Rondot (1994).

4.2 Background

4.2.1 Geologic setting

The CSZ lies in a structurally complex setting created by a series of tectonic events spanning the last 1.1 billion years (Figure 4.2A). The oldest tectonic episode recorded in the region consists of the 1100-990 Ma Grenville orogeny, which resulted from a series of exotic terranes accreting onto the southeast margin of Laurentia (Rivers, 1997). The upper amphibolite to granulite metamorphic facies rocks of the Grenville Province make up the core of this orogen and now form the basement of the Charlevoix area (Figure 4.2B). Following a period of erosion the area was subjected to a late Proterozoic to early Paleozoic rifting event associated with the breakup of the Rodinia supercontinent and the formation of the Iapetus Ocean (Kumarapeli, 1985). A series of normal faults forming the St. Lawrence paleorift system represented the passive margin of the proto-North American continent onto which carbonate rocks of the St. Lawrence platform were deposited (St-Julien & Hubert, 1975). The next major tectonic phase was associated with the closing of the Iapetus Ocean and the formation of the Appalachian orogen. Appalachian Nappes were thrust over the North American continent as far west as the St. Lawrence in the Charlevoix area. The deformation front, known as Logan's Line, runs through the CSZ (Rondot, 1994). Following this, in the Devonian ($\sim$350 Ma) the region was subjected to a meteorite impact resulting in a large ($\sim$56 km diameter) crater (Rondot, 1971). The last significant tectonic episode to effect the region was the normal sense reactivation of the Iapetan rift faults due to the open-

ing of the Atlantic in the Mesozoic (Lemieux *et al.*, 2003).

Since the Appalachian Nappes are confined to the upper few kilometeres, and most of the seismicity is located in the deeper Grenville basement rocks, the most pertinent structural features are the rifted faults and the impact structure (Figure 4.2B). The NE-SW trending St. Lawrence rift is a half-graben represented by a series of parallel normal faults steeply dipping to the SE, which extend into the Grenville basement (Tremblay *et al.*, 2003). In the Charlevoix region these faults include the Gouffre North-West and St. Laurent faults that parallel the St. Lawrence river along its north shore, the Charlevoix fault, which lies under the river, and the South Shore fault, which does not outcrop on surface but is inferred from gravity and magnetic data (Lamontagne, 1999)(Figure 4.2A,B).

The Charlevoix impact structure forms a $\sim$56 km diameter damaged zone exhibiting varied fault orientations. The faults include a polygonal ring graben system between 16 and 20 km from the centre (Rondot, 1994) in which rocks of the St. Lawrence platform are locally preserved (Figure 4.2). In the interior portion of the crater the faults are more scattered in orientation (Lemieux *et al.*, 2003). Faulting associated with the crater is estimated to extend to a depth of approximately 12 km (Rondot, 1994).

4.2.2 Seismicity

The CSZ has been the locus of five earthquakes greater than **M** 6 in recent history (in 1663, 1791, 1860, 1870, and 1925) (Adams & Basham, 1991). The site is also host to an abundance of background seismicity. Over 200 events are recorded each

year, most of which are lower than Nuttli magnitude (m_N) 3.0. Earthquakes occur almost entirely within the Grenville basement, with most activity between 7–15 km depth, but with some as deep at 30 km (Figure 4.2C).

The spatial distribution of the background seismicity appears to be largely controlled by the St. Lawrence rift and the impact structure. The seismically active region spans approximately 30 by 85 km covering the area of overlap between the two structures and extending beyond the boundaries of the crater along the rift to the northeast (Figure 4.2A). A cross-sectional view of the seismicity across the strike of the rift reveals that earthquakes cluster into two distinct elongate zones, with the northwest cluster steeply dipping to the southeast (Figure 4.2B). The similarity in orientation of these clusters with the St. Lawrence rift faults led Anglin (1984) to conclude that most of the seismicity was related to reactivation of the faults. Improvements in hypocentre locations over the years, however, combined with evidence of varied slip planes from microseismic focal mechanisms suggest that much of the activity is not located on the major faults but within a fractured volume bounded by the rift faults (Lamontagne, 1999).

Although the active region of the CSZ extends beyond the boundaries of the crater, most of the low magnitude background activity occurs either within or beneath it (Figures 4.2C and 4.3). The large increase in shallow events within the crater area relative to the surrounding regions is strongly suggestive of its influence on the seismicity of the area. This is unusual, however, since most large impact structures found worldwide are seismically inactive (Solomon & Duxbury, 1987).

While the impact structure appears to be strongly associated with low-level

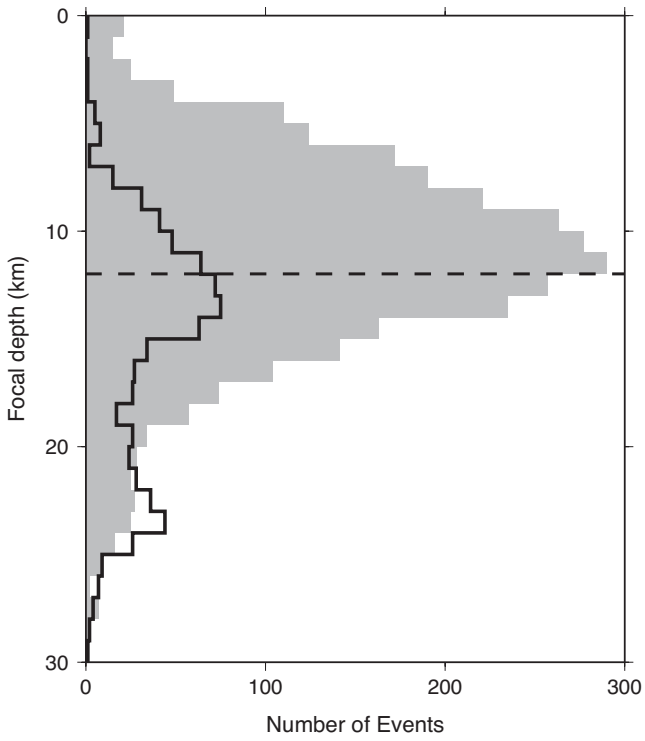

Figure 4.3: Earthquake depth distribution for events located within or directly below the crater (epicentres within 28 km from crater centre, grey) and for the surrounding area (epicentres 28-70 km from crater centre, black outline). Dashed line indicates approximate lower boundary of the crater. Data compiled from the Geological Survey of Canada earthquake catalogue.

background seismicity, the opposite is true for larger events. As shown in Figure 4.2, all events larger than m_N 4.0 (red circles) since 1985 have occurred outside the crater, with most clustering at the northeast end. Additionally most large events over the last century have occurred to the northeast of the crater, including the 1925 **M** 6.2 event and the 1979 m_N 5.0 event (Hasegawa & Wetmiller, 1980; Bent, 1992). Bearing in mind that rupture surfaces of events of this magnitude are estimated to be on the order of several kilometres wide (Johnston, 1993), the localization of large events outside the crater as well as a common SE dipping nodal plane (Figure 4.4) suggest that the rift faults form the locus of these large events.

4.2.3 Stress Field

The CSZ is located within the Midplate stress province of eastern North America, which is dominated by NE- to ENE- oriented maximum horizontal compressive stress (S_H) (Zoback & Zoback, 1991). Plate-driving forces from the mid-Atlantic ridge likely provide the greatest source of stress (Richardson & Reding, 1991; Adams & Bell, 1991; Zoback & Zoback, 1991). The orientation of the stress field is inferred from a variety of data sources, which have been included in the World Stress Map database. In eastern Canada and the northeastern United States these are primarily borehole breakouts and earthquake focal mechanisms (Heidbach *et al.*, 2008).

Borehole breakout data from the World Stress Map database for southeastern Canada are shown in Figure 4.1. These include a large number of measurements along the St. Lawrence river approximately 100–250 km southwest of the CSZ, between Québec City and Montréal, which are all consistently oriented NE-SW,

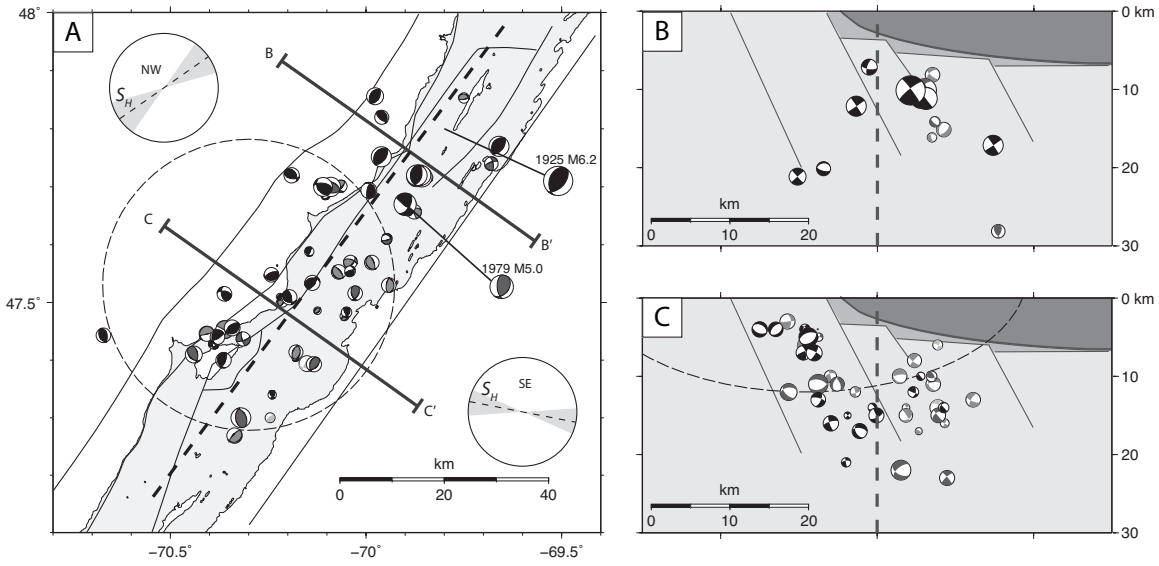

Figure 4.4: (A) Earthquake focal mechanisms from the Charlevoix seismic zone. Mechanisms are scaled by magnitude. Black, dark grey, and light grey mechanisms refer to quality rankings of A, B, and C, respectively. The two largest events (**M** 6.2 1925 event and m_N 5.0 1979 event) are indicated. (B) Cross-section showing mechanisms northeast of the crater. (C) Cross-section showing mechanisms within or below the crater. Circles with dashed line and grey angular sectors indicate the average and 90% confidence region of the maximum horizontal compressive stress direction in the NE and SW clusters of seismicity from the stress inversion of Mazzotti & Townend (2010). Thick dashed line indicates the separation of the NW and SE clusters of seismicity used in the analysis.

subparallel to the river.

Earthquake focal mechanisms provide another source of stress data where the P, B, and T axes are used to provide an estimate of the principal stress orientations (Zoback, 1992b). However, P and T axes can potentially differ significantly from the actual stress orientations with the only strict constraint being that the orientation of the major principal stress must lie within the dilatational field of the focal mechanism (e.g. McKenzie, 1969). Consequently it is current practice that all stress orientations inferred from individual focal mechanisms are given a quality ranking of no more than C ($\pm 25^{\circ}$ uncertainty) regardless of how well the mechanism is constrained (Barth *et al.*, 2008). Despite these problems, focal mechanisms do provide some constraint on the stress orientation and also contain useful information on the geometry of fault slip.

A case study was carried out by Zoback (1992a), examining the focal mechanisms of 32 moderate earthquakes in eastern North America to determine whether slip was compatible with the regional stress field. A similar study by Du *et al.* (2003) supplemented the data with 16 more moderate events since 1990. Of the events examined, most were broadly compatible with the regional stress field, with NE-SW oriented P-axes. However, there were a few notable exceptions including four events located along the St. Lawrence river (two from the CSZ), which had P-axes oriented NW-SE (Figure 4.1). Zoback (1992a) found that while the 1979 Charlevoix earthquake was geometrically possible in the inferred regional stress field, it was frictionally unlikely, requiring either very weak faults, or superlithostatic pore pressure. Alternatively it was argued that it was related to a local stress perturbation, possibly due to the presence of a dense rift pillow beneath the St.

Lawrence (Zoback, 1992a). Similar models have been proposed to explain earthquake concentration in the New Madrid seismic zone in the central United States, which is located within the Reelfoot rift (Grana & Richardson, 1996), and to explain an apparent stress rotation near the Amazonas rift in Brazil (Zoback & Richardson, 1996). Published studies, however, are insufficient to support or refute the existence on a rift pillow beneath the St. Lawrence (Du *et al.*, 2003). These models also fail to account for the large number of borehole breakout data indicating rift parallel compression between Québec City and Montréal (Figure 4.1).

One of the major shortcomings of these broad regional focal mechanism studies is the limited datasets used. All four of the anomalous events examined along the St. Lawrence were larger than **M** 4. Examining a variety of focal mechanisms from the CSZ, however, reveals that while larger events ($m_N > 4$) typically have NW-SE oriented P-axes, smaller events are considerably more varied (Figure 4.4). A formal stress inversion of 60 focal mechanisms carried out by Mazzotti & Townend (2010) yields a S_H orientation of 086° for the whole of the CSZ, an approximately 30° clockwise rotation from S_H inferred from borehole measurements. A more detailed analysis into spatial variations of stress within the CSZ, however, reveals two distinct estimates of S_H orientation between events clustering northwest of the Saint-Laurent fault versus those from the southeast (Figure 4.4). A 47° apparent rotation exists between the two groups, with the NW cluster roughly parallel to the borehole data and the rift trend, and the SW cluster strongly oblique (Mazzotti & Townend, 2010).

The significance of the large apparent rotation between the borehole and focal mechanism inferred S_H orientations is not clear at this time. However, the varia-

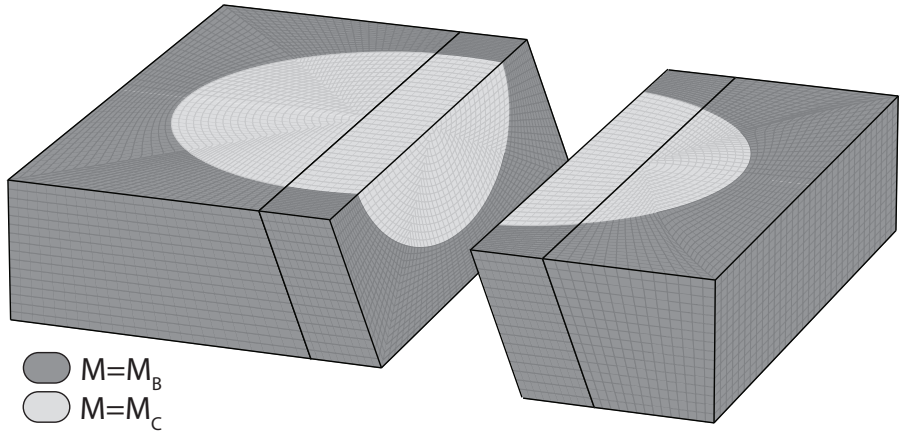

Figure 4.5: Internal geometry of the model. The crater is represented as an ellipsoid with a horizontal radius of 30 km and depth of 15 km at its centre. Rift faults strike at 35° and are steeply dipping to the SE. Colours indicate variations of the elastic moduli (M) in the model between the background rock (M_B) and the weakened crater rock (M_C).

tions in S_H derived from microseismicity from within the CSZ suggest that it is a very localized effect and likely not due to a regional stress perturbation. Discussion of possible mechanisms causing the rotation is addressed later in this paper.

4.3 Numerical Approach

Baird *et al.* (2009) used a 2-D stress analysis code to investigate the interaction between the rift faults and crater by locally altering the regional stress field and controlling the distribution of seismicity. In this paper we take a similar approach using the 3-D code FLAC3D (Fast Lagrangian Analysis of Continua) (Itasca Consulting Group Inc., 2005b). FLAC3D uses finite difference techniques to compute stress and strain within discretized continuum blocks while permitting the inclusion of a small number of discontinuities to represent discrete faults.

The main reason for using a 3-D code is to better represent the true architecture of the system and to allow oblique slip displacements along modelled faults, which were previously restricted to strike-slip. For simplicity we limit the structures included to only those features which play an important role in the distribution of seismicity, namely the rift faults and the impact crater (Figure 4.5). The rift faults are represented as a series of three parallel frictional discontinuities striking at N035° and steeply dipping to the southeast. Due to difficulty in including curved interfaces to model listric faults, the models are tested with fault dips of 60° and 70°. The faults roughly correspond to the Gouffre North-West, Saint-Laurent and South Shore faults, which appear to form the main boundaries of the seismicity (Figure 4.2). The Impact structure is represented in the models as the lower half of an oblate spheroid, with a 30 km radius at the surface and extending to a depth of 15 km below the centre. Rather than represent the complex faulted volume with explicit faults, the damaged volume is simulated by using a continuum of lowered elastic modulus following the well established concept of an equivalent continuum for fractured rock (e.g. Fossum, 1985).

4.3.1 Initial and boundary conditions

An elastic continuum constitutive model is chosen to represent the crust in which density, bulk, and shear moduli must be prescribed. Density is assumed to be 2700 kg m^{-3}, typical of upper crustal rock. The background moduli for the region outside the crater (both bulk and shear, hereby denoted collectively as M_B) is derived from P and S-wave velocity models for the Saguenay region to the north of

the CSZ (Somerville *et al.*, 1990). The variation of M_B with depth is shown in Figure 4.6A. Within the crater, the elastic modulus values (denoted M_C) are lowered to simulate the damaged zone. Since the equivalent modulus is not known it was tested at $1/4$ and $1/2$ the value of the surrounding rock (M_B).

Eastern Canada is characterized by a triaxial thrust regime state of stress (i.e. $S_H > S_h > S_V$) (Adams & Bell, 1991). However, rather than initializing a differential stress in the models, a simple lithostatic stress field is initialized, and the horizontal compressive stress is then slowly increased through boundary displacements. This procedure ensures compatibility between the stresses and fault displacement. Since it is assumed that the largest contribution to stress in the region is from far-field tectonic sources, boundary displacements are applied in the direction of tectonic loading over a series of computational time steps. The stress field is slowly built up until the differential stress at a depth of 10 km is approximately 200 MPa (Figure 4.6B), which is of the same order as estimates of stress differences at that depth (e.g. Hasegawa *et al.*, 1985; Zoback *et al.*, 1993; Lamontagne & Ranalli, 1996).

4.3.2 Processing technique

The main purpose of the modelling is to understand the partitioning and distribution of seismicity. For this, we distinguish two classes of earthquakes: (a) Earthquakes that occur off the main rift faults, on fractures and minor faults which are not explicitly modelled, and (b) Earthquakes that nucleate along the major rift faults. We use a different technique to interpret the two classes of events.

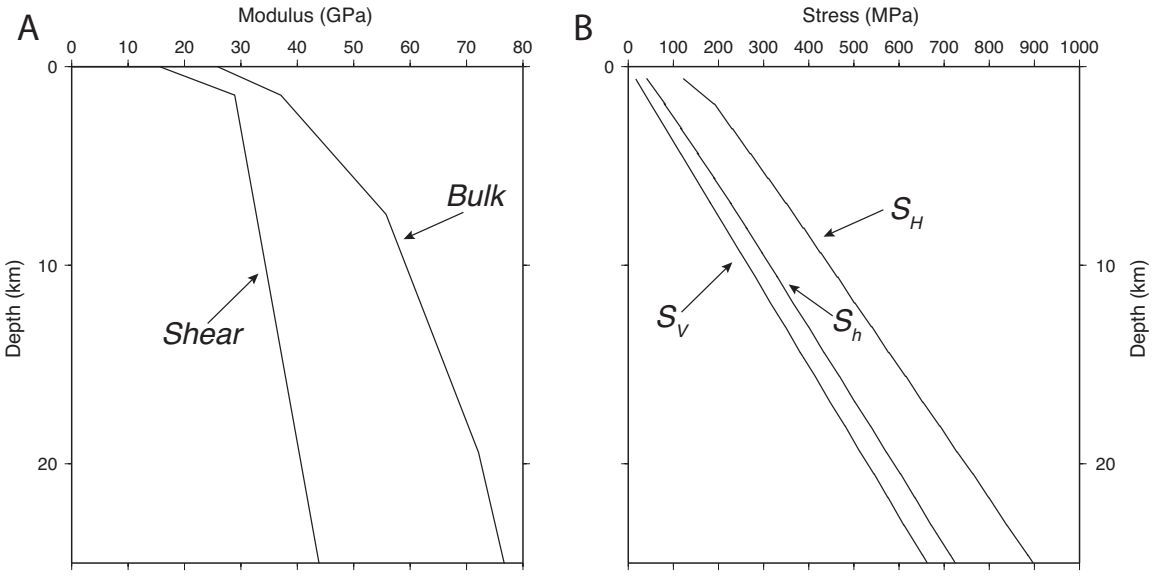

Figure 4.6: (A) Variation of bulk and shear modulus with depth at a region outside of the impact structure, as computed from the 1-D velocity model in the Saguenay region of Somerville *et al.* (1990). (B) Final stress profile in region outside on the crater resulting from boundary displacements. S_H, S_h, and S_V refer to the maximum horizontal-, minimum horizontal-, and vertical-stresses, respectively.

Earthquakes off the rift faults Events located away from the rift faults constitute the bulk of the low-level background seismicity that is observed in the CSZ, which are interpreted to cluster within fractured volumes bounded by the rift faults. Because the faults associated with these events are not explicitly included in the models, their stability must be inferred using alternative means. One of the main influences on the stability of damaged zones is the level of differential stress ($\sigma_1 - \sigma_3$). However, there are many other important factors, such as the presence of pre-exiting faults and fractures, or the brittle strength of rocks that also play an important role.

Given that large impact structures are typically aseismic (Solomon & Duxbury, 1987), we make the assumption that much of the seismicity that occurs off the main rift faults is due to the influence these faults have on the state of stress in the crater and surrounding rock. Therefore, by isolating the effect that weak rift faults have on the state of stress in the vicinity of the crater, we can make some inferences on the state of stability. To achieve this we follow the technique of Baird *et al.* (2009). For each model tested we compute differential stress in each discretized zone for two cases: (1) with the rift faults at a weak frictional strength (S_{Weak}) and (2) with rift faults locked (S_{Locked}). The second case, with the faults locked, is equivalent to removing the faults from the model, and the resulting state of stress is assumed to be compatible with an aseismic impact structure. The influence of the weak rift faults on the state of differential stress can then be computed for each discretized zone by using the following equation:

$$\frac{S_{Weak} - S_{Locked}}{S_{Locked}} \tag{4.1}$$

which expresses the change in differential stress in terms of a percentage. Regions where this value is positive correspond to regions of increased deviatoric stress relative to an assumed aseismic model, and thus indicate an increased potential for earthquakes to occur.

Earthquakes on the rift faults Since the large-scale rift faults are modelled explicitly, we can infer the fault stability simply by monitoring slip activity as the background differential stress is built up though boundary displacements. The build up of the stress in the model is done over 10,000 computational time-steps (not linked to true time). To monitor temporal changes in slip activity a 100 step interval is arbitrarily choosen to represent a "small" amount of time. Relative slip displacement accumulated over the interval is then calculated for each fault grid-point and plotted as a vector field indicating both magnitude and direction of slip of the hanging wall relative to a stable footwall. By viewing these vector fields in sequence, slip activity in the model can be observed.

4.4 Results

4.4.1 Seismicity off the rift faults

To analyze the stress models for seismicity off the main faults, the data is processed to calculate the increase in deviatoric stress caused by weak rift faults as defined in

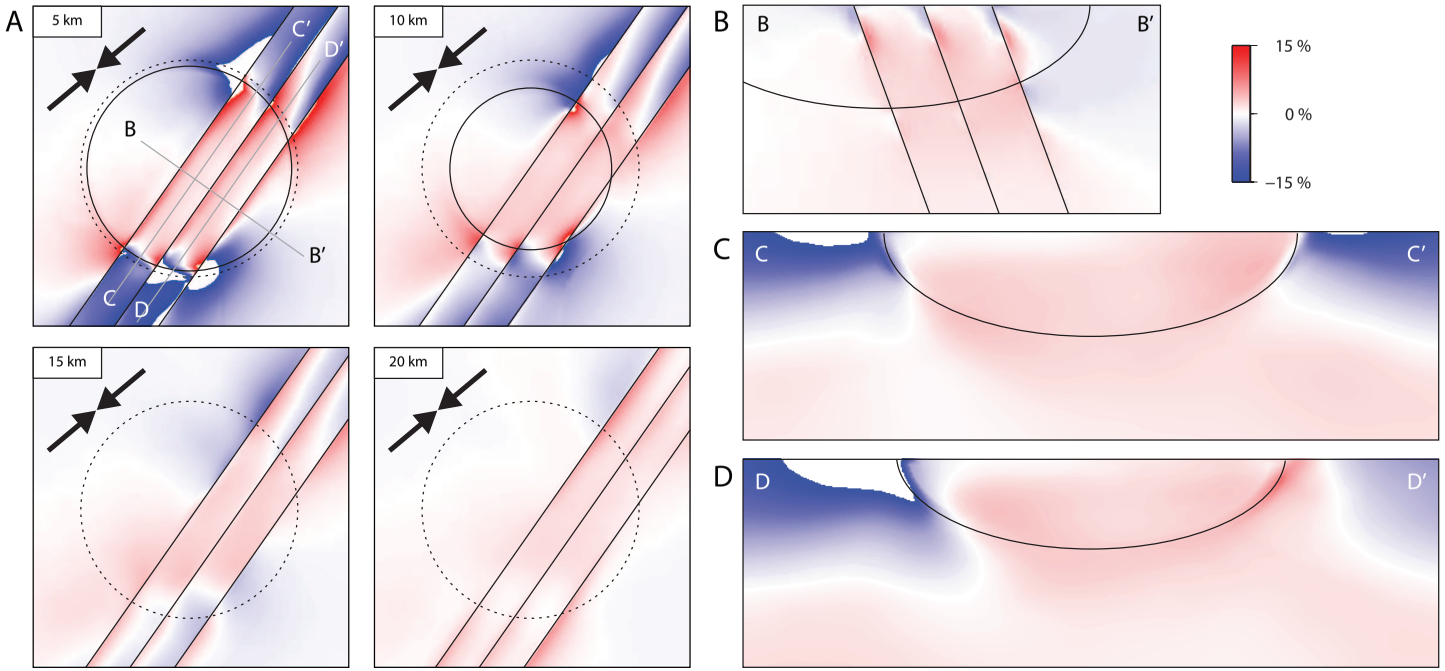

Figure 4.7: Sectional contour plots showing changes in deviatoric stress using equation 4.1 for a model with $M_C = 1/4M_B$, a fault strength of 5°, and an applied regional S_H orientation of 050°. (A) A series of horizontal depth-sections. (B) A cross-section through the centre of the crater oriented perpendicular to the rift strike. (C and D) Cross-sections parallel to rift strike, located between the northern and central fault (C), and between the central and southern fault (D).

equation 4.1. Using this definition, positive values are expected to indicate regions where seismicity is promoted, particularly in areas where pre-existing faults and fractures occur, such as in the crater and rift. Figure 4.7 shows a series of sectional contour plots of this value, showing its 3-D distribution through a model with $M_C = 1/4M_B$, a fault strength of 5°, and an applied regional orientation of S_H of N050° as inferred from borehole measurements (Heidbach *et al.*, 2008).

At the shallower levels within the depth range of the crater (5 km and 10 km, Figure 4.7A), there is a clear increase in stress in the region of the crater bounded by the rift faults, which corresponds to the general pattern of background seismicity observed in the CSZ (Figure 4.2A). At deeper levels (15 km and 20 km) a similar pattern exists, although not as prominent as at shallow depths. Cross-sectional views, both across and along strike (Figures 4.7B–D) show a pattern of increased stress concentrations between the rift faults, both within and beneath the crater, which match the general pattern of seismicity observed in the CSZ (Figure 4.2).

To understand the reason for these stress concentrations, the effect of the relevant structures on the flow of regional stresses must be examined. When the crater is considered on its own, without the influence of the rift, the stress field tends to flow around the structure (Figure 4.8A). This leaves the mechanically weaker material in the interior of the crater at a lower state of stress, thus diminishing the probability of earthquakes. When weak rift faults are also included in the model (Figure 4.8B), the largest effect is a local rotation of S_H such that it becomes more parallel to the faults. While the effect of the re-orientation is subtle ($< 15°$ rotation), it does disrupt the flow of stress around the crater such that higher stress concentrations form in the interior of the crater between the rift faults. In cross-section the

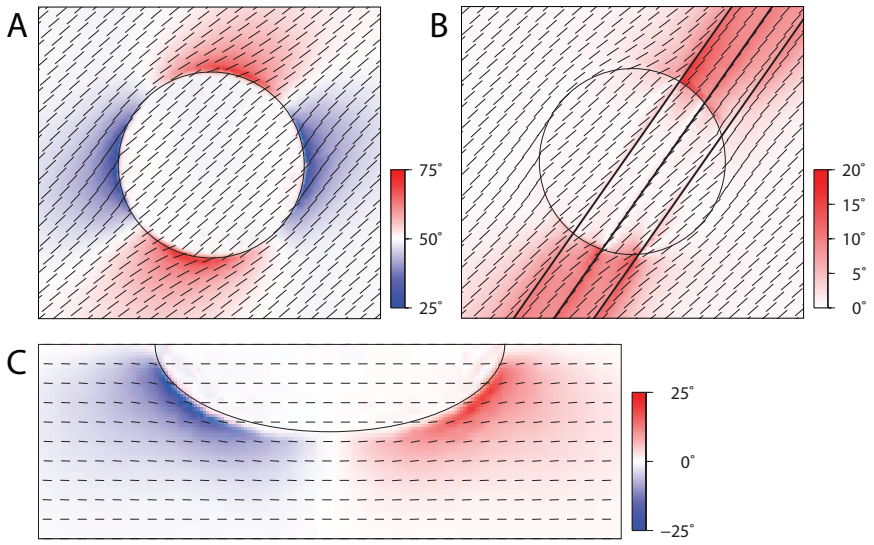

Figure 4.8: (A) S_H orientation for stress applied to a crater with modulus 1/4 of the background at a depth of 5 km. Applied loading at 50°. (B) Same model as (A) but with weak (5°) frictional faults included, contour plot indicates amount of rotation of S_H relative to locked fault model shown in (A). (C) NW-SE vertical cross-section, showing the flow of stress beneath the crater.

stress field also flows beneath the crater, thus resulting in a higher concentration in this area as well (Figure 4.8C).

The general pattern of stress partitioning is very similar to the main findings from Baird *et al.* (2009). However, the 3-D models reveal some additional details observed in the CSZ that were not found in the 2-D models. One of the notable details of the seismicity distribution is an extension of the active zone along the rift to the northeast of the crater, while there is minimal background seismicity to the southwest (Figure 4.2). A similar pattern of increased stress to the northeast of the crater is observed in the model, most clearly at the 10 and 15 km depth sections (Figure 4.7A) and also in the cross-sections along fault strike (Figure 4.7C). This effect is mainly a consequence of the asymmetry imposed on the system by

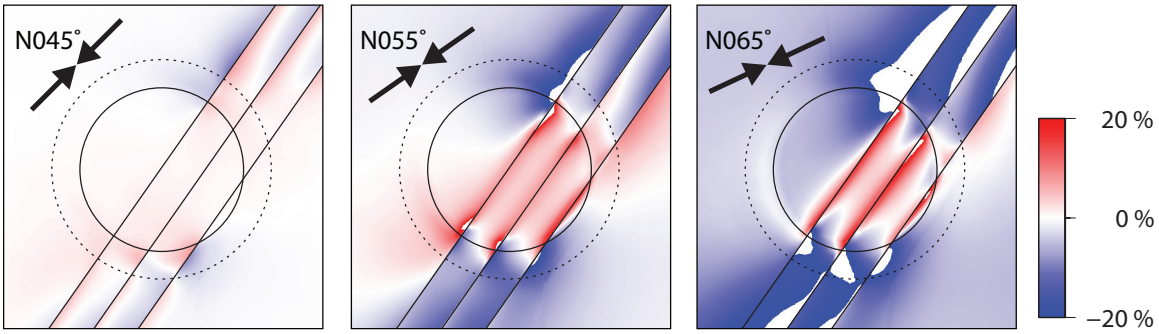

Figure 4.9: Contour plots of change in deviatoric stress, showing the effect of varying the applied stress orientation.

the inclination of the applied stress field orientation relative to the rift fault orientation. This is illustrated in Figure 4.9 where the stress concentration is plotted for models with applied loading at N045°, N055°, and N065° (equal to a 10°, 20° and 30° clockwise rotation from the strike of the rift). When the applied stress is at low angles to the rift, the region of increased stress extends out of the crater the most, however, the magnitude of stress concentration is low. At higher angles the extension out of the crater is reduced, but stress concentration inside the crater increases. An applied stress orientation of N050° as shown in Figure 4.7 forms a pattern which best matches the observed seismicity, and is consistent with the inferred orientation of S_H from borehole breakout measurements (Heidbach *et al.*, 2008).

4.4.2 Seismicity on the rift faults

To analyze seismicity localized on the rift faults, the slip activity is monitored as stresses are progressively built up through boundary displacements. While this is not strictly equivalent to the build-up of tectonic stresses, it can be used to make

some inferences of the relative stability of different portions of the faults. The behaviour is best observed by viewing the animations provided in the supplementary material[1]. Figure 4.10 shows a vector field of the hanging wall shear displacement relative to a stable footwall for: (A) All three faults at one snapshot of time during the progressive boundary displacement and (B) a closeup of the northern fault at the northeastern side of the crater before (top), during (middle) and after (bottom) the activity shown in part (A). At early times the stress field is effectively lithostatic and there is little motion along the faults. As differential stress is built up, the induced strain begins to be accommodated by fault slip, with most initial activity localized near the surface gradually migrating deeper. The sense of slip is a combination of thrust and dextral strike-slip. Although the locations of activity vary over time, over the course of the progressive loading slip on the faults outside of the crater is approximately evenly distributed. Inside the crater, the amount of slip is noticeably lower, and occasionally slip is accentuated just outside the crater (Figure 4.10A and B middle), to the northeast in particular, and to a lesser degree to the southwest. After these large slip events the activity returns to its background level.

The slip partitioning along the rift faults appears to be largely the consequence of the modulus contrast between the crater and the surrounding rock. The rift faults represent a large-scale regional weak zone within a relatively strong crust. As a consequence of this, much of the far-field strain is accommodated by concentrated deformation along the rift. Along most of its extent the rift is surrounded

[1]Animations are available online through the Qspace website: `https://qspace.library.queensu.ca/handle/1974/799`

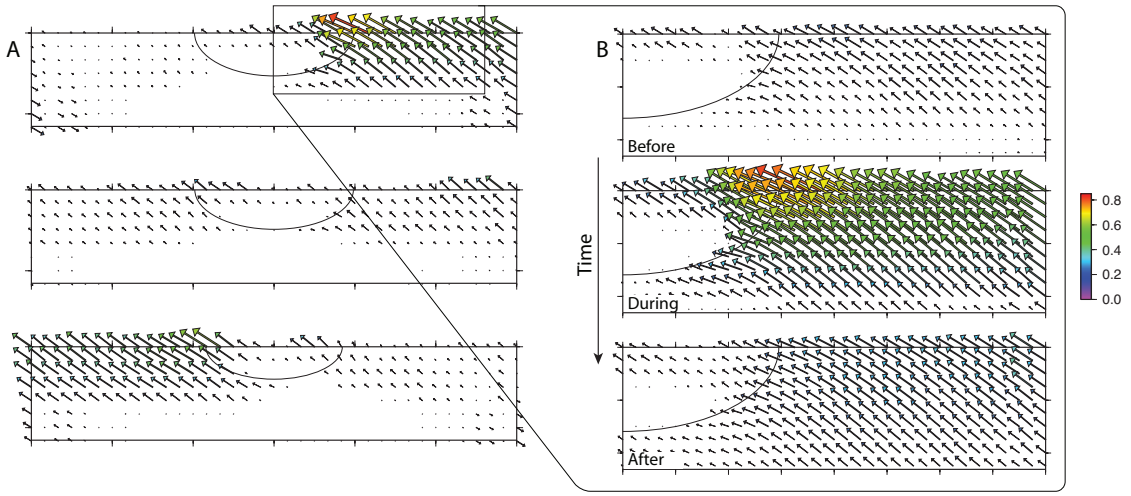

Figure 4.10: Vector plot showing relative shear displacement of the hanging wall of the rift faults. (A) The northern (top) middle and southern (bottom) faults during one of the pulses of activity just outside the crater. (B) A close-up along the north-eastern portion of the north rift fault before, during and after a pulse event. Animations of the behaviour are available online at `https://qspace.library.queensu.ca/handle/1974/799`

by relatively stiff rocks, favouring slip along the discrete bounding faults. Where the rift passes through the crater there is a noticeable decrease in slip activity along the faults, however there is a corresponding increase of stress within the crater as a result of its interaction with the weak rift faults (Figure 4.7). This suggests that the decrease of fault slip is simply due to the transition from strain accommodation by discrete fault slip along the rift boundary faults to accommodation by bulk deformation of the interior rock where the rift passes through the damaged impact zone. The periodic large slip activity just outside the crater boundaries appears to be resulting from the build up of shear stress on these faults due to the flow of stress around the crater (Figure 4.8).

4.4.3 Stress and focal mechanisms

Perhaps the most puzzling aspect of the CSZ is the apparent inconsistencies in the inferred orientation of stress. Focal mechanism based stress inversions suggest that stress is directed parallel to the rift in the NW cluster of events, while oriented strongly oblique to the rift in the SE cluster (Figure 4.4) (Mazzotti & Townend, 2010). Most available stress information is derived from focal mechanisms of events from within the seismic zone, therefore for comparison purposes, modelled principal stress orientations from the approximate dimensions of the seismic zone are plotted in Figure 4.11A. It shows stress orientations from all gridpoints between the rift faults for depths shallower than 15 km between the southwest boundary of the crater, to 30 km past the northeast boundary of the crater (Figure 4.11B). The data show an orientation of S_H very similar to the applied loading directions, but with a minor counterclockwise rotation of a few degrees. The small rotation is due to the weak rift faults, which locally reorient stress as shown in Figure 4.8. This matches the inferred S_H orientation from the NW cluster of events, but is inconsistent with the SE cluster, which shows a strong ($\sim$45°) clockwise rotation (Figure 4.4)(Mazzotti & Townend, 2010).

Modelled focal mechanism parameters for events on the rift faults are computed using the fault geometry and slip vector data. Figure 4.11C shows a contour plot of the modelled P, T and B axes in a lower hemisphere projection. The most notable characteristic of this is the large ($\sim$35°) clockwise rotation of the P-axes orientation relative to the direction of loading. The mechanism is similar in style to some of the large earthquakes observed in the CSZ, although the natural events

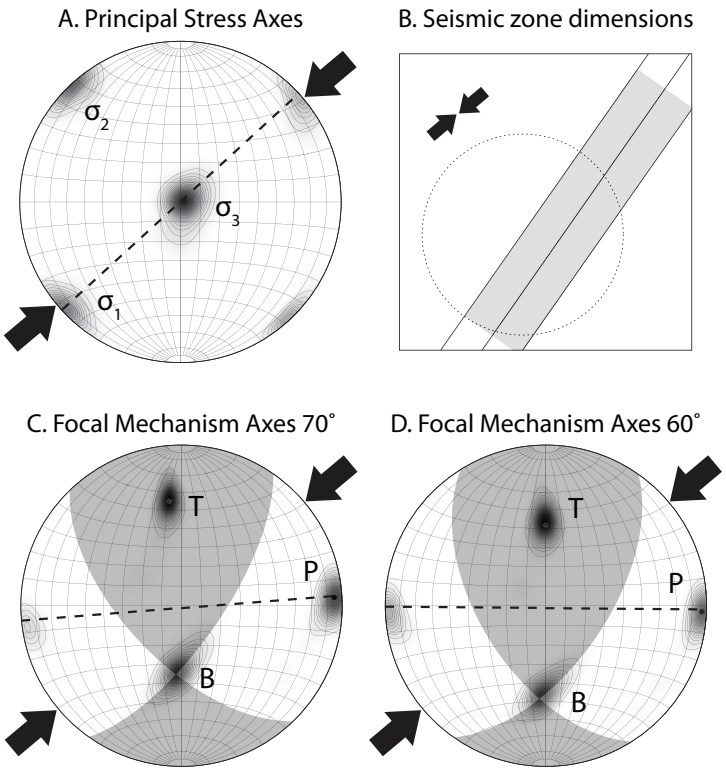

Figure 4.11: (A) Lower hemisphere stereonet contour plot of the principal stress orientations computed in the model within the upper 15 km of the region defined in (B). (C) The P, T, and B focal mechanism axes calculated using rift-fault slip vectors, with overlaid best fit focal mechanism solution for rift faults dipping at 70°, and (D) best fit focal mechanism for faults dipping at 60°. Large black arrows indicated the direction of loading applied to the model.

typically have a larger thrust component. Figure 4.11D shows the resulting average mechanism if the fault dip is lowered to 60°. This results in further rotation of the P-axis as well as a larger thrust component to slip providing a better match to the observed large events. It is likely that some variation of fault dip with depth (i.e. listric faults) could account for some variability in the style of mechanisms.

4.5 Discussion

The models are able to reproduce many of the observed characteristics of the CSZ. The region of increased deviatoric stress between the rift faults in the models shows a remarkably similar pattern to the observed background seismicity (Figure 4.7), including details such as the extension of seismicity to the NE of the crater, which only occurs when the applied boundary conditions are close the regional orientation of S_H as inferred by borehole data. The comparatively soft impact crater is shown to influence the stability of the rift faults intersecting it as it responds to regional strain from far-field boundary displacements (Figure 4.8). Rift fault slip is significantly reduced within the crater, where strain accommodation due to bulk deformation is preferred (Figure 4.10). However, just outside the boundaries of the crater slip is locally promoted (Figure 4.10B); this corresponds spatially to the regions of large events observed in the CSZ (Figure 4.2). Additionally, the sense of slip along the faults implies a significantly rotated P-axis compared to the applied regional stress (Figures 4.11C and D), which is similar in style to the focal mechanisms of large events at the CSZ (Figure 4.4).

Although the models do address the apparent stress field rotation observed when considering only large events, they do not adequately explain the difference in S_H orientation between the two rift parallel clusters of seismicity (Figure 4.4)(Mazzotti & Townend, 2010). These stress orientations were calculated by a formal stress inversion technique using both large and small events. The main simplifications made to the structures in the model, however, may provide some insight into the difference between the model results and observations. The three

large rift faults are the only true failure planes included in the models. All other material is represented by an isotropic continuum. The impact crater in reality is a complex faulted structure, which is simulated by representing the damaged zone as a continuum with reduced elastic properties. However, in doing so, much of the complexity is removed. The reduced elastic modulus representation is likely most valid in the central portion of the crater, which is characterized by a wide scattering of fracture orientations (Lemieux *et al.*, 2003). In the outer portion of the crater, fault geometry is dominated by a ring graben structure, such that the prominent fault orientation is roughly parallel to the boundary (Rondot, 1994). Mechanisms from the NW cluster yielded a S_H orientation roughly parallel to the regional field. This is encouraging, as this cluster runs through the centre of the crater, where the isotropic representation is likely more valid given the scattered orientation of fractures. The SE cluster, however, yielded a S_H orientation strongly oblique to the rift, similar to the P-axis orientation from large events (Mazzotti & Townend, 2010). It is notable that this cluster occurs near the southeast boundary of the crater, where crater faults are likely to be preferentially oriented NE-SW similar to the rift faults. Perhaps more importantly, a large number of the focal mechanisms in this cluster extend beneath the lower boundary of the crater, into the rifted crust below (Figure 4.4C). In the models the rift is represented as three discrete faults, with no structure in the rocks between them. In reality these rocks likely exhibit minor faulting in a similar style to the regional faults, and thus have a prominent NE-SW orientation. The rifted block beneath the crater is still affected by stress concentration due to the stress flow beneath the crater; however, by analogy with the larger events, much of the minor event focal mechanisms in this area would be expected

to reflect the local structure.

One troubling requirement of the models is that the regional rift faults must be very weak, as they are poorly oriented for reactivation in the regional stress field. This weakness can be due to an unusually low frictional strength (as was used in the model), a very large pore-fluid pressure, or by some combination of the two. While this is unusual it has been proposed as a possible explanation for the large thrust events in the CSZ (e.g. Zoback, 1992a; Du *et al.*, 2003). Lamontagne (1999) proposed a model for the CSZ in which the rift faults could act as a conduit for fluids under pressure, causing an inherent weakness. Regardless of the source of fault weakness, its effect in the models leads to the formation of patterns of stress and seismicity compatible with observations.

4.6 Implications

The suggestion that the St. Lawrence rift faults are inherently weak has broad implications for seismicity of the St. Lawrence as a whole. While monitoring slip along the modelled faults (Figure 4.10), it is noted that outside of the crater zone, slip is on average evenly distributed along the rift, with the exception of somewhat increased pulses of slip just outside the crater. At any one time, however, only small segments of the faults are active. It is difficult to ascertain the significance of this, given the limitations of the models, since the boundary conditions are not equivalent to tectonic strain. However, it can be speculated that slip activity along the St. Lawrence may migrate over time, in which case seismic hazard in currently quiescent areas may be underestimated. Seismic hazard maps based

on historical seismicity often contain 'bulls eyes' of high hazard around areas with recent large earthquakes (Stein, 2007). This may, however, be an artifact of the relatively brief seismic record. Current hazard maps published by the Geological Survey of Canada now employ a robust approach to hazard estimation, which uses both historic seismicity and recognized regional structures that allow for increased estimates between active seismic zones (Adams & Atkinson, 2003).

The models also help to clarify the unusually large range of focal mechanism patterns observed in the CSZ. In particular, the models highlight a possible scale dependence between large and small events, which has broad implications for interpreting focal mechanisms at regional scales, particularly in intraplate settings. The models indicate that while stress tensors show little deviation from the applied orientation of S_H, focal mechanisms computed from slip along the weak rift faults produce a P-axis at high angles to the applied stress (Figure 4.11). Restricting focal mechanisms to only those that occur along the rift faults would therefore result in a misleading estimate of S_H orientation. It is argued that by restricting their dataset to only moderate and large earthquakes, the regional focal mechanism studies of Zoback (1992a) and Du *et al.* (2003) introduced a structural bias to events occurring along larger-scale faults, resulting in a substantial apparent stress rotation along the St. Lawrence river ($\sim$60–90°, Figure 4.1). Studies that incorporate smaller magnitude focal mechanisms (e.g. Adams & Bell, 1991; Mazzotti & Townend, 2010) include events that occur on more variably oriented minor faults. These generally result in stress orientation estimates closer to the regional field, but still with a significant clockwise rotation ($\sim$30–45°). The detailed stress inversion results from within the CSZ of Mazzotti & Townend (2010) showed that

mechanisms from the NW cluster of events yielded a S_H approximately parallel to the regional field. Many of the events in this cluster are located within the central portion of the impact crater (Figure 4.4a,c). This is notable because the central part of the crater is the region of most intense impact related faulting and fracturing (Rondot, 1994; Lemieux *et al.*, 2003), resulting in a variably oriented collection of potential failure planes. Results of the models also suggest that the interior of the crater is a region of reduced rift fault slip (Figure 4.10). The large availability of failure planes as well as the reduced rift fault slip suggest that focal mechanisms in this region would be amongst those least biased by the geometry of the St. Lawrence rift, and thus provide the best local stress field estimates.

The large structural geometric bias in focal mechanisms in the St. Lawrence valley lies in marked contrast to many stress inversion results from California and Japan, which are typically consistent with borehole derived stress estimates (Townend & Zoback, 2001, 2006). The contrast, however, may be due to a fundamental difference between the seismicity of tectonically active regions versus continental interiors. Since a single stress tensor is capable of reactivating faults in a variety of orientations (McKenzie, 1969), stress inversion techniques generally rely on sampling events from many variably oriented structures in a small geometric area to constrain a single stress tensor compatible with all derived slip directions (e.g. Gephart & Forsyth, 1984; Arnold & Townend, 2007). Tectonically active areas surrounding plate boundaries are characterized by broad deformation at relatively high strain rates; consequently the conditions necessary for stress inversion are easily met and cover large areas. The seismically active faults are also typically geologically young features which formed in the current tectonic regime, and there-

fore, would be expected to be favourably oriented for reactivation and produce good stress inversions. The conditions in intraplate seismic zones, however, are considerably different. Structures in continental interiors are characterized by significantly lower strain rates than those in tectonically active areas. Inevitably most intraplate regions produce an inadequate number of events to carry out a stress inversion. The few areas where there are sufficient seismic events are often associated with prominent pre-existing weak structure (e.g. a rift zone or aulacogen) which formed in a different tectonic regime than what exists today. Under these conditions it is possible that the most prominent structures (i.e the St. Lawrence rift) are poorly oriented for reactivation, although they may be the largest source of weakness.

The discrepancy between the focal mechanisms from the rift faults and the regional stress orientation is similar in many respects to plate boundary-related mechanisms in tectonically active areas. Plate boundaries, as opposed to the broad deformation zone around them, are characterized by a preferred orientation of faults with low frictional strength, which can be reactivated under very poorly oriented stress conditions. The archetypal example of this is the plate boundary strike-slip San Andreas fault in California. Here the orientation of S_H in the surrounding crust, as inferred from both borehole measurements and focal mechanism stress inversion is nearly perpendicular to the fault (e.g. Zoback *et al.*, 1987; Townend, 2006). The influence of the plate boundary geometry dominates the overall kinematics, such that the focal mechanisms from slip along the fault gives misleading results. Consequently, focal mechanisms which are thought to be possible plate boundary events are flagged as such in the World Stress Map database,

and are omitted by default from stress maps (Barth *et al.*, 2008). Away from the plate boundary, faults are more varied in orientations such that stress inversion produces acceptable results. If similar behaviour affects the St. Lawrence, it implies that mechanisms within the rift zones with nodal planes consistent with slip along the fault should be treated as suspect.

The apparent inherent weakness of the St. Lawrence rift raises the question as to whether similar behaviour should be expected in other intraplate seismic zones. Johnston (1993) noted that there is a global correlation between intraplate seismicity and regions of crustal extension, with about two thirds of events occurring within them. This correlation is particularly evident in eastern North America where most of the $\mathbf{M} > 6$ events have occurred within the Atlantic and Iapetan rift basins, rifted margin, and aulocagens (Mazzotti, 2007). This correlation is also reflected in the background seismicity (Figure 4.1). However, unlike the St. Lawrence rift, most events along these other rift structures produce focal mechanisms broadly consistent with the regional stress field (Zoback, 1992a; Du *et al.*, 2003). This consistency may be partially due to arrangement of structural orientation relative to the stress field. In eastern Canada, for example, besides the CSZ and Lower St. Lawrence which lie along the NE trending St. Lawrence rift, many of the seismic zones lie along NW-SE oriented structures, such as the Ottawa and Saguenay grabens (Figure 4.1). These structures are approximately perpendicular to the regional orientation of S_H and therefore are optimally oriented to reactivate in the thrust sense, which is prominent in eastern Canada. In the eastern United States paleotectonic rift structures are prominently oriented NE–SW, similar to that of the St. Lawrence. The transition south is also marked by some changes in the regional

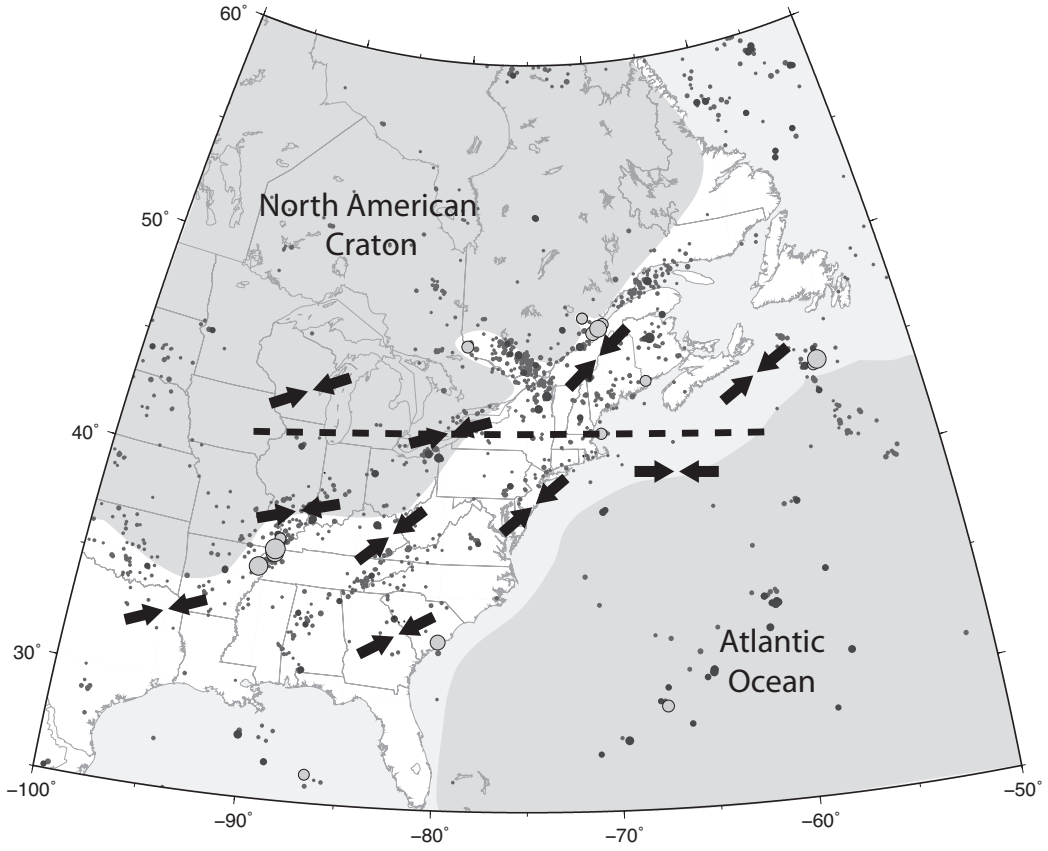

Figure 4.12: Seismicity and simplified stress map of eastern North America. Background seismicity since 1973 is shown by dark grey ($M \geq 3$) and black ($M \geq 4.5$) circles. Historical large earthquakes (mostly $M \geq 6.0$) are shown by large grey circles. Grey shaded area indicates the low seismicity regions of the North American craton and the Atlantic Ocean (modified from Mazzotti, 2007). Inverted arrows show a generalized variation of S_H orientation based on data from the World Stress Map (Heidbach *et al.*, 2008). Dashed line indicates transition in earthquake focal mechanism style from predominately thrust in the North to predominately strike-slip to the south. Seismicity data are from the Geological Survey of Canada and United States Geological Survey catalogues, historic Canadian events are from Lamontagne *et al.* (2007).

stress field, including a slight clockwise rotation in S_H to ENE-WSW in the eastern central United States, and perhaps more importantly a transition from prominently thrust regime in Canada to strike-slip in the United States (Figure 4.12). The result is that the stress field is oriented at an acute angle to the major rift faults, which is more favourably oriented for reactivation in a strike-slip sense. The implication is that the apparent consistency between the S_H orientation and P-axes may be due to a serendipitous arrangement of weak structures in the stress field that is optimally oriented for fault slip.

4.7 Conclusions

The results of the 3-D stress models of the CSZ agree well with the main findings of the previously published 2-D models (Baird *et al.*, 2009). Much of the background seismicity patterns can be explained by the intersection of weak faults of the St. Lawrence rift with the damage zone created by the Charlevoix impact. The weak faults modify the flow of stress around the crater resulting in a stress concentration in the volume between the rift faults within and beneath the crater. In addition to matching broad patterns in seismicity, the 3-D models are able to explain subtle details in the seismicity distribution including the extension of background events to the NE of the crater. The best matching patterns from the models occur when the applied stress field is oriented parallel to the regional field as inferred from borehole breakout data. This suggests that there is no significant local source of stress driving the seismicity; however, to achieve the best calibration, the modelling results require that the rift faults be inherently weak.

Modelled slip distribution along the main rift faults in response to boundary displacements shows that while slip is distributed throughout the rift, it is locally diminished inside the crater and locally enhanced just outside its boundaries. The area of enhanced slip agrees well with the location of large earthquakes just outside the boundary of the crater. Analysis of the slip vectors of events on the rift fault reveals an inferred P-axis strongly oblique to the regional orientation of S_H, and broadly matching the style of large event focal mechanisms.

The models suggest that the inherent weakness of the St. Lawrence rift may be producing a systematic rotation of focal mechanisms P-axes relative to the surrounding orientation of S_H. The effect appears to have a greater influence on large events, which preferentially occur along the regional faults, suggesting that small events may provide better indications of the true local state of stress. It is speculated that similar behaviour may be expected in other seismically active intraplate rift zones, highlighting a potential caveat for the use of focal mechanisms for stress field estimation in intraplate settings.

4.8 Acknowledgements

We thank Stéphane Mazzotti for providing us with an early version of his manuscript as well as a compilation of focal mechanism parameters. Financial support for this work was provided by the Ontario Reseach and Development Challenge Fund, Natural Sciences and Engineering Research Council of Canada Discovery Grants to Steve McKinnon and Laurent Godin, and by an Ontario Graduate Scholarship in Science and Technology to Alan Baird.

Chapter 5

Discussion and conclusions

5.1 Introduction

Research presented in the preceding chapters explores the relationship between ancient lithospheric structures and the present-day tectonic stress field through the use of geomechanical models to better understand the structural controls for intraplate seismicity. While the work deals specifically with the areas of southern Ontario and Charlevoix Québec, the results have potential implications for other intraplate seismic zones. In this chapter the concepts and relationships explored in the previous chapters are used to discuss possible controls on the seismicity of another area, the Eastern Tennessee seismic zone. Using this latter site, along with southern Ontario and Charlevoix regions, a generalized model of eastern North American intraplate seismicity is proposed.

5.2 The eastern Tennessee seismic zone

The eastern Tennessee seismic zone (ETSZ) forms a pronounced NE-SW oriented ~300 km by 50 km trend of seismicity located in the southern Appalachian region of the United States, mainly in eastern Tennessee, northwestern Georgia, and northeastern Alabama (Figure 5.1) (Johnston *et al.*, 1985; Bollinger *et al.*, 1991). More diffuse seismicity surrounding the zone also extends into eastern North Carolina, southwestern Virginia, and southeastern Kentucky. The zone constitutes the third highest concentration of seismicity in eastern North America, following the New Madrid seismic zone in the eastern-central United States, and the Charlevoix area in eastern Canada (Powell *et al.*, 1994). Unlike these other seismic zones, however, most events in the ETSZ are of relatively low magnitude, the largest being the **M** 4.6 earthquake, which occurred April 29, 2003 near Fort Payne Alabama (Figure 5.1).

The ETSZ is located mostly within the Valley and Ridge physiographic province of the southern Appalachians (Figure 5.1), which consists of Paleozoic sedimentary rocks within a foreland fold and thrust belt northwest of the Blue Ridge-Piedmont megathrust sheet indentor (Hatcher *et al.*, 2007). The fold and thrust sheets override Grenville-aged crystalline basement rock along a shallow subhorizontal detachment fault at approximately 5 km depth below the ETSZ (Cook & Vasudevan, 2006). The internal structure of the Grenville basement rock is difficult to ascertain as it is generally not seismically reflective (Nelson *et al.*, 1987; Cook & Vasudevan, 2006). Most of what is known about the basement structure has been inferred from magnetic and gravity data. Two large-scale magnetic lineaments related to base-

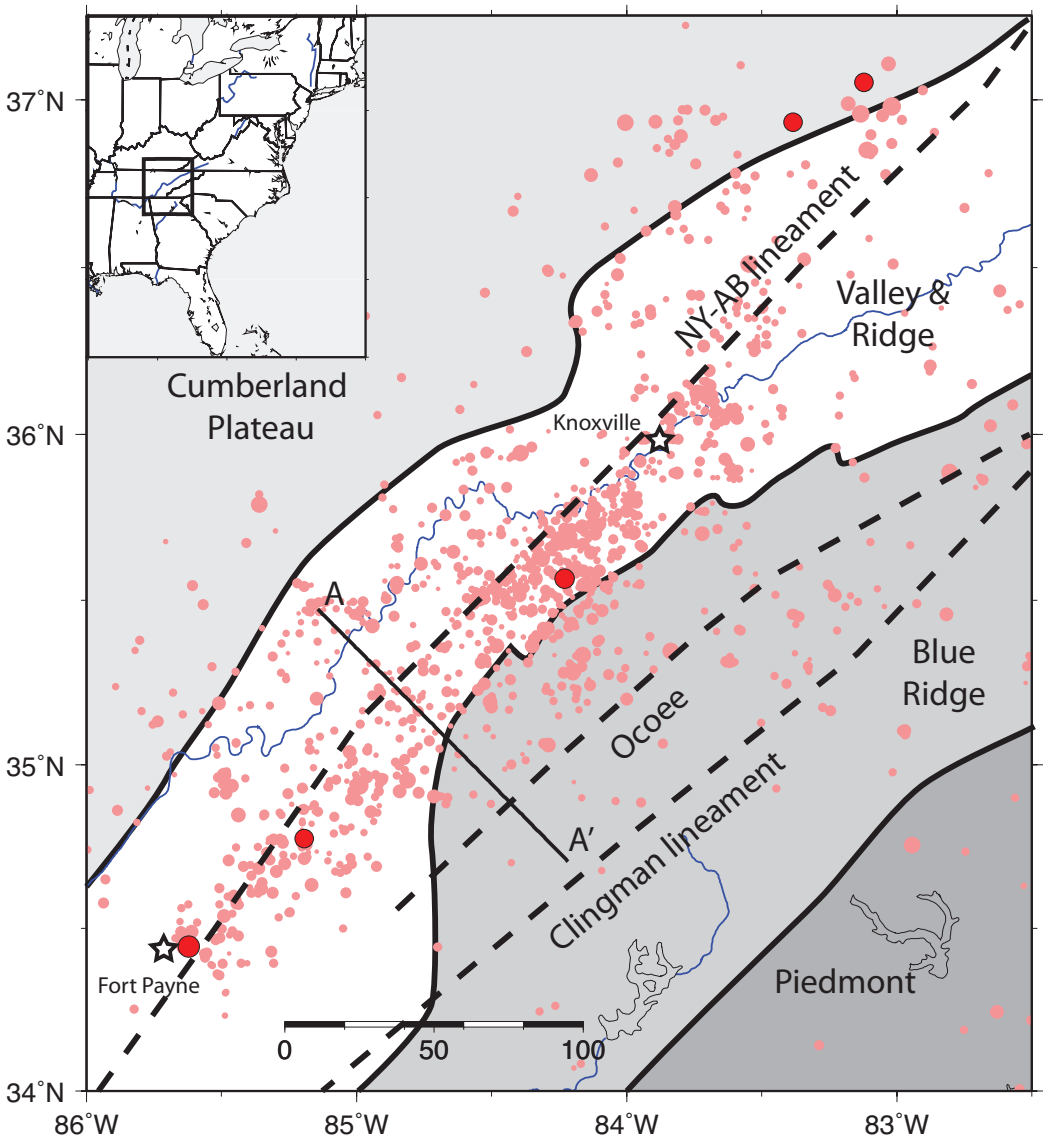

Figure 5.1: Seismicity and geology of the Eastern Tennessee seismic zone. Shades of grey indicate the extent of the major geologic provinces: Piedmont, Blue Ridge, Valley and Ridge, and Cumberland Plateau. Pink and red circles represent earthquake magnitudes of less than 4.0 and greater than 4.0, respectively. Dashed line indicates potential field lineaments (see Figure 5.2) (Johnston *et al.*, 1985). Line A–A′ refers to cross-section shown in Figure 5.3. Stars indicate locations of cities. Earthquake data from the United States Geological Survey for the period 1980-2009.

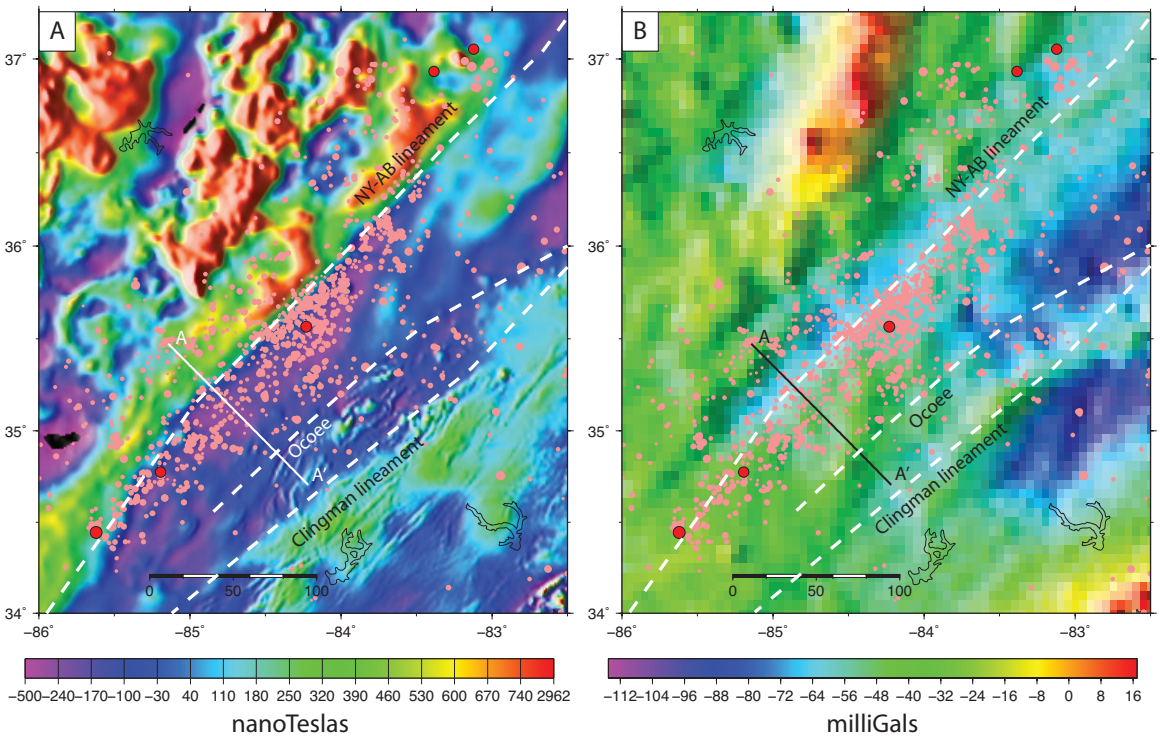

Figure 5.2: (A) Total magnetic intensity and (B) Bouguer gravity anomaly of the Eastern Tennessee seismic zone. Dashed lines indicate the New York-Alabama, Ocoee, and Climgman potential field lineaments (King & Zietz, 1978; Nelson & Zietz, 1983; Johnston *et al.*, 1985). Line A–A′ refers to cross-section shown in Figure 5.3. Magnetic data from NAMAG (2002). Gravity data from Kucks (1999).

ment structures run through the region. The prominent New York-Alabama (NY-AB) lineament (King & Zietz, 1978), which strikes NE-SW and spans ∼1600 km beneath much of the Appalachians in the eastern United States, and the somewhat less prominent Clingman lineament, which parallels the NY-AB to the east and spans ∼1000 km (Nelson & Zietz, 1983) (Figure 5.2). Both lineaments separate basement blocks of distinctly different magnetic signatures and are interpreted to be the result of major faults active during the Grenville orogeny (Nelson & Zietz, 1983; Hatcher *et al.*, 1987).

Most of the seismicity of the ETSZ occur at depths ranging from 5 to 26 km, be-

low the Appalachian décollement and within the Grenville basement (Figure 5.3) (Johnston *et al.*, 1985; Powell *et al.*, 1994; Vlahovic *et al.*, 1998); consequently the earthquake distribution has no clear association with the surface geology. Johnston *et al.* (1985) recognized a correlation between the boundaries of seismic zone and basement features. The NY-AB magnetic lineament has a strong spatial relationship with the western boundary of the seismic zone, separating highly seismogenic crust in the SE from more diffuse seismicity to the NW (Figures 5.2 and 5.3). The Ocoee magnetic lineament, a branch of the larger Clingman lineament lies roughly along the eastern boundary of the seismicity (Johnston *et al.*, 1985). It is speculated that these magnetic lineaments mark the boundaries of a crustal zone, referred to as the Ocoee block, which is relatively weak compared to the adjacent crust (Johnston *et al.*, 1985; Powell *et al.*, 1994).

While the general trend of the seismic zone appears to be controlled by major NE trending basement shear zones, the broad area over which the earthquakes are clustered is indicative of a more complex fault system. Focal mechanisms from within the ETSZ indicate primarily strike-slip displacement along steeply-dipping faults (Chapman *et al.*, 1997). Some mechanisms contain a NE-striking nodal plane, consistent with the overall shape of the seismic zone. Most mechanisms, however, imply either left-lateral slip along E-W faults, or right-lateral slip along N-S faults, suggesting a more complex fault system than what is implied by the magnetic lineaments (Johnston *et al.*, 1985; Powell *et al.*, 1994; Chapman *et al.*, 1997). Wheeler (1995) suggested that the most probable source of faulting would be from a buried rift zone, noting the tabular shape of the seismicity cluster and the similarity in seismicity to the Giles County seismic zone in Virginia that has been convincingly

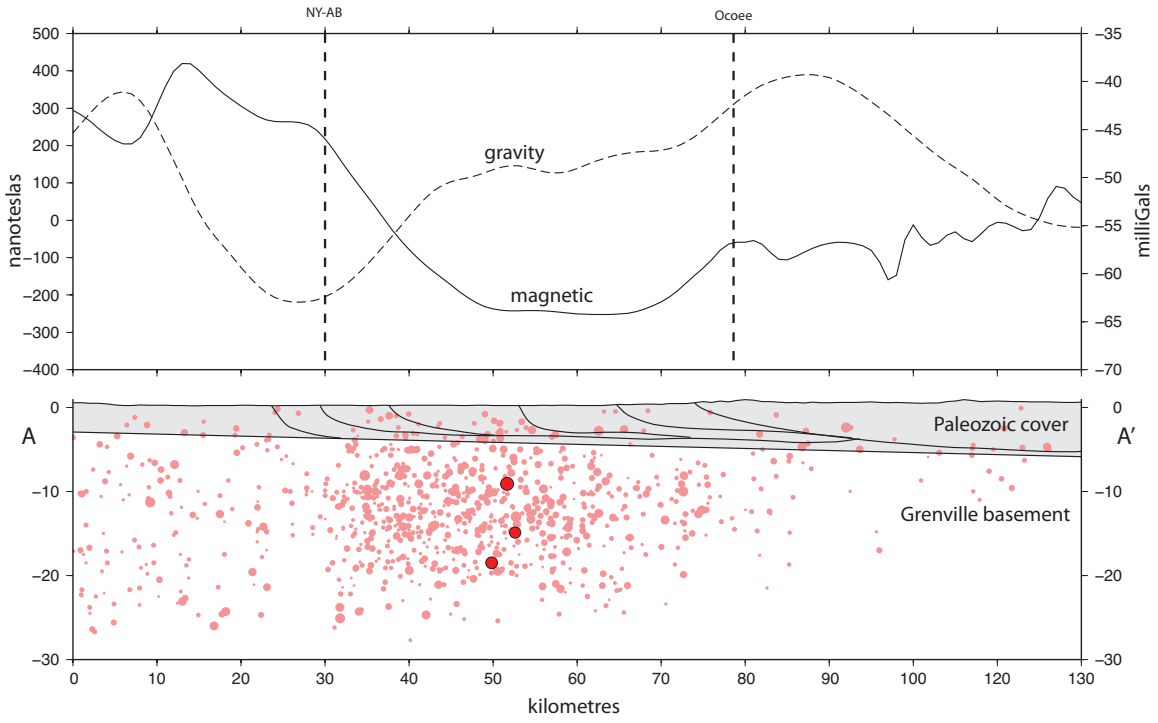

Figure 5.3: Cross-section through the Eastern Tennessee seismic zone showing magnetic and bouguer gravity anomalies (top) and seismicity (bottom). Location of cross-sections shown in Figures 5.1 and 5.2. Paleozoic fault interpretation after Johnston *et al.* (1985) and Hatcher *et al.* (2007). Pink and red circles represent earthquake magnitudes of less than 4.0 and greater than 4.0, respectively.

attributed to the reactivation of rifted faults (Bollinger & Wheeler, 1988). Powell *et al.* (1994) also speculated that the faults may have originated from Iapetan rifting, but suggested that they may have been modified by Paleozoic compression or Mesozoic extension to form a current configuration of predominantly E-W and N-S faults. They proposed that slip along the east and north striking planes may be coalescing into a through-going strike slip fault along the NY-AB lineament.

In an effort to ascertain seismogenic fault geometry, Chapman *et al.* (1997) carried out a statistical earthquake epicentre cluster analysis for the ETSZ. They found that epicentres clustered along preferred NE and E trends. On the basis of this they concluded that most seismicity in the ETSZ occurs on a series of E and NE striking faults. These general conclusions were supported by a subsequent hypocentre relocation study (Dunn & Chapman, 2006).

The stress field in the ETSZ is dominated by a NE-SW orientation of maximum horizontal compressive stress (S_H) as determined from borehole data (Heidbach *et al.*, 2008). This is roughly parallel to the orientation of the magnetic lineaments and is consistent with stress estimates inferred from focal mechanism data (Teague *et al.*, 1986; Chapman *et al.*, 1997; Mazzotti & Townend, 2010).

5.2.1 Comparison with southern Ontario

As discussed in greater detail in Chapter 2, the seismicity of the western Lake Ontario region lies primarily beneath the Paleozoic cover rocks in the Grenville basement. As a result of this, individual seismogenic features cannot be identified. Many authors, however, have noted an apparent correlation between trends of

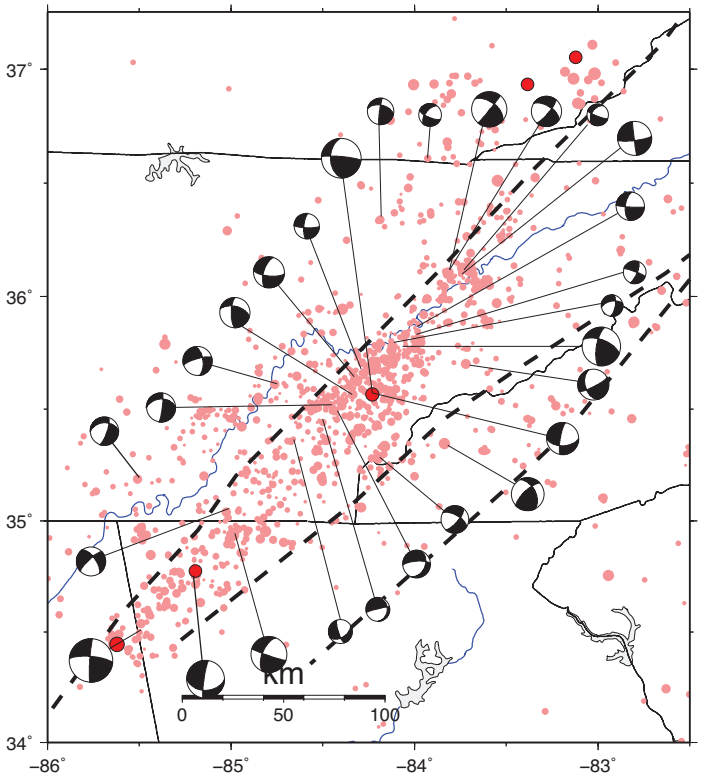

Figure 5.4: Focal mechanisms from the eastern Tennessee seismic zone scaled by earthquake magnitude (modified from Chapman *et al.*, 1997). Focal mechanism data compiled by Mazzotti & Townend (2010). Pink and red circles represent earthquake magnitudes of less than 4.0 and greater than 4.0, respectively.

seismicity and prominent magnetic lineaments associated with the southward continuation of major Grenville terrane boundaries beneath the Paleozoic cover (e.g. Wallach & Mohajer, 1990; Thomas *et al.*, 1993; Mohajer, 1993; Wallach *et al.*, 1998; Dineva *et al.*, 2004). The correlation implies that there is a preferred trend in brittle failure planes which is defined by the overall structural grain of the Grenville orogen. Ductile shear zones are in general not known to be seismogenic in other regions of the Grenville orogen. However, the localization of seismicity is notable in that it occurs along a major southward bend of the dominantly NE-SW striking orogen, suggesting that the local seismicity may simply be due to a more preferable orientation of brittle structures for reactivation with respect to the regional stress field. Analysis of stress data shows an apparent perturbation of the stress field in the region of western Lake Ontario, such that S_H orientations appear to mimic the structural grain of the Grenville basement rocks (Baird & McKinnon, 2007). The spatial correlation between the region of stress misalignment and the region of low-level background seismicity suggests a common root cause of both phenomena.

The greatest similarity between the ETSZ and western Lake Ontario is the association of seismicity with magnetic lineaments thought to be related to large scale basement shear zones beneath the overlying cover rock. The Ontario model relied on the assumption that the basement fabric defined by magnetic lineaments would control a preferred orientation for brittle features. The recognition of NE-SW alignments of epicentres suggests a similar mechanism may exist in the ETSZ (Chapman *et al.*, 1997). Both the NY-AB and Clingman lineaments extend for over 1000 km and underly a significant portion of the Appalachian fold and thrust-

belt of the eastern United States (Figure 5.5A). While the lineaments association with seismicity is most clearly demonstrated in the ETSZ, a correlation is observed over its entire length (King & Zietz, 1978). The correlation suggests that the lineaments may represent mechanically weak structures, or form the boundaries of weak basement blocks. Although it has been shown that Iapetan rifting does cross Grenville suture zones (Thomas, 2006), the alignment of the NY-AB lineament with the Birmingham and Rome Iapetan graben systems to the south and north of the ETSZ, respectively (Figure 5.5A), as well as the inferred faulting within the ETSZ suggests that the NY-AB lineament may have been a preferred site for rifting during breakup of Rodinia, further suggesting that it may represent a deep-rooted weak zone.

Another major feature of the southern Ontario model is a stress perturbation associated with the active portion of the Grenville fabric. Given the possibility that the NY-AB and Clingman lineaments may be related to a large-scale weakness zone, it raises the question as to whether they may be producing a similar perturbation. S_H orientations from the World Stress Map database for the eastern United States are plotted on Figure 5.5A. Over most of the length of the NY-AB and Clingman lineaments S_H is relatively consistently oriented NE-SW, sub-parallel to the strike of the lineaments. Possible relationships between stress field variations and geologic structures have been addressed in the past, however, these have focused primarily on surface geology rather than deeper basement structures. The consistency of the stress field orientation over much of the relatively sinuous trend of the Appalachians has been cited as evidence that Proterozoic orogenic belts do not significantly perturb regional stress fields (Evans, 1989; Zoback, 1992b). In contrast

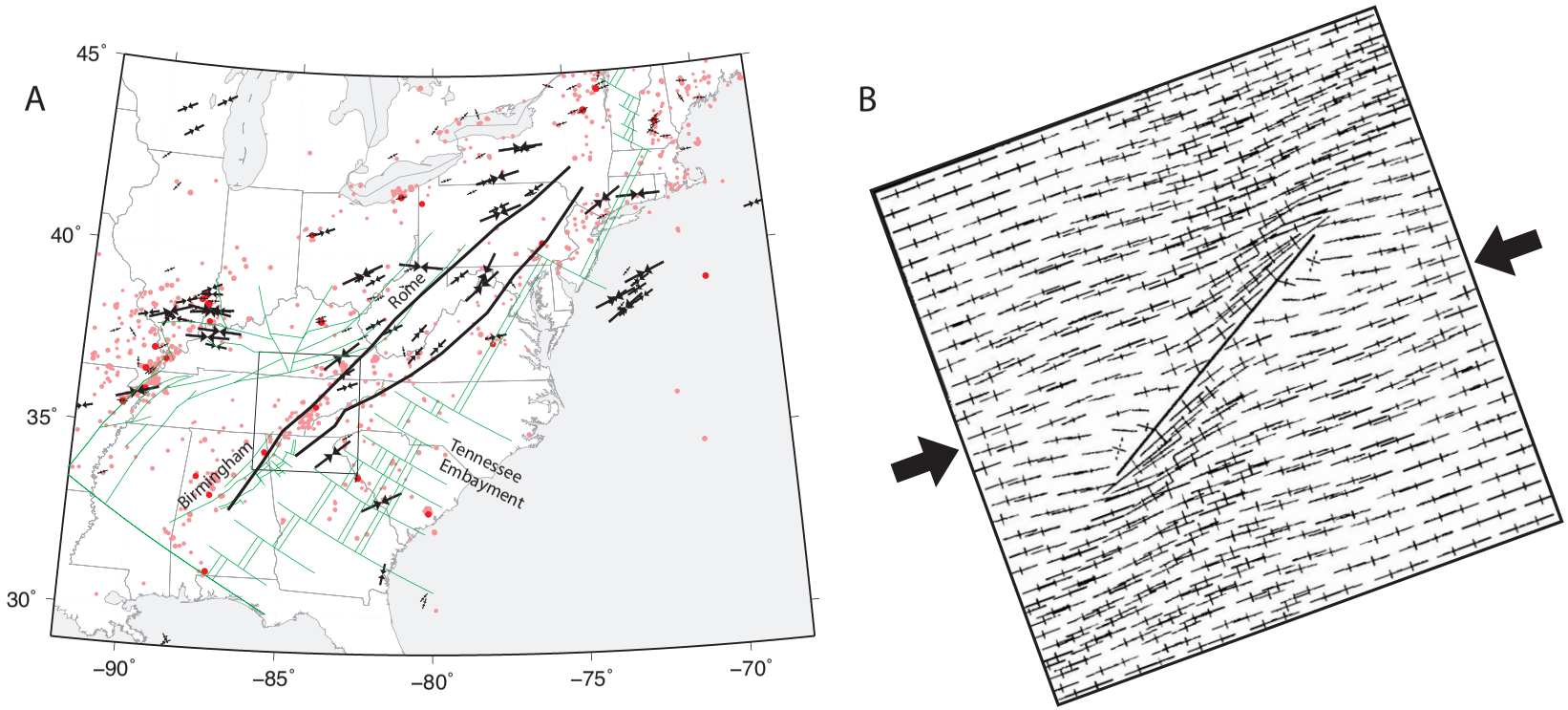

Figure 5.5: (A) Seismicity of the eastern United States relative to some major basement structures. Black lines indicate the NY-AB and Clingman magnetic lineaments, and green lines indicate Iapetan rift margin geometry and major Iapetan basement faults (Thomas, 1991). Inverted black arrows indicate the orientation of S_H inferred from borehole measurements (Heidbach *et al.*, 2008). (B) Modelled stress perturbations around a weak discontinuity (modified from Homberg *et al.*, 1997). Large black arrows indicate loading direction.

the underlying lineaments are relatively straight and consistently oriented NE-SW over their entire extent. Consequently, a basement-structure-influenced stress field might be expected to have little variation along its strike, although variation may be expected across strike since the influence of the weak structure on the stress field would diminish at greater distances. To the west of the lineaments in the central United States, stress measurements indicate a significant clockwise rotation in S_H (Figure 5.5A). While the ultimate cause of this stress rotation is unclear, the general pattern with respect to the NY-AB lineament is similar to what may be expected from the stress perturbation around a weak discontinuity (Figure 5.5B) (Homberg *et al.*, 1997). Thus a weak zone defined by the NY-AB and Clingman magnetic lineaments is consistent with the broad scale stress patterns.

5.2.2 Comparison with Charlevoix

The Charlevoix seismic zone constitutes a region of persistent low-level seismicity and repeated, though less frequent large events. The seismicity is clustered along a segment of the St. Lawrence rift which is overlapped by a meteorite impact crater, resulting in a locally complex structure. 2-D and 3-D stress models (presented in Chapters 3 and 4) were constructed to explore the interplay between the rift faults and impact structure within the regional tectonic stress field and were ultimately successful in reproducing many of the seismicity patterns and characteristics observed in the area. The models require that the St. Lawrence rift faults be inherently weak, such that they slip in response to regional stresses despite being poorly-oriented for reactivation. The regional scale fault slip forms a stress

perturbation along the rift that results in a local enhancement of stresses in the portion of the impact structure that is bounded by the rift faults, thus creating a tabular shaped cluster of background seismicity. Stress perturbations associated with stress flow around the impact structure in turn results in enhanced fault slip and localization of large events along the rift, at the periphery of the crater.

The juxtaposition of the impact structure and the rift in the CSZ creates an unusual structural setting unlikely to be found in other seismic zones. Nevertheless, there are a number of striking similarities between background seismicity patterns observed in the ETSZ and those in the CSZ suggesting similar controlling processes. The ETSZ, like the CSZ, is interpreted to cluster along regional scale structures defining a tabular zone of seismogenic crust which is bounded by regional faults. Focal mechanisms from each seismic zone suggest that background seismicity is distributed throughout a complex network of faults, rather than simply by faults parallel to the regional structure. Both regions lie within a local stress field with S_H oriented nearly parallel to the structural trend.

One notable difference between the seismic zones, however, is the degree of complexity indicated by the focal mechanism patterns. Mechanisms from the CSZ show a wide degree of scatter in nodal plane orientations indicating a very complex fracture network, which is to be expected for an impact structure. The ETSZ, in contrast, shows a considerably more ordered faulting network with dominant faults striking NE-SW and E-W. The E-W striking faults create the complexity in the ETSZ, analogous to the heavily-fractured impact structure in the CSZ. However, because the fault zone lies beneath the Appalachian fold and thrust belt, the source of the E-W striking faults cannot be clearly determined. One possibility,

as some have suggested (e.g. Powell *et al.*, 1994; Wheeler, 1995), is that the seismogenic fault network in the ETSZ is related to Iapetan rifting. If this is the case then the E-W faults may be a result of complexities in the rift geometry to the east of Tennessee. Reconstructions of the late Precambrian–early Paleozoic continental margin define a zigzag pattern of short rift segments offset by transform faults along the Tennessee embayment (Figure 5.5A) (Thomas, 1991). The E-W faults may simply be the result of inbord extensions of these transform faults active during the Iapetan rifting event, which may have subsequently been modified during later deformation events.

The focal mechanism patterns from the ETSZ imply that most of the events are slipping along the E-W trending faults. If this is the case, then the sharp truncation of activity at the western edge of the zone suggests that the structure defined by NY-AB lineament is controlling the stability of the faults. This behaviour is analogous to the abrupt breaks in the seismicity of the impact structure observed in the CSZ marked by the Gouffre North-West and Saint-Laurent rift faults. Based on numerical modelling it was shown that the selective reactivation of impact crater faults could be caused by a local enhancement of stress induced by slip along the inherently weak rift faults (Chapter 3). By analogy with the CSZ it is suggested that the NY-AB lineament represents a similarly weak fault.

A second major difference between the CSZ and the ETSZ is the partitioning of seismicity between regional and local structures. In the CSZ all the earthquakes larger than **M** 5.0 and many of those larger than 4.0 are localized outside the crater and have focal mechanisms consistent with slip along the rift faults. Smaller magnitude events, conversely, tend to spread relatively evenly throughout the seismic

zone and with more variable focal mechanisms. In the ETSZ, however, all recorded earthquakes are of relatively low magnitude (the largest being **M** 4.6), and generally do not show a clear partitioning between the regional and local structures. Since 1980 there have only been three $\mathbf{M} > 4.0$ events recorded (compared to 10 since 1985 in the CSZ), and while two of them were located in the northern part of the zone and the other one at the southern tip, it is difficult to pick out any clear patterns with so few events.

Ultimately, the ETSZ closely resembles the CSZ but without the large regional fault earthquakes. This, however, does not imply that large events have not happened in the past, or that they will not happen in the future. Indeed, the high concentration of microseismicity suggests that a notable level of seismic hazard exists. If the stress channelling model is correct then the paucity of large events on record suggest a few possible explanations. It could be that the recurrence time between large events is simply longer than at Charlevoix such that none have been instrumentally or historically recorded. Alternatively, as suggested by Powell *et al.* (1994), the ETSZ may be an evolving fault system, and the background activity may mark the precursors to a potential future large event along the NY-AB lineament. Another possibility suggested by some (e.g. Ebel, 2008) is that the elevated level of microseismicity may simply represent an aftershock sequence of a prehistoric large event, and that a future large event is unlikely.

5.3 A generalized model of eastern North American seismicity

The research presented thus far has focussed on site specific conditions to explain local stress perturbations and seismicity patterns. Many of the concepts explored in the local models and discussion will now be applied on a broader scale to explain some of the spatial and temporal patterns of stress and seismicity over eastern North America.

Earthquakes in eastern North America are concentrated mainly within a ∼1000 km wide band of crust between the interior North American craton and the Atlantic margin. The geology of the region is dominated by a pervasive NE-SW oriented structural fabric formed by a series of alternating compression and extension events associated with the assemblage and breakup of the Rodinia and Pangea supercontinents. The resulting succession of suture zones and rifted faults all show a preferred NE-SW strike and show significant degree of overprinting and tectonic inheritance, suggesting that the structures remained sufficiently weak to remain preferred sites of reactivation over a large period of time (Thomas, 2006). Given the propensity for reactivation of the structures evident in the rock record, it is unsurprising that much of the current seismicity is associated with them. Nearly all known $\mathbf{M} > 6$ earthquakes in eastern North America have occurred within Atlantic or Iapetan rifted basins, margins and aulacogens (Johnston *et al.*, 1994). While current seismicity patterns are not evenly distributed throughout the paleotectonic structures, seismic zones do preferentially cluster along NE-SW trends, mimicking the underlying structural grain (Figure 5.6).

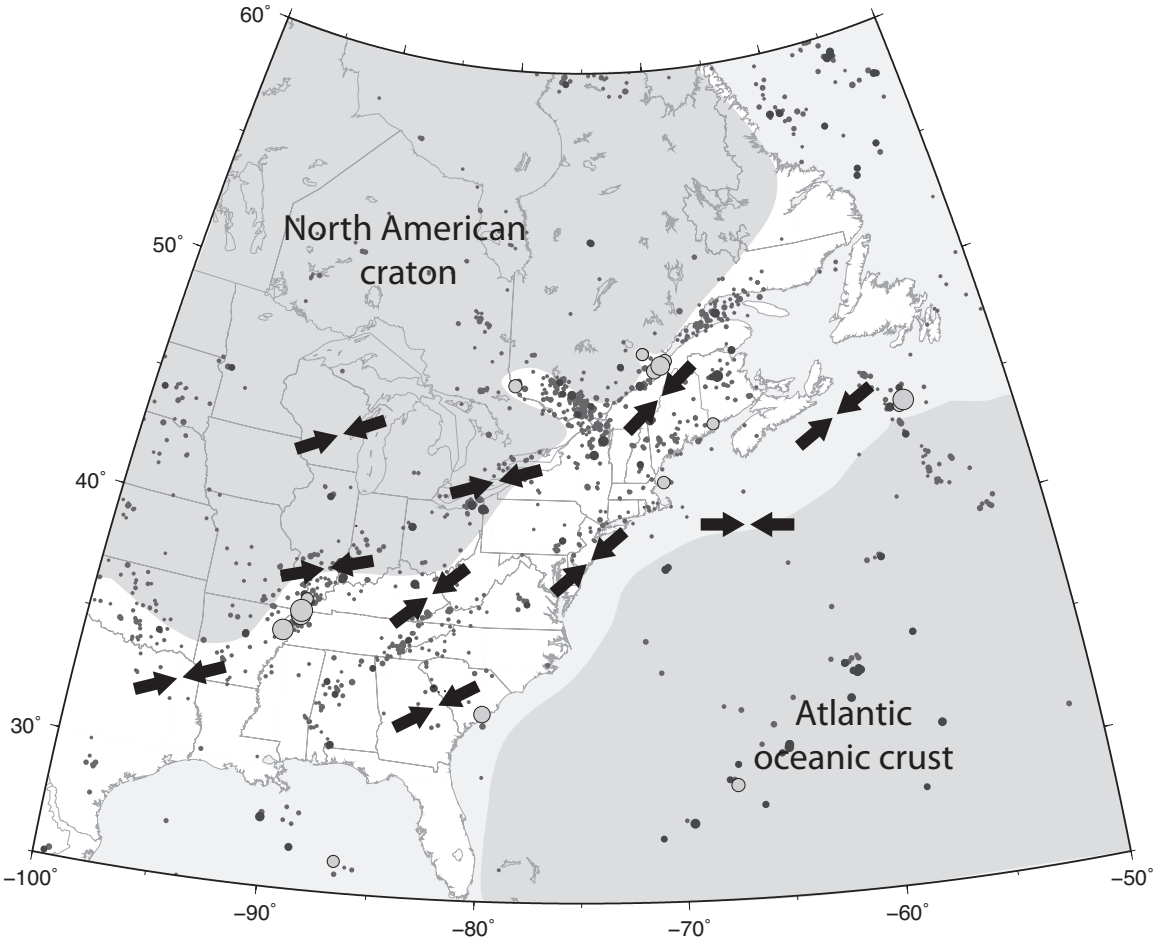

Figure 5.6: Background and historic seismicity of eastern North America. Background seismicity since 1973 is shown by dark grey ($M \geq 3$) and black ($M \geq 4.5$) circles. Historical large earthquakes (mostly $M \geq 6.0$) are shown by large grey circles. Grey shaded area indicates the low seismicity rigid regions of the North American craton and the Atlantic Ocean (modified from Mazzotti, 2007). Inverted arrows show a generalized variation of S_H orientation based on data from the World Stress Map (Heidbach *et al.*, 2008).

While the broad scale correlation of earthquakes with ancient rift and suture zones is apparent, in detail the nature of the relationship is unclear. In many areas, seismicity cannot be definitively linked to any known faults. The difficulty is partially attributed to a general lack of high quality data as a result of the short time period of instrument measurements over a relatively sparse seismic network. In other cases the difficulty arises from the relevant seismogenic structures being obscured by thick sedimentary sequences or cover rock. In regions where seismicity can clearly be associated with paleotectonic structures, the relationship can still be confusing. The unusual partitioning of earthquakes in the Charlevoix seismic zone, where large earthquakes cluster along the rift faults, and small ones cluster between them, is an example of this complexity.

If the assertion that these predominantly NE trending structures are preferred sites for reactivation is true, then one puzzling question is why they would reactivate, given that the present day stress field is dominated NE-SW compression, subparallel to the regional strike (Figure 5.6)? In this configuration a NE striking plane would have very little resolved shear stress acting on it, and would therefore not be expected to slip. The problem with this line of reasoning is that it treats the structures and the stress field as independent parameters, which in fact they are not. Both the southern Ontario and Charlevoix models rely on the interplay between the stress field and local structures in order to explain seismicity patterns, and perhaps a similar relationship can be found at a regional scale. Figure 5.6 shows a generalized variation in S_H orientation over much of eastern North America based on data from the World Stress Map. Although, to first order, S_H orientations are relatively consistent over a large region, there are some perturbations

apparent in the trend. The largest changes in orientation appear to be related to the transition from the craton to the younger, thinner and more seismically active crust to the east and south. While the interior of the craton is rather poorly sampled by stress data (Zoback & Zoback, 1991), S_H in the central United States is dominantly oriented ENE, as opposed to the NE preferred orientation in the eastern part of the continent. Perhaps this could be indicative of a large stress scale perturbation.

Mazzotti (2007) proposed a variety of end member dynamic models to explain eastern North American seismicity. In one very compelling model he proposes that the seismic activity could be the result of distributed deformation between two rigid blocks defined by the thick North American craton, and the relatively strong oceanic lithosphere of the western Atlantic. Under this framework the behaviour of eastern North America could be considered as analogous to plate boundary regions, with the key difference that the differential velocities between the blocks are considerably lower than at typical plate boundaries, and deformation is spread over a wide ($\sim$1000 km) zone, rather than over a narrow band. If the overall stress field applied to the craton-oceanic block assemblage is ENE-WSW oriented compression as suggested by stress data in the central United States, then the resulting kinematics as defined by the block geometry would imply a broad dextral transpressive deformation zone as illustrated in Figure 5.7. One could imagine that the deformation would be largely accommodated by slip along the major NE-SW oriented paleotectonic structures, which, over long time scales, should be relatively evenly distributed.

This long-term slip accumulation could have a lasting effect on the regional orientation of S_H. It has been demonstrated in the Mediterranean region that stress

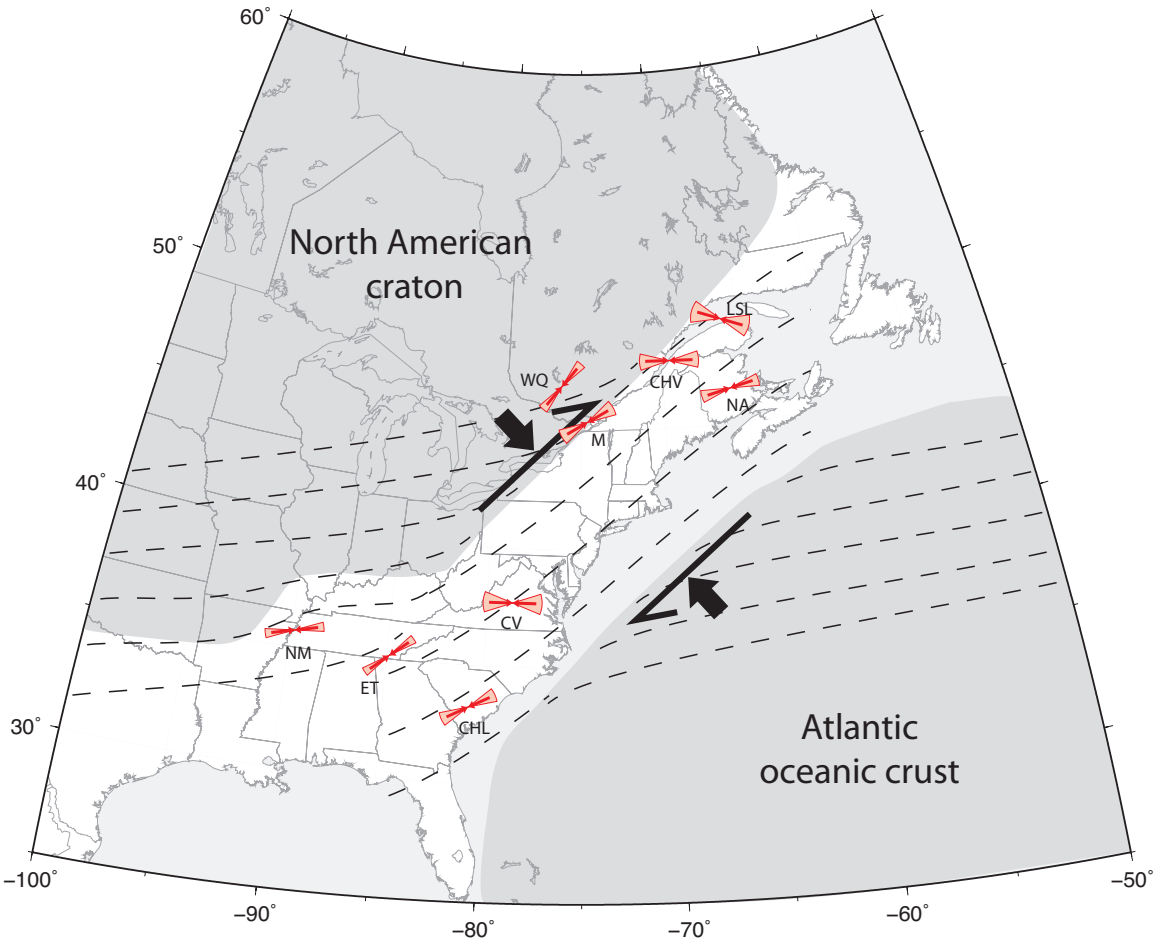

Figure 5.7: Proposed model for eastern North American seismicity. Earthquakes are the result of a broad dextral transpressive deformation zone caused by slow differential motion between the North American craton and the rigid Atlantic crust. Dashed lines indicate orientation of maximum horizontal compression (S_H). Red arrows indicate estimates of the maximum horizontal compressive stress direction within nine seismic zones based on the focal mechanism stress inversion results of Mazzotti & Townend (2010). The seismic zones are CHL: Charleston, CHV: Charlevoix, CV: Central Virginia, ET: Eastern Tennessee, LSL: Lower St. Lawrence, M: Montréal, NA: Northern Appalachians, NM: New Madrid, WQ: Western Québec.

domains can be defined by structures at different scales (Rebaï *et al.*, 1992). Large stress domains can be controlled by regional structures, while smaller sub-domains may be defined by local variations in structure. The stress perturbation in southern Ontario explored using numerical models in Chapter 2 may be an example of one of these subdomains within a larger stress domain controlled by the craton-oceanic block assemblage. By analogy with the smaller Ontario model the regional stress field between the blocks would be expected to rotate counterclockwise to an orientation closer to the strike of the main block boundaries and paleotectonic structures as illustrated in Figure 5.7.

One of the implications of this model is that over time earthquakes should be more or less evenly distributed throughout the paleotectonic structure network. This suggests that the pattern of seismicity expressed by the current data, with concentrated clusters of earthquakes separated by regions of relative seismic quiescence, may simply be an artifact of having only a relatively short sampling of a long-term transient process (e.g. Swafford & Stein, 2007). There is geologic evidence to support the temporal migration of seismic activity within the Reelfoot rift system in the Central United States. While current activity is concentrated mainly in the New Madrid seismic zone, the general lack of significant topography suggests that the onset of high magnitude activity has been relatively recent (e.g. Schweig & Ellis, 1994). Geologic studies have also found liquifaction deposits along rift segments outside of the NMSZ area, providing evidence for large paleoearthquakes in regions that are currently aseismic (e.g. Tuttle *et al.*, 2006). There is reason to suggest that seismicity along the St. Lawrence may be transient as well. Seismic reflection profiles in the Charlevoix area fail to show significant accumu-

lated slip across Quaternary deposits, suggesting that significant seismic activity in the CSZ is relatively young, perhaps only a few thousand years (Lamontagne, 1999). Additionally the behaviour of the 3-D model in Chapter 4 suggests that over long time periods slip along the rift faults is more or less evenly distributed, thus the current activity observed there may not continue indefinitely.

The model of migrating seismicity due to distributed deformation across eastern North America is an appealing one for the Charlevoix seismic zone, as it may help to explain some of its unusual characteristics. One of the unresolved issues with the CSZ is why there are such large events that localize along the rift faults despite the fact that local stresses are poorly oriented to induce slip. If the seismic activity is simply due to the transient effect of long term regional deformation, it would be reasonable to assume that most of the strain release should be localized along regional scale structures. Although the kinematics of the large events, with typically E-W to NW-SE oriented P-axes, are difficult to reconcile with local stress measurements, one could argue that perhaps they are more compatible with the broad scale kinematics of the proposed North America-Atlantic block hypothesis (Figure 5.7).

While the spatially migrating nature of large scale, long term deformation may explain the localization of large events in the CSZ, most observed earthquakes are lower magnitude background events which display quite different behaviour. As discussed in great detail in Chapters 3 and 4, the partitioning of seismicity in the CSZ is such that large events cluster along the rift faults, while small events cluster between them, within the damaged zone formed by the impact structure. The numerical models suggest that the localization of these events is the result of stress

perturbations induced by slip along the rift faults, which act to enhance the state of stress in portions of the crater. In this respect the background seismicity can be considered aftershocks of the large events (Ebel *et al.*, 2000; Stein & Liu, 2009). Unlike the main shocks, however, the aftershocks nucleate along smaller scale faults with more variable orientations, and generally produce slip that is compatible with the local state of stress.

The recognition that the background seismicity may represent aftershocks has an important implication for the long term understanding of the seismic zone. If the hypothesis that high concentrations of seismicity is a transient feature, then at some point in the future it would be expected that the large slipping events located on the rift faults of the CSZ will cease, as the region of high activity migrates elsewhere along-strike. The aftershock sequence would therefore be expected to continue for some time after the main activity has stopped. It has been argued that in low strain rate areas like eastern North America, aftershock sequences from strong earthquakes could stand out over background seismicity for hundreds of years or more (Ebel *et al.*, 2000). In this new configuration the seismicity of the CSZ would show a cluster of events clearly trending along the rift, but with most events slipping on planes inconsistent with the regional faults. This pattern is very similar to what is currently observed in the ETSZ, and suggests that the activity there may be due to aftershocks from geologically recent large events along the major NE-SW basement structure. In fact this relationship could be extended to a broader scale. Given the broad scale NE-SW trend of background seismicity even between the localized zones of higher seismic activity, perhaps much of the seismicity observed in eastern North America are simply aftershocks of prehistoric

larger events migrating along the major weak structures (Ebel *et al.*, 2000; Stein & Liu, 2009).

In regional studies, focal mechanisms have been shown to be broadly compatible with the tectonic stress field over most of eastern North America with a few exceptions (Zoback, 1992a; Du *et al.*, 2003). Within seismic zones, however, there is often more complexity evident in the focal mechanism patterns. In the Charlevoix seismic zone this complexity has been argued to be caused by a mixture of fault geometry controlled large events, and local stress-controlled small events. Mazzotti & Townend (2010) carried out focal mechanism stress inversion within ten seismic zones in eastern North America, the results of which are shown in Figure 5.7. Of the ten studied, four (including the ETSZ) were shown to have inferred stress orientations parallel to local stress measurements. The Charlevoix, Lower St. Lawrence, and Central Virginia zones showed significant clockwise rotations of 30-50° relative to the local field (Figure 5.7). The sense of rotation is consistent with what would be expected from reactivation of dominant NE-SW oriented structures. This consistency suggests that these areas may be the present day sites of far-field strain accommodation, in accordance with the broad shear zone migrating seismicity model proposed in this thesis.

5.3.1 Tests for model

The proposed block-assemblage hypothesis is somewhat speculative and would require further investigation. The model is based on a relatively limited dataset, however, additional data may be used to test the predictions of the model in order

to support, reject or revise the proposed hypothesis.

One of the major predictions of the hypothesis is that the long term distribution of seismicity within eastern North America should be approximately evenly distributed along the major paleotectonic structures. The relatively short seismic record suggests that within a 500 year period only a few **M** 7 earthquakes should be expected in the entire region. With such a long recurrence interval between large events, simply waiting for the gaps to fill in is clearly an impractical way to validate the model. An alternative approach, however, is to look for geological evidence of prehistoric large earthquakes, particularly in regions where seismicity rates are currently low, in order to gain a better understanding of the long-term seismicity trends. Evidence of long-term migration of seismicity along strike of rift zones would support the hypothesis.

In addition to elevated levels of seismicity, the differential motion between the North American craton and the Atlantic would likely result in a broad-scale stress perturbation between the two blocks (Figure 5.7). Although signs of stress perturbations can be identified in the current data (Figure 5.6), additional high quality data would be invaluable in ascertaining whether a true large-scale perturbation exists or if current variations are merely local effects. In particular a larger sampling of high quality stress measurements are needed in the interior craton region. Currently the largest source of stress orientation data, as well as the fastest growing source, is from earthquake focal mechanisms (Barth *et al.*, 2008). Unfortunately these are of relatively low quality, and may contain a systematic bias controlled by the regional structural fabric. Additionally the data is most prevalent in the seismically active regions, which are already relatively well sampled by measurements.

High quality stress data require expensive borehole drilling, and primarily come from industry-related drilling projects. While collection of these data is possible, it may be impractical.

A third possible test for the hypothesis is the use of high precision geodetic techniques to observe and quantify deformation patterns throughout the eastern North American region. With the advent of satellite technology over the past few decades the use of GPS derived velocity measurements has become a valuable tool in understanding the seismotectonics of actively deforming plate boundary regions (e.g. Hackl *et al.*, 2009). The application of these techniques to intraplate regions has been considerably more difficult and controversial due to their comparatively low strain rates. Much of the recently calculated residual horizontal velocities in eastern North America are smaller than their uncertainty at a 95% confidence level (Calais *et al.*, 2006), meaning that they currently cannot be distinguished from zero velocity. However, because of the nature of GPS strain techniques, error will diminish with longer time periods of measurement. Thus with continued monitoring of GPS stations combined with a continual expansion of permanent network of stations, GPS derived strain patterns will likely become an increasingly valuable tool in understanding intraplate dynamics (Stein, 2007).

5.4 Future research considerations

This thesis represents a significant contribution to our understanding of the interrelationship between stress, structure and seismicity in intraplate settings. However, there remain some unanswered questions and room for further investigation

to contribute to our understanding of the seismotectonics of continental interiors, some of which are highlighted here.

Structural fabric modelling One of the major motivations for the numerical modelling of southern Ontario in Chapter 2 was to test whether reactivation of weak planes defined by tectonic fabric could result in a stress perturbation as observed in the area. While the model was successful in illustrating this as a potential mechanism of stress rotation it is not clear whether the effect is better modelled by slip along a few discrete weak faults or along a more diffuse series of closely spaced but stronger faults. The difficulty in producing the 3-D geometry of the models made testing a variety of fault configurations impractical. A revised approach may be to use more sophisticated anisotropic constitutive models to represent the continuum portions between the faults, in order to simulate variations in internal fabric.

Focal mechanisms in fractured mediums In the 3-D Charlevoix model of Chapter 4 much of the discussion deals with the variation of focal mechanism patterns between large and small events, and between mechanisms inside and outside the fractured rocks of the impact crater. However, the representation of the impact structure as a region of lowered elastic modulus rather than with the explicit modelling of individual fractures precludes any direct modelling of slip along crater-related faults. Thus the focal mechanism discussion was mainly qualitative in nature. The conclusions of the chapter, however, have some important implications for the interpretation of focal mechanisms in regions of preferred structural trend, particularly in regard to their applicability to stress orientation estimation, which

highlights a need for a more formal, quantitative investigation. A possible approach would be to use a discontinuum geomechanical modelling code such as 3DEC in order to test the response of a fractured medium to an applied stress. The effect of structural anisotropy on earthquake characteristics can be explored by introducing varying degrees of preferred orientation of fractures in the model, and monitoring the slip behaviour given orientations and magnitudes of applied stress. The model could also be used to test the effectiveness of stress inversion techniques in regions with a dominant structural fabric by using modelled fault slip data to simulate earthquake focal mechanisms, and comparing inversion results with the known applied stress field.

Spatio-temporal response of fault networks One of the major shortcomings of the models presented in this thesis is that they only consider relatively small geographic areas surrounding seismic zones. Limiting the extent is beneficial in that it allows greater detail to be included in the model, and the large amount of seismicity data collected from the seismic zone provides useful constraints for the modelled behaviour. However, while detailed studies of individual seismic zones are certainly valuable, it is important to recognize that they are not truly isolated systems. The seismically active structures are merely components of a much broader network of faults that are all interrelated. Additionally the geographical extent of seismic zones are entirely based on the historic seismic record, which covers only a small time period and likely does not represent the long-term trends. The main motivation for studying intraplate seismicity is to gain a better indication of the risk posed to the public. In order to effectively assess the risk it is essential

to understand how each seismic zone fits into the broader system, and how the behaviour may change in the future. The problem may be addressed by the use of numerical models to study the spatio-temporal response of fault networks to long-term far-field strain. By combining these models with extended earthquake histories from paleoseismic field studies, and constraints from high resolution GPS strain data, we may gain a much clearer understanding of regional intraplate seismicity behaviour.

Bibliography

Adams, J., 1995. The Canadian crustal stress database; a compilation to 1994. *Geological Survey of Canada Open File*, **3122**, 38.

Adams, J. & Atkinson, G., 2003. Development of seismic hazard maps for the proposed 2005 edition of the National Building Code of Canada. *Canadian Journal of Civil Engineering*, **30**(2), 255–271.

Adams, J., Basham, P.W., & Halchuk, S., 1995. Northeastern North American earthquake potential – new challenges for seismic hazard mapping. In *Current Research*, 1995–D, pp. 91–99. Geological Survey of Canada.

Adams, J. & Halchuk, S., 2003. Fourth generation seismic hazard maps of Canada: Values for over 650 Canadian localities intended for the 2005 National Building Code of Canada. *Geological Survey of Canada Open File*, **4459**, 1–155.

Adams, J. & Basham, P., 1991. The seismicity and seismotectonics of eastern Canada. In D.B. Slemmons, E.R. Engdahl, M.D. Zoback, & D.D. Blackwell, eds., *Neotectonics of North America*, pp. 261–275. Geological Society of America, Boulder, Colorado, United States.

Adams, J. & Bell, J.S., 1991. Crustal stresses in Canada. In D.B. Slemmons, E.R. Engdahl, M.D. Zoback, & D.D. Blackwell, eds., *Neotectonics of North America*, pp. 367–386. Geological Society of America, Boulder, Colorado, United States.

Anglin, F.M., 1984. Seismicity and faulting in the Charlevoix zone of the St. Lawrence valley. *Bulletin of the Seismological Society of America*, **74**(2), 595–603.

Argus, D.F. & Gordon, R.G., 1991. No-net-rotation model of current plate velocities incorporating plate motion model NUVEL-1. *Geophysical Research Letters*, **18**(11), 2039–2042.

Arnold, R. & Townend, J., 2007. A Bayesian approach to estimating tectonic stress from seismological data. *Geophysical Journal International*, **170**(3), 1336–1356. DOI:10.1111/j.1365-246X.2007.03485.x.

Assameur, D.M. & Mareschal, J.C., 1995. Stress induced by topography and crustal density heterogeneities: implication for the seismicity of southeastern Canada. *Tectonophysics*, **241**(3-4), 179–192.

Baird, A.F. & McKinnon, S.D., 2007. Linking stress field deflection to basement structures in southern Ontario: Results from numerical modelling. *Tectonophysics*, **432**(1-4), 89–100. DOI:10.1016/j.tecto.2006.12.002.

Baird, A.F., McKinnon, S.D., & Godin, L., 2009. Stress channelling and partitioning of seismicity in the Charlevoix seismic zone, Québec, Canada. *Geophysical Journal International*, **179**(1), 559–568. DOI:10.1111/j.1365-246X.2009.04275.x.

Baird, A.F., McKinnon, S.D., & Godin, L., in review. Relationship between struc-

tures, stress and seismicity in the Charlevoix seismic zone revealed by 3-D geomechanical models: Implications for the seismotectonics of continental interiors. *Journal of Geophysical Research*.

Barth, A., Reinecker, J., & Heidbach, O., 2008. World Stress Map project guidelines: Stress derivation from earthquake focal mechanisms. URL `http://dc-app3-14.gfz-potsdam.de/pub/guidelines/WSM_analysis_guideline_focal_mechanisms.pdf`.

Bendick, R., Bilham, R., Fielding, E., Gaur, V.K., Hough, S.E., Kier, G., Kulkarni, M.N., Martin, S., Mueller, K., & Mukul, M., 2001. The 26 January 2001 "Republic Day" earthquake, India. *Seismological Research Letters*, **72**(3), 328–335.

Bent, A.L., 1992. A re-examination of the 1925 Charlevoix, Québec, earthquake. *Bulletin of the Seismological Society of America*, **82**(5), 2097–2113.

Bollinger, G.A., Johnston, A.C., Talwani, P., Long, L.T., Shedlock, K.M., Sibol, M.S., & Chapman, M.C., 1991. Seismicity of the southeastern United States; 1698 to 1986. In D.B. Slemmons, E.R. Engdahl, M.D. Zoback, & D.D. Blackwell, eds., *Neotectonics of North America*, pp. 291–308. Geological Society of America.

Bollinger, G.A. & Wheeler, R.L., 1988. The Giles County, Virginia seismic zone: seismological results and geological interpretations. *United States Geological Survey Professional Paper*, **1355**, 85.

Boyce, J.I. & Morris, W.A., 2002. Basement-controlled faulting of Paleozoic strata in southern Ontario, Canada: new evidence from geophysical lineament mapping. *Tectonophysics*, **353**(1-4), 151–171. DOI:10.1016/S0040-1951(02)00280-9.

Calais, E., Han, J.Y., DeMets, C., & Nocquet, J.M., 2006. Deformation of the North American plate interior from a decade of continuous GPS measurements. *Journal of Geophysical Research*, **111**(B6). DOI:10.1029/2005JB004253.

Calais, E., Mattioli, G., DeMets, C., Nocquet, J.M., Stein, S., Newman, A., & Rydelek, P., 2005. Tectonic strain in plate interiors? *Nature*, **438**(7070), E9–E10. DOI:10.1038/nature04428.

Carr, S.D., Easton, R.M., Jamieson, R.A., & Culshaw, N.G., 2000. Geologic transect across the Grenville orogen of Ontario and New York. *Canadian Journal of Earth Sciences*, **37**(2-3), 193–216. DOI:10.1139/CJES-37-2-3-193.

Célérier, J., Sandiford, M., Hansen, D.L., & Quigley, M., 2005. Modes of active intraplate deformation, Flinders Ranges, Australia. *Tectonics*, **24**(6), TC6006. DOI:10.1029/2004TC001679.

Chapman, M.C., Powell, C.A., Vlahovic, G., & Sibol, M.S., 1997. A statistical analysis of earthquake focal mechanisms and epicenter locations in the eastern Tennessee seismic zone. *Bulletin of the Seismological Society of America*, **87**(6), 1522–1536.

Cook, F.A. & Vasudevan, K., 2006. Reprocessing and enhanced interpretation of the initial COCORP Southern Appalachians traverse. *Tectonophysics*, **420**(1-2), 161–174.

Cox, R.T., Arsdale, R.B.V., Harris, J.B., & Larsen, D., 2001. Neotectonics of the southeastern Reelfoot rift zone margin, central United States, and implications for regional strain accommodation. *Geology*, **29**(5), 419–422.

Cox, R.T., Cherryhomes, J., Harris, J.B., Larsen, D., Van Arsdale, R.B., & Forman, S.L., 2006. Paleoseismology of the southeastern Reelfoot rift in western Tennessee and implications for intraplate fault zone evolution. *Tectonics*, **25**(3), TC3019. DOI:10.1029/2005TC001829.

Cundall, P.A., 1988. Formulation of a three-dimensional distinct element model – Part I: A scheme to detect and represent contacts in a system composed of many polyhedral blocks. *International Journal of Rock Mechanics and Mining Sciences & Geomechanics Abstracts*, **25**(3), 107–116.

Dineva, S., Eaton, D., & Mereu, R., 2004. Seismicity of the southern Great Lakes; revised earthquake hypocenters and possible tectonic controls. *Bulletin of the Seismological Society of America*, **94**(5), 1902–1918. DOI:10.1785/012003007.

Du, W.X., Kim, W.Y., & Sykes, L.R., 2003. Earthquake source parameters and state of stress for the northeastern United States and southeastern Canada from analysis of regional seismograms. *Bulletin of the Seismological Society of America*, **93**(4), 1633–1648. DOI:10.1785/0120020217.

Dunn, M.M. & Chapman, M.C., 2006. Fault orientation in the eastern Tennessee seismic zone: A study using the double-difference earthquake location algorithm. *Seismological Research Letters*, **77**(4), 494–504. URL `http://srl.geoscienceworld.org/cgi/content/abstract/77/4/494`.

Easton, R.M., 1992. The Grenville Province and the Proterozoic history of central and southern Ontario. In *Geology of Ontario, Part 2*, Special Volume 4, pp. 714–904. Ontario Geological Survey.

Ebel, J.E., 2008. The importance of small earthquakes. *Seismological Research Letters*, **79**(4), 491.

Ebel, J.E. & Tuttle, M., 2002. Earthquakes in the eastern Great Lakes basin from a regional perspective. *Tectonophysics*, **353**(1-4), 17–30. DOI:10.1016/S0040-1951(02)00277-9.

Ebel, J.E., Bonjer, K.P., & Oncescu, M.C., 2000. Paleoseismicity: seismicity evidence for past large earthquakes. *Seismological Research Letters*, **71**(2), 283–294.

Ellis, W.L., 1994. Summary and discussion of crustal stress data in the region of the New Madrid seismic zone. *United States Geological Survey Professional Paper*, **1538**, B1–B13.

Evans, K.F., 1989. Appalachian stress study 3: Regional scale stress variations and their relation to structure and contemporary tectonics. *Journal of Geophysical Research*, **94**(B12), 17619–17645.

Eyles, N., Boyce, J., & Mohajer, A.A., 1993. The bedrock surface of the western Lake Ontario region: evidence of reactivated basement structures? *Géographie Physique et Quaternaire*, **47**(3), 269–283.

Forsyth, D.A., Milkereit, B., Davidson, A., & Hanmer, S., 1994a. Seismic images of a tectonic subdivision of the Grenville Orogen beneath lakes Ontario and Erie. *Canadian Journal of Earth Sciences*, **31**(2), 229–242.

Forsyth, D.A., Milkereit, B., Zelt, C.A., White, D.J., Easton, R.M., & Hutchinson,

D.R., 1994b. Deep structure beneath Lake Ontario: crustal-scale Grenville subdivisions. *Canadian Journal of Earth Sciences*, **31**(2), 255–270.

Fossum, A.F., 1985. Effective elastic properties for a randomly jointed rock mass. *International Journal of Rock Mechanics and Mining Sciences & Geomechanics Abstracts*, **22**(6), 467–470.

Gephart, J.W. & Forsyth, D.W., 1984. An improved method for determining the regional stress tensor using earthquake focal mechanism data; application to the San Fernando earthquake sequence. *Journal of Geophysical Research*, **89**(B11), 9305–9320.

Grana, J.P. & Richardson, R.M., 1996. Tectonic stress within the New Madrid seismic zone. *Journal of Geophysical Research*, **101**(B3), 5445–5458.

Hackl, M., Malservisi, R., & Wdowinski, S., 2009. Strain rate patterns from dense gps networks. *Natural Hazards and Earth System Sciences*, **9**, 1177–1187.

Hart, R., Cundall, P.A., & Lemos, J., 1988. Formulation of a three-dimensional distinct element model – Part II: Mechanical calculations for motion and interaction of a system composed of many polyhedral blocks. *International Journal of Rock Mechanics and Mining Sciences & Geomechanics Abstracts*, **25**(3), 117–125.

Hart, R.D., 1993. An introduction to distinct element modeling for rock engineering. In C. Fairhurst & J.A. Hudson, eds., *Comprehensive rock engineering*, vol. 2, pp. 245–261. Pergamon Press, Oxford, United Kingdom.

Hasegawa, H.S., Adams, J., & Yamazaki, K., 1985. Upper crustal stresses and ver-

tical stress migration in eastern Canada. *Journal of Geophysical Research*, **90**(B5), 3637–3648.

Hasegawa, H.S. & Wetmiller, R.J., 1980. The Charlevoix earthquake of 19 August 1979 and its seismo-tectonic environment. *Earthquake Notes*, **51**(4), 23–37.

Hatcher, Jr., R.D., Lemiszki, P.J., & Whisner, J.B., 2007. Character of rigid boundaries and internal deformation of the southern Appalachian foreland fold-thrust belt. In J.W. Sears, T. Harms, & C.A. Evenchick, eds., *Whence the mountains?: inquiries into the evolution of orogenic systems: a volume in honor of Raymond A. Price*, vol. 433 of *Geological Society of America Special Paper*, p. 243. Geological Society of America. DOI:10.1130/2007.2433(12).

Hatcher, Jr., R.D., Zietz, I., & Litehiser, J.J., 1987. Crustal subdivisions of the eastern and central United States and a seismic boundary hypothesis for eastern seismicity. *Geology*, **15**(6), 528–532.

Heidbach, O., Tingay, M., Barth, A., Reinecker, J., Kurfeß, D., & Müller, B., 2008. The 2008 release of the World Stress Map. URL `http://www.world-stress-map.org`.

Homberg, C., Hu, J.C., Angelier, J., Bergerat, F., & Lacombe, O., 1997. Characterization of stress perturbations near major fault zones: insights from 2-D distinct-element numerical modelling and field studies (Jura mountains). *Journal of Structural Geology*, **19**(5), 703–718. DOI:10.1016/S0191-8141(96)00104-6.

Horton, S.P., Kim, W.Y., & Withers, M., 2005. The 6 June 2003 Bardwell, Kentucky, earthquake sequence: Evidence for a locally perturbed stress field in the Missis-

sippi Embayment. *Bulletin of the Seismological Society of America*, **95**(2), 431–445. DOI:10.1785/0120040052.

Hutchinson, D.R., Pomeroy, P.W., Wold, R.J., & Halls, H.C., 1979. A geophysical investigation concerning the continuation of the Clarendon-Linden fault across Lake Ontario. *Geology*, **7**(4), 206–210.

Itasca Consulting Group Inc., 2003. *3DEC (3 Dimensional Distinct Element Code), Version 3.0*. Minneapolis, MN.

Itasca Consulting Group Inc., 2005a. *FLAC (Fast Lagrangian Analysis of Continua), Version 5.0*. Minneapolis, MN.

Itasca Consulting Group Inc., 2005b. *FLAC3D (Fast Lagrangian Analysis of Continua in 3 Dimensions), Version 3.0*. Minneapolis, MN.

Jacobi, R.D. & Fountain, J., 2002. The character and reactivation history of the southern extension of the seismically active Clarendon-Linden fault system, western New York State. *Tectonophysics*, **353**(1-4), 215–262.

Jacobi, R.D. & Fountain, J., 1993. The southern extension and reactivations of the Clarendon-Linden fault system. *Géographie Physique et Quaternaire*, **47**(3), 285–302.

James, T.S. & Bent, A.L., 1994. A comparison of eastern North American seismic strain-rates to glacial rebound strain-rates. *Geophysical Research Letters*, **21**(19), 2127–2130.

Johnston, A.C., 1993. Average stable continental earthquake source parameters based on constant stress drop scaling. *Seismological Research Letters*, **64**, 261.

Johnston, A.C., 1996. Seismic moment assessment of earthquakes in stable continental regions—III. New Madrid 1811–1812, Charleston 1886 and Lisbon 1755. *Geophysical Journal International*, **126**(2), 314–344.

Johnston, A.C., Coppersmith, K.J., Kanter, L.R., & Cornell, C.A., 1994. *The earthquakes of stable continental regions*, vol. 1–5. Electric Power Research Institute (EPRI), Palo Alto, CA, USA.

Johnston, A.C., Reinbold, D.J., & Brewer, S.I., 1985. Seismotectonics of the southern Appalachians. *Bulletin of the Seismological Society of America*, **75**(1), 291–312.

King, E.R. & Zietz, I., 1978. The New York-Alabama lineament: Geophysical evidence for a major crustal break in the basement beneath the Appalachian basin. *Geology*, **6**(5), 312–318.

Kucks, R.P., 1999. Bouguer gravity anomaly data grid for the conterminous US. *U.S. Geological Survey Digital Data Series*, **DDS-9**.

Kumarapeli, P.S., 1985. Vestiges of Iapetan rifting in the craton west of the northern Appalachians. *Geoscience Canada*, **12**(2), 54–59.

Lamontagne, M., Halchuk, S., Cassidy, J.F., & Rogers, G.C., 2007. Significant Canadian earthquakes 1600–2006. *Geological Survey of Canada Open File*, **5539**.

Lamontagne, M. & Ranalli, G., 1996. Thermal and rheological constraints on

the earthquake depth distribution in the Charlevoix, Canada, intraplate seismic zone. *Tectonophysics*, **257**(1), 55–69.

Lamontagne, M., 1987. Seismic activity and structural features in the Charlevoix region, Quebec. *Canadian Journal of Earth Sciences*, **24**(11), 2118–2129.

Lamontagne, M., 1999. Rheological and geological constraints on the earthquake distribution in the Charlevoix seismic zone, Québec, Canada. *Geological Survey of Canada Open File*, **D3778**, 1 CD–ROM.

Leblanc, G. & Buchbinder, G., 1977. Second microearthquake survey of the St. Lawrence Valley near La Malbaie, Quebec. *Canadian Journal of Earth Sciences*, **14**(12), 2778–2789.

Leblanc, G., Stevens, A.E., Wetmiller, R.J., & DuBerger, R., 1973. A micro-earthquake survey of the St. Lawrence valley near La Malbaie, Quebec. *Canadian Journal of Earth Sciences*, **10**(1), 42–53.

Lemieux, Y., Tremblay, A., & Lavoie, D., 2003. Structural analysis of supracrustal faults in the Charlevoix area, Quebec: Relation to impact cratering and the St-Laurent fault system. *Canadian Journal of Earth Sciences*, **40**(2), 221 – 235. DOI:10.1139/E02-046.

Liu, L. & Zoback, M.D., 1997. Lithospheric strength and intraplate seismicity in the New Madrid seismic zone. *Tectonics*, **16**(4), 585–595.

Martignole, J. & Calvert, A.J., 1996. Crustal-scale shortening and extension across the Grenville Province of western Quebec. *Tectonics*, **15**(2), 376–386.

Mazzotti, S., James, T.S., Henton, J., & Adams, J., 2005. GPS crustal strain, postglacial rebound, and seismic hazard in eastern North America: The Saint Lawrence valley example. *Journal of Geophysical Research*, **110**, B11301. DOI:10.1029/2004JB003590.

Mazzotti, S., Wu, P., Wada, I., Bent, A., & Adams, J., 2006. Role of plate tectonic and post-glacial rebound forces in the present-day state of stress and fault reactivation along the St Lawrence and Ottawa valleys. In *GAC-MAC Annual Meeting Abstracts, Montréal, Québec, 14-17 May*, vol. 31, p. 99. Geological Association of Canada.

Mazzotti, S., 2007. Geodynamic models for earthquake studies in intraplate North America. In S. Stein & S. Mazzotti, eds., *Continental intraplate earthquakes: science, hazard, and policy issues*, vol. 425 of *Geological Society of America Special Paper*, pp. 17–33. Geological Society of America. DOI:10.1130/2007.2425(02).

Mazzotti, S. & Townend, J., 2010. State of stress in central and eastern North American seismic zones. *Lithosphere*, **2**(2), 76–83. DOI:10.1130/L65.1.

McFall, G.H., 1993. Structural elements and neotectonics of Prince Edward County, southern Ontario. *Géographie Physique et Quaternaire*, **47**(3), 303–312.

McKenzie, D.P., 1969. The relation between fault plane solutions for earthquakes and the directions of the principal stresses. *Bulletin of the Seismological Society of America*, **59**(2), 591–601.

McKinnon, S.D., 2006. Triggering of seismicity remote from active mining excava-

tions. *Rock Mechanics and Rock Engineering*, **39**(3), 255–279. DOI:10.1007/s00603-005-0072-5.

McKinnon, S.D. & Garrido de la Barra, I., 2003. Stress field analysis at the El Teniente Mine: evidence for N-S compression in the modern Andes. *Journal of Structural Geology*, **25**(12), 2125–2139. DOI:10.1016/S0191-8141(03)00068-3.

Michael, A.J., 1984. Determination of stress from slip data: faults and folds. *Journal of Geophysical Research*, **89**(B13), 11517–11526.

Mitchell, F., 2007. *Structural analysis of brittle deformation features along Grenvillian shear zones in southeastern Ontario*. Master's thesis, Queen's University.

Mohajer, A.A., 1993. Seismicity and seismotectonics of the western Lake Ontario region. *Géographie Physique et Quaternaire*, **47**(3), 353–362.

Mount, V.S. & Suppe, J., 1987. State of stress near the San Andreas fault: implications for wrench tectonics. *Geology*, **15**(12), 1143–1146.

Müller, B., Wehrle, V., Hettel, S., Sperner, B., & Fuchs, K., 2003. A new method for smoothing orientated data and its application to stress data. *Geological Society Special Publication*, **209**, 107–126. DOI:10.1144/GSL.SP.2003.209.01.11.

NAMAG, 2002. Digital data grids for the magnetic anomaly map of North America, Compiled by North American Magnetic Anomaly Group (NAMAG). *United State Geological Survey Open-File*, **02-414**.

Nelson, A.E. & Zietz, I., 1983. The Clingman lineament, other aeromagnetic fea-

tures, and major lithotectonic units in part of the southern Appalachian mountains. *Southeastern Geology*, **24**, 147–157.

Nelson, K.D., McBride, J.H., Arnow, J.A., Wille, D.M., Brown, L.D., Oliver, J.E., & Kaufman, S., 1987. Results of recent COCORP profiling in the southeastern United States. *Geophysical Journal of the Royal Astronomical Society*, **89**(1), 141–146.

O'Dowd, C.R., Eaton, D., Forsyth, D., & Asmis, H.W., 2004. Structural fabric of the Central Metasedimentary Belt of southern Ontario, Canada, from deep seismic profiling. *Tectonophysics*, **388**(1-4), 145–159. DOI:10.1016/j.tecto.2004.07.041.

Onasch, C.M. & Kahle, C.F., 1991. Recurrent tectonics in a cratonic setting: An example from northwestern Ohio. *Geological Society of America Bulletin*, **103**(10), 1259–1269.

Ouellet, M., 1997. Lake sediments and Holocene seismic hazard assessment within the St. Lawrence valley, Québec. *Geological Society of America Bulletin*, **109**, 631–642.

Pascal, C. & Gabrielsen, R.H., 2001. Numerical modeling of Cenozoic stress patterns in the mid-Norwegian margin and the northern North Sea. *Tectonics*, **20**(4), 585–599.

Powell, C.A., Bollinger, G.A., Chapman, M.C., Sibol, M.S., Johnston, A.C., & Wheeler, R.L., 1994. A seismotectonic model for the 300-kilometer-long eastern Tennessee seismic zone. *Science*, **264**(5159).

Rebaï, S., Philip, H., & Taboada, A., 1992. Modern tectonic stress field in the

Mediterranean region: evidence for variation in stress directions at different scales. *Geophysical Journal International*, **110**(1), 106–141.

Richardson, R.M. & Reding, L.M., 1991. North American plate dynamics. *Journal of Geophysical Research*, **96**(B7), 12,201–12,223.

Rivers, T., 1997. Lithotectonic elements of the Grenville Province: review and tectonic implications. *Precambrian Research*, **86**(3-4), 117–154.

Rondot, J., 1971. Impactite of the Charlevoix structure, Quebec, Canada. *Journal of Geophysical Research*, **76**(23), 5414–5423.

Rondot, J., 1994. Recognition of eroded astroblemes. *Earth-Science Reviews*, **35**(4), 331–365. DOI:10.1016/0012-8252(94)90001-9.

Rutty, A.L. & Cruden, A.R., 1993. Pop-up structures and the fracture pattern in the Balsam Lake area, southern Ontario. *Géographie Physique et Quaternaire*, **47**(3), 379–388.

Sanford, B.V., Thompson, F.J., & McFall, G.H., 1985. Plate tectonics – a possible controlling mechanism in the development of hydrocarbon traps in southwestern Ontario. *Bulletin of Canadian Petroleum Geology*, **33**(1), 52–71.

Schulte, S.M. & Mooney, W.D., 2005. An updated global earthquake catalogue for stable continental regions: reassessing the correlation with ancient rifts. *Geophysical Journal International*, **161**(3), 707–721. DOI:10.1111/j.1365-246X.2005.02554.x.

Schweig, E.S. & Ellis, M.A., 1994. Reconciling short recurrence intervals with minor deformation in the New Madrid seismic zone. *Science*, **264**(5163), 1308.

Seeber, L. & Armbruster, J.G., 1993. Natural and induced seismicity in the Lake Erie-Lake Ontario region: reactivation of ancient faults with little neotectonic displacement. *Géographie Physique et Quaternaire*, **47**(3), 363–378.

Sella, G.F., Stein, S., Dixon, T.H., Craymer, M., James, T.S., Mazzotti, S., & Dokka, R.K., 2007. Observation of glacial isostatic adjustment in "stable" North America with GPS. *Geophysical Research Letters*, **34**(2), 2306.

Sibson, R.H., 1994. An assessment of field evidence for "Byerlee" friction. *Pure and Applied Geophysics*, **142**(3-4), 645–662.

Smalley, R., Ellis, M.A., Paul, J., & Van Arsdale, R.B., 2005a. Space geodetic evidence for rapid strain rates in the New Madrid seismic zone of central USA. *Nature*, **435**(7045), 1088–1090. DOI:10.1038/nature03642.

Smalley, R., Ellis, M.A., Paul, J., & Van Arsdale, R.B., 2005b. Tectonic strain in plate interiors? (reply). *Nature*, **438**(7070), E10. DOI:10.1038/nature04428.

Solomon, S.C. & Duxbury, E.D., 1987. A test of the longevity of impact-induced faults as preferred sites for later tectonic activity. *Journal of Geophysical Research*, **92**(B4), 759 – 768.

Somerville, P.G., McLaren, J.P., Saikia, C.K., & Helmberger, D.V., 1990. The 25 November 1988 Saguenay, Quebec, earthquake: Source parameters and the attenuation of strong ground motion. *Bulletin of the Seismological Society of America*, **80**(5), 1118–1143.

St-Julien, P. & Hubert, C., 1975. Evolution of the Taconian orogen in the Quebec Appalachians. *American Journal of Science*, **275-A**, 337–362.

Stein, S. & Liu, M., 2009. Long aftershock sequences within continents and implications for earthquake hazard assessment. *Nature*, **462**, 87–89. DOI:10.1038/nature08502.

Stein, S. & Sella, G., 2002. Plate boundary zones: Concepts and approaches. *Plate Boundary Zones, American Geophysical Union Geodynamic Series*, **30**, 1–26.

Stein, S., 2007. Approaches to continental intraplate earthquake issues. In S. Stein & S. Mazzotti, eds., *Continental intraplate earthquakes: science, hazard, and policy issues*, vol. 425 of *Geological Society of America Special Paper*, pp. 1–16. Geological Society of America. DOI:10.1130/2007.2425(01).

Stein, S. & Wysession, M., 2003. *An introduction to seismology, earthquakes, and earth structure*. Wiley-Blackwell.

Stepp, J.C., Price, R.A., Coppersmith, K.J., Klimkiewicz, G.C., & McGuire, R.K., 1995. AECB workshop on seismic hazard assessment in southern Ontario. Tech. rep., Atomic Energy Control Board of Canada. INFO-0604.

Stevens, A.E., 1980. Reexamination of some larger La Malbaie, Quebec, earthquakes (1924-1978). *Bulletin of the Seismological Society of America*, **70**(2), 529–557.

Stevens, A.E., 1994. Earthquakes in the Lake Ontario region: intermittent scattered activity, not persistent trends. *Geoscience Canada*, **21**(3), 105–111.

Stevenson, D., Gangopadhyay, A., & Talwani, P., 2006. Booming plutons: Source of microearthquakes in South Carolina. *Geophysical Research Letters*, **33**(3). DOI:10.1029/2005GL024679.

Stewart, I.S., Sauber, J., & Rose, J., 2000. Glacio-seismotectonics: Ice sheets, crustal deformation and seismicity. *Quaternary Science Reviews*, **19**(14-15), 1367–1389. DOI:10.1016/S0277-3791(00)00094-9.

Swafford, L. & Stein, S., 2007. Limitations of the short earthquake record for seismicity and seismic hazard studies. *Geological Society of America Special Papers*, **425**, 49.

Sykes, L.R., 1978. Intraplate seismicity, reactivation of preexisting zones of weakness, alkaline magmatism, and other tectonism postdating continental fragmentation. *Reviews of Geophysics and Space Physics*, **16**(4), 621–688.

Teague, A.G., Bollinger, G.A., & Johnston, A.C., 1986. Focal mechanism analyses for eastern Tennessee earthquakes (1981-1983). *Bulletin of the Seismological Society of America*, **76**(1), 95–109.

Thomas, R.L., Wallach, J.L., McMillan, R.K., Bowlby, J.R., Frape, S., Keyes, D., & Mohajer, A.A., 1993. Recent deformation in the bottom sediments of western and southeastern Lake Ontario and its association with major structures and seismicity. *Géographie Physique et Quaternaire*, **47**(3), 325–335.

Thomas, W.A., 1991. The Appalachian-Ouachita rifted margin of southeastern North America. *Geological Society of America Bulletin*, **103**(3), 415.

Thomas, W.A., 2006. Tectonic inheritance at a continental margin. *GSA Today*, **16**(2), 4–11. DOI:10.1130/1052-5173(2006)016[4:TIAACM]2.0.CO;2.

Townend, J., 2006. What do faults feel? Observational constraints on the stresses acting on seismogenic faults. In R. Abercrombie, A. McGarr, H. Kanamori, & G. Di Toro, eds., *Earthquakes: Radiated Energy and the Physics of Faulting*, Geophysical Monograph Series 170, pp. 313–327. American Geophysical Union. DOI:10.1029/170GM31.

Townend, J. & Zoback, M.D., 2001. Implications of earthquake focal mechanisms for the frictional strength of the San Andreas fault system. *Geological Society Special Publication*, **186**, 13–21.

Townend, J. & Zoback, M.D., 2006. Stress, strain, and mountain building in central Japan. *Journal of Geophysical Research*, **111**, B03411. DOI:10.1029/2005JB003759.

Tremblay, A., Long, B., & Massé, M., 2003. Supracrustal faults of the St. Lawrence rift system, Québec: kinematics and geometry as revealed by field mapping and marine seismic reflection data. *Tectonophysics*, **369**(3-4), 231–252.

Tuttle, M.P. & Dyer-Williams, K.M., 2009. Charlevoix seismic zone, southeastern Canada: Source of repeated large earthquakes during the past 10,000 years, in Abstracts of the Eastern Section of the Seismological Society of America Meeting, Kingston, Ontario, 5-7 October 2008. *Seismological Research Letters*, **80**(1), 174.

Tuttle, M.P., Al-Shukri, H., & Mahdi, H., 2006. Very large earthquakes centered southwest of the New Madrid seismic zone 5,000-7,000 years ago. *Seismological Research Letters*, **77**(6), 755–770.

Vlahovic, G., Powell, C.A., Chapman, M.C., & Sibol, M.S., 1998. Joint hypocenter-velocity inversion for the eastern Tennessee seismic zone. *Journal of geophysical research*, **103**(B3), 4879–4896.

Vlahovic, G., Powell, C., & Lamontagne, M., 2003. A three-dimensional P wave velocity model for the Charlevoix seismic zone, Quebec, Canada. *Journal of Geophysical Research*, **108**(B9), 2439. DOI:10.1029/2002JB002188.

Wallach, J.L., 2002. The presence, characteristics and earthquake implications of the St. Lawrence fault zone within and near Lake Ontario (Canada-USA). *Tectonophysics*, **353**(1-4), 45–74. DOI:10.1016/S0040-1951(02)00285-8.

Wallach, J.L. & Mohajer, A.A., 1990. Integrated geoscientific data relevant to assessing seismic hazard in the vicinity of the Darlington and Pickering nuclear power plants. In *Prédiction et Performance en Géotechnique. Canadian Geotechnical Conference, Québec*, vol. 2, pp. 679–686.

Wallach, J.L., Mohajer, A.A., & Thomas, R.L., 1998. Linear zones, seismicity, and the possibility of a major earthquake in the intraplate western Lake Ontario area of eastern North America. *Canadian Journal of Earth Sciences*, **35**(7), 762–786.

Wheeler, R.L., 1995. Earthquakes and the cratonward limit of Iapetan faulting in eastern North America. *Geology*, **23**(2), 105–108.

White, D.J., Forsyth, D.A., Asudeh, I., Carr, S.D., Wu, H., Easton, R.M., & Mereu, R.F., 2000. A seismic-based cross-section of the Grenville Orogen in southern Ontario and western Quebec. *Canadian Journal of Earth Sciences*, **37**(2-3), 183–192. DOI:10.1139/CJES-37-2-3-183.

Wu, P. & Mazzotti, S., 2007. Effects of a lithospheric weak zone on postglacial seismotectonics in eastern Canada and the northeastern United States. In S. Stein & S. Mazzotti, eds., *Continental intraplate earthquakes: science, hazard, and policy issues*, vol. 425 of *Geological Society of America Special Paper*, pp. 113–128. Geological Society of America. DOI:10.1130/2007.2425(09).

Zoback, M.D. & Zoback, M.L., 1989. In situ stress, crustal strain, and seismic hazard assessment in eastern North America. *Annals of the New York Academy of Sciences*, **558**(1), 54–65.

Zoback, M.D., Zoback, M.L., Mount, V.S., Suppe, J., Eaton, J.P., Healy, J.H., Oppenheimer, D., Reasenberg, P., Jones, L., Raleigh, C.B., Wong, I.G., Scotti, O., & Wentworth, C., 1987. New evidence on the state of stress of the San Andreas fault system. *Science*, **238**(4830), 1105–1111.

Zoback, M.L., 1992a. Stress field constraints on intraplate seismicity in eastern North America. *Journal of Geophysical Research*, **97**(B8), 11,761–11,782.

Zoback, M.L. & Richardson, R.M., 1996. Stress perturbation associated with the Amazonas and other ancient continental rifts. *Journal of Geophysical Research*, **101**(B3), 5459–5476.

Zoback, M.D., Apel, R., Baumgartner, J., Brudy, M., Emmermann, R., Engeser, B., Fuchs, K., Kessels, W., Rischmuller, H., Rummel, F., & Vernik, L., 1993. Upper-crustal strength inferred from stress measurements to 6 km depth in the KTB borehole. *Nature*, **365**(6447), 633–635. DOI:10.1038/365633a0.

Zoback, M.D. & Zoback, M.L., 1991. Tectonic stress field of North America and relative plate motions. In D.B. Slemmons, E.R. Engdahl, M.D. Zoback, & D.D. Blackwell, eds., *Neotectonics of North America*, pp. 339–366. Geological Society of America, Boulder, Colorado, United States.

Zoback, M.L., 1992b. First- and second-order patterns of stress in the lithosphere: the World Stress Map Project. *Journal of Geophysical Research*, **97**(B8), 11,703–11,728.

Zoback, M.L., Zoback, M.D., Adams, J., Assumpção, M., Bell, S., Bergman, E.A., Blümling, P., Brereton, N.R., Denham, D., Ding, J., Fuchs, K., Gay, N., Gregersen, S., Gupta, H.K., Gvishiani, A., Jacob, K., Klein, R., Knoll, P., Magee, M., Mercier, J.L., Müller, B.C., Paquin, C., Rajendran, K., Stephansson, O., Suarez, G., Suter, M., Udias, A., Xu, Z.H., & Zhizin, M., 1989. Global patterns of tectonic stress. *Nature*, **341**, 291–298.

Appendix A

3DEC code for southern Ontario model

A.1 Model background

The geometry of the southern Ontario 3DEC model is formed by first calculating the 2-D geometry of seven cross-sections perpendicular to the strike of the Grenville orogen (Figure A.1). These were then combined with the adjacent cross-section to define six wedges (labelled A-F), which are split into six blocks each (labelled 1-6). Outer blocks are then defined to generate N-S and E-W oriented boundaries. Corresponding blocks in adjacent wedges are then joined to form continuous blocks and piecewise continuous fault surfaces along strike.

Prominent seismogenic features in the region such as the Ottawa-Bonnechère graben and the Western Québec seismic zone were not included in the model geometry. These features have no apparent connection to the seismicity in the west-

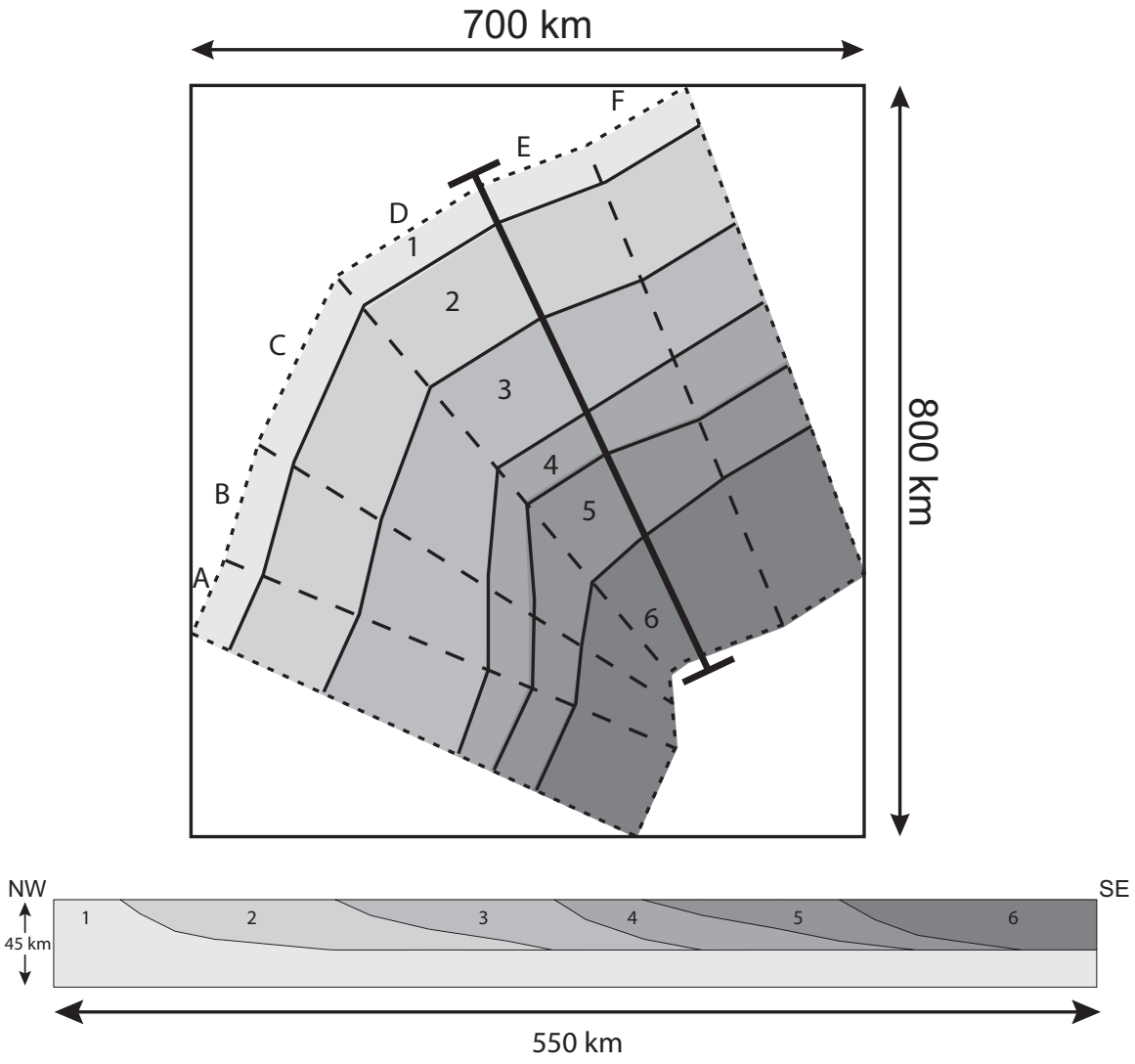

Figure A.1: Southern Ontario 3DEC model geometry

ern Lake Ontario region which is the main focus of the study. Additionally, these features strike approximately perpendicular to the regional stress field orientation, and would likely have little influence of the stress orientation in the Great Lakes region.

Stresses are initially set to lithostatic pressure (equal to the weight of overlying rocks) in order to ensure compatibility with the structures. The model assumes that the stress field is largely tectonic in origin and can be simulated through boundary loading in the direction of absolute plate motion. Differential stresses are gradually built up through small boundary displacements over a series of time steps. The model is run in a pseudo-static manner, although time-stepping and boundary velocities are used they are not linked to a true time scale, they are chosen to maintain an unbalanced force at a stable low level.

A.2 Initial conditions

The following code sets up the material properties prior to running model.

```
;====================
;= Model Properties =
;====================
find
change mat 1
hide
find region 0
change mat 2
find
property material 1 ym=40000 pr=0.25 density=0.00275
property material 2 ym=40000 pr=0.25 density=0.00275
gravity 0 -9.81 0
;=================
;= Define joints =
;=================
```

```
change rint 1 2 jmat 2
change rint 1 3 jmat 2
change rint 1 4 jmat 2
change rint 1 5 jmat 2
change rint 1 6 jmat 2
change rint 2 3 jmat 2
change rint 2 4 jmat 2
change rint 2 5 jmat 2
change rint 2 6 jmat 2
change rint 3 4 jmat 2
change rint 3 5 jmat 2
change rint 3 6 jmat 2
change rint 4 5 jmat 2
change rint 4 6 jmat 2
change rint 5 6 jmat 2
change rint 0 1 jmat 3
change rint 0 2 jmat 3
change rint 0 3 jmat 3
change rint 0 4 jmat 3
change rint 0 5 jmat 3
change rint 0 6 jmat 3
;========================
;= Set joint properties =
;========================
property jmat 1 fr 89 jkn 5500 jks 5500 jco 5000 jte 500
property jmat 2 fr 15 jkn 5500 jks 5500 jco 0 jte 500
property jmat 3 fr 89 jkn 5500 jks 5500 jco 5000 jte 500
call bound.txt
bound -1 716373 -45001 -44999 -215642 580436 yvel 0
insitu stress  0 0 0 0 0 0 &
ygrad 0.026977 0.026977 0.026977 0 0 0
hist unbal
hist xvel 0 -20000 -215641
hist zvel 0 -20000 -215641
call changevelocity.fis
ret
```

A.3 Subroutine

The following subroutine monitors the maximum unbalanced forces and adjusts boundary velocities so that the model is stable.

```
Define velpt
   velpt = gp_near(0, -20000, -215641)
end
DEFINE change_vel
   whilestepping
   incv = 1
   if unbal > high_unbal then
      incv = 0.975
   end_if
   if unbal < low_unbal then
      incv = 1.025
      if gp_xvel(velpt) > max_vel then
         incv = 0.975
      end_if
   end_if
   cri_=bou_head
   loop while cri_ # 0
           fmem(cri_ + 21) = fmem(cri_ + 21)*incv
           fmem(cri_ + 23) = fmem(cri_ + 23)*incv
        cri_=imem(cri_ + $KBDV)
   endloop
end
set high_unbal=4e+10
set low_unbal=2e+9
set incv=1
set max_vel = 2
hist incv
change_vel
ret
```

Appendix B

FLAC code for 2-D Charlevoix model

B.1 Model background

The geometry of the model is defined by a 30 km radius circular region of lowered elastic modulus representing the heavily fractured Charlevoix impact structure, and a serious of parallel discontinuities representing the main faults of the St. Lawrence rift. These two main features show the clearest relationship to the seismicity patterns of both large and small events in the seismic zone

One potentially relevant seismogenic feature that was left out of the model is the Saguenay graben, marked by the Saguenay river, which meets the St. Lawrence approximately 60 km NE of the Charlevoix crater and strikes NW-SE. The Saguenay graben has hosted one large (m_N 6) earthquake in 1989, but unlike the CSZ it has not experienced prolonged background seismicity. The structure has no apparent influence on the distribution pattern of activity within the CSZ, which was apparent prior to the 1989 event. Additionally, due to the NW-SE strike of the

Saguenay graben, approximately perpendicular to the regional stress field, it is assumed to have little influence on the orientation of stresses in the Charlevoix area.

Stresses are built up slowly through boundary displacements in the direction of tectonic loading over a series of time steps, and evolve internally through interaction with the local structure. For the purposes of interpreting seismicity patterns, it is acknowledged that earthquake activity depends both on stress conditions and the material properties of the rock. It is assumed that within regions of similar material properties, that a higher deviatoric stress will lead to a higher likelihood of earthquake activity. However, a high deviatoric stress within a mechanically strong material may not necessarily lead to seismicity.

B.2 Model code

The following is some example FLAC code for the 2-D Charlevoix model used in Chapter 3.

```
;==============================
;= FLAC model nw-km-5-mod2.dat =
;==============================

new
config ex 1
grid 130 230
mod elastic
set large
mod null i=42
mod null i=55
mod null i=68
mod null i=101
mod null i=116
mod null j=201
mod null j=216
```

```
;==================================
;= Deform grid to proper geometry =
;==================================

;mainpart
gen 0,0 0,200 24,200 60,0 i=1,42 j=1,201
gen 86,0 50,200 100,200 100,0 i=69,101 j=1,201
gen 60,0 24,200 37,200 73,0 i=43,55 j=1,201
gen 73,0 37,200 50,200 86,0 i=56,68 j=1,201

;top and bottom
;top
gen 0,200 0,230 24,230 24,200 i=1,42 j=202,216
gen 24,200 24,230 37,230 37,200 i=43,55 j=202,216
gen 37,200 37,230 50,230 50,200 i=56,68 j=202,216
gen 50,200 50,230 100,230 100,200 i=69,101 j=202,216

attach aside from 42,202 to 42,216 bside from 43,202 to 43,216
attach aside from 55,202 to 55,216 bside from 56,202 to 56,216
attach aside from 68,202 to 68,216 bside from 69,202 to 69,216

attach aside from 1,202 to 42,202 bside from 1,201 to 42,201
attach aside from 43,202 to 55,202 bside from 43,201 to 55,201
attach aside from 56,202 to 68,202 bside from 56,201 to 68,201
attach aside from 69,202 to 101,202 bside from 69,201 to 101,201

;bottom
gen 0,-30 0,0 60,0 60,-30 i=1,42 j=217,231
gen 60,-30 60,0 73,0 73,-30 i=43,55 j=217,231
gen 73,-30 73,0 86,0 86,-30 i=56,68 j=217,231
gen 86,-30 86,0 100,0 100,-30 i=69,101 j=217,231

attach aside from 42,217 to 42,231 bside from 43,217 to 43,231
attach aside from 55,217 to 55,231 bside from 56,217 to 56,231
attach aside from 68,217 to 68,231 bside from 69,217 to 69,231

attach aside from 1,1 to 42,1 bside from 1,231 to 42,231
attach aside from 43,1 to 55,1 bside from 43,231 to 55,231
attach aside from 56,1 to 68,1 bside from 56,231 to 68,231
attach aside from 69,1 to 101,1 bside from 69,231 to 101,231

;leftside
gen -50,0 -50,200 0,200 0,0 rat 0.833 1 i=102,116 j=1,201
gen -50,-30 -50,0 0,0 0,-30 rat 0.833 1 i=102,116 j=217,231
gen -50,200 -50,230 0,230 0,200 rat 0.833 1 i=102,116 j=202,216
```

```
;rightside
gen 100,0 100,200 150,200 150,0 rat 1.2 1 i=117,131 j=1,201
gen 100,-30 100,0 150,0 150,-30 rat 1.2 1 i=117,131 j=217,231
gen 100,200 100,230 150,230 150,200 rat 1.2 1 i=117,131 j=202,216

gen cir 50,100 29

;attach sides
attach aside from 116,1 to 116,201 bside from 1,1 to 1,201
attach aside from 101,1 to 101,201 bside from 117,1 to 117,201

;attach side tops and bottoms
attach aside from 102,201 to 116,201 bside from 102,202 to 116,202
attach aside from 102,231 to 116,231 bside from 102,1, to 116,1

attach aside from 117,201 to 131,201 bside from 117,202 to 131,202
attach aside from 117,231 to 131,231 bside from 117,1 to 131,1

;attach side tops and bottoms to middle

attach aside from 116,202 to 116,216 bside from 1,202 to 1,216
attach aside from 101,202 to 101,216 bside from 117,202 to 117,216

attach aside from 116,217 to 116,231 bside from 1,217 to 1,231
attach aside from 101,217 to 101,231 bside from 117,217 to 117,231

ini x=86 var 0,-36 i=68,69 j=1,201
ini x=73 var 0,-36 i=55,56 j=1,201
ini x=60 var 0,-36 i=42,43 j=1,201

;==============================
;= Define interfaces (faults) =
;==============================

int 1 aside from 42,1 to 42,201 bside from 43,1 to 43,201
int 2 aside from 55,1 to 55,201 bside from 56,1 to 56,201
int 3 aside from 68,1 to 68,201 bside from 69,1 to 69,201

;============================================================
;= Define geometric regions for material property assignment =
;============================================================

group outside region 1 1
group outside region 100 1
```

```
group outside region 102,1
group outside region 117,1

group rift region 50 1
group rift region 50 200
group rift region 60 1
group rift region 60 200
group crat region 41 100
group crat region 75 100
group crat_rift region 60 100
group crat_rift region 50 100

;=========================================
;= Set material and interface properties =
;=========================================

prop bulk 18250 dens 0.0027 shear 11000

prop bulk 73000 dens 0.0027 shear 44000 group outside
prop bulk 73000 dens 0.0027 shear 44000 group rift
prop bulk 36500 dens 0.0027 shear 22000 group crat
prop bulk 36500 dens 0.0027 shear 22000 group crat_rift
int 1 coh 0 fric 5 kn 5500 ks 5500
int 2 coh 0 fric 5 kn 5500 ks 5500
int 3 coh 0 fric 5 kn 5500 ks 5500

;=============================================
;= Set initial stresses and boundary conditions =
;=============================================

initial sxx -20 syy -20 szz -20

apply yvel 0.05 from 102,217 to 116,217
apply yvel 0.05 from 1,217 to 42,217
apply yvel 0.05 from 43,217 to 55,217
apply yvel 0.05 from 56,217 to 68,217
apply yvel 0.05 from 69,217 to 101,217
apply yvel 0.05 from 117,217 to 131,217

apply yvel -0.05 from 102,216 to 116,216
apply yvel -0.05 from 1,216 to 42,216
apply yvel -0.05 from 43,216 to 55,216
apply yvel -0.05 from 56,216 to 68,216
apply yvel -0.05 from 69,216 to 101,216
apply yvel -0.05 from 117,216 to 131,216
```

```
apply xvel 0 from 102,217 to 102,231
apply xvel 0 from 102,1 to 102,201
apply xvel 0 from 102,202 to 102,216

apply xvel 0 from 131,217 to 131,231
apply xvel 0 from 131,1 to 131,201
apply xvel 0 from 131,202 to 131,216

;================================
;= Expand model to proper scale =
;================================

call expand.fis
expand

;================================
;= Run model for 5000 time-steps =
;================================

hist 1 unbalance
step 5000
save nw-km-5-mod2-5k.sav

ret
```

B.3 Subroutines

The following subroutines, shearout and thetaout, are used to calculate and export maximum deviatoric stresses and the orientation of S_H respectively for each model zone. The exported data are then used to produce contour plots.

```
;=========================================
;= subroutine shearout, exports coordinates =
;= and deviatoric stress for each zone      =
;=========================================
def shearout
loop i (1, izones)
   loop j (1, jzones)
      if model(i,j) # 1
```

```
         xpos = (x(i,j) + x(i+1,j) + x(i,j+1) + x(i+1,j+1))/4.0
         ypos = (y(i,j) + y(i+1,j) + y(i,j+1) + y(i+1,j+1))/4.0
         $sdif = sxx(i,j) - syy(i,j)
         $s0   = 0.5 * (sxx(i,j) + syy(i,j))
         $st   = 4.0 * sxy(i,j)^2
         rad  = 0.5 * sqrt($sdif^2 + $st)
         oo = out(string(xpos) +' '+string(ypos)+' '+string(rad))
      endif
   endloop
endloop
end

;=================================================================
;= subroutine thetaout, exports coordinates and orientation of    =
;= maximum compressive stress relative to model loading direction =
;=================================================================
def thetaout
loop i (1, izones)
   loop j (1, jzones)
      if model(i,j) # 1
         xpos = (x(i,j) + x(i+1,j) + x(i,j+1) + x(i+1,j+1))/4.0
         ypos = (y(i,j) + y(i+1,j) + y(i,j+1) + y(i+1,j+1))/4.0
         sigx = -sxx(i,j)
         sigy = -syy(i,j)
         tauxy = -sxy(i,j)
         sig1 = (sigx + sigy + sqrt(4*tauxy^2+(sigx-sigy)^2))/2
         theta1 = (90 - atan(tauxy/(sig1-sigy))*180/pi)
         if theta1 > 270 then
            theta1 = theta1-180
         endif
         if theta1 < 90 then
            theta1 = theta1+180
         endif
         oo = out(string(xpos) +' '+string(ypos)+' '+string(theta1))
      endif
   endloop
endloop
end
```

Appendix C

FLAC3D code for 3-D Charlevoix model

C.1 Model background

The 3-D Charlevoix model uses a similar approach as the 2-D model with the major difference being a more accurate representation of the three-dimensional structural architecture of the system. The geometry is defined by the lower half of an ellipsoidal volume of lowered elastic modulus representing the heavily fractured impact structure. The modelled structure has a 30 km radius at surface and extends to a maximum depth of 15 km at the centre. The St. Lawrence rift faults are represented as three parallel planar discontinuities steeply dipping to the SE. The dip of the faults is varied between 60° and 70°.

The elastic moduli in the model varies with depth and is derived from P and S-wave velocity models for the Saguenay region to the north of Charlevoix (Somerville

et al., 1990). Stresses are initially set to lithostatic (equal to the weight of the overlying rock). Deviatoric stresses are built up slowly through boundary displacements in the direction of tectonic loading over a series of time steps, and evolve internally through interaction with the local structure.

For the purposes of interpreting seismicity patterns, it is acknowledged that earthquake activity depends both on stress conditions and the material properties of the rock. It is assumed that within regions of similar material properties, that a higher deviatoric stress will lead to a higher likelihood of earthquake activity. However, a high deviatoric stress within a mechanically strong material may not necessarily lead to seismicity.

C.2 Model code

The following is the FLAC3D code used for generating the 3-D geometry of the Charlevoix region for the model used in Chapter 4.

```
;===============
;= 3D geometry =
;===============

def parm
  rad=30.0     ; radius of spherical cavity
  len=40.0    ; length of outer box edge
end
parm

;================
;= Build blocks =
;================

gen zone radtunnel p0 (6,0,0) p1 (6,40,0) p2 (16,0,0) p3 (13.28,0,-40) &
  p4 (16,40,0) p5 (23.28,0,-40) p6 (13.28,40,-40) p7 (23.28,40,-40) &
  p8 (6,30,0) p9 (11.46,0,-30) p10 (16,30,0) p11 (21.46,0,-30) &
```

```
  p12 (11.46,30,-30) p13 (21.46,30,-30) &
  size 16 10 16 16 &
  rat 1.0 1.0 1.0 1.0 dim 30 30 group rwedge fill group crwedge
gen zone radtunnel p0 (-4,0,0) p1 (-4,40,0) p2 (6,0,0) p3 (3.28,0,-40) &
  p4 (6,40,0) p5 (13.28,0,-40) p6 (3.28,40,-40) p7 (13.28,40,-40) &
  p8 (-4,30,0) p9 (1.46,0,-30) p10 (6,30,0) p11 (11.46,0,-30) &
  p12 (1.46,30,-30) p13 (11.46,30,-30) &
  size 16 10 16 16 &
  rat 1.0 1.0 1.0 1.0 dim 30 30 group lwedge fill group clwedge
gen zone radbrick p0 (16,0,0) p1 (40,0,0) p2 (23.28,0,-40) p3 (16,40,0)&
  p4 (40,0,-40) p5 (23.28,40,-40) p6 (40,40,0) p7 (40,40,-40) &
  p8 (30,0,0) p9 (21.46,0,-30) p10 (16,30,0) p11 (30,0,-30) &
  p12 (21.46,30,-30) p13 (30,30,0) p14 (30,30,-30) &
  size 14 16 16 16 &
  rat 1.0 1.0 1.0 1.0 dim 14 30 30 group rightb fill group cright
gen zone radbrick p0 (-4,0,0) p1 (-40,0,0) p2 (-4,40,0) p3 (3.28,0,-40)&
  p4 (-40,40,0) p5 (3.28,40,-40) p6 (-40,0,-40) p7 (-40,40,-40) &
  p8 (-30,0,0) p9 (-4,30,0) p10 (1.46,0,-30) p11 (-30,30,0) &
  p12 (1.46,30,-30) p13 (-30,0,-30) p14 (-30,30,-30) &
  size 26 16 16 16 &
  rat 1.0 1.0 1.0 1.0 dim 26 30 30 group leftb fill group cleft

;============================================================
;= Subroutines to deform blocks into spherical crater shape =
;============================================================

def make_innersphere
; Loop over all GPs and remap their coordinates:
  section
  p_gp=gp_head
  loop while p_gp#null
; Get gp coordinate: P=(px,py,pz)
    px=gp_xpos(p_gp)
    py=gp_ypos(p_gp)
    pz=gp_zpos(p_gp)
; Get group name: grou
    grou=gp_group(p_gp,1)
; Origin shift depends on group
    if grou='cright' then
      shift=16.0
    else
      if grou='cleft' then
        shift=-4.0
      else
         if grou='crwedge' then
```

```
           shift=px+pz*(5.46/30)
    else
      if grou='clwedge' then
        shift=px+pz*(5.46/30)
      else
        exit section
          end_if
        end_if
      end_if
    end_if
; New origin coordinates A=(ax,ay,az)
    ax=shift
    ay=0.0
    az=0.0
; new point coordinates relative to A, H=(hx,hy,hz)
; If py is negative, make hy positive
    if py<0 then
      hx=px-shift
      hy=-py
      hz=pz
    else
      hx=px-shift
      hy=py
      hz=pz
    end_if
; find radial distance from A to sphere shifted by -shift
; coordinates of this point (relative to A) are B=bx,by,bz
      dist=abs(sqrt(hx*hx+hy*hy+hz*hz))
      if dist>0 then
        th=atan2(hy,hx)
        ph=acos(hz/dist)
        atemp=(cos(th)*sin(ph))^2 + (sin(th)*sin(ph))^2 +(cos(ph))^2
        btemp=(2*shift*cos(th)*sin(ph))
        ctemp=shift^2-(rad)^2
        radtemp=(-btemp+sqrt(btemp^2-4*atemp*ctemp))/(2*atemp)
        k=radtemp/dist
        bx=hx*k
        by=hy*k
        bz=hz*k
; Find distance to point on cube radially above H
; could be xboxdist, yboxdist, or zboxdist
        xtemp=30-abs(shift)
        ytemp=30
        ztemp=30
        if th>pi/2 then
```

```
          thtemp=pi-th
        else
          thtemp=th
        end_if
        phtemp=ph-(pi/2)
        dentemp=cos(phtemp)*cos(thtemp)
        if dentemp>0 then
          xboxdist=xtemp/dentemp
        else
          xboxdist=10000.0
        end_if
        dentemp=cos(phtemp)*sin(thtemp)
        if dentemp>0 then
          yboxdist=ytemp/dentemp
        else
          yboxdist=10000.0
        end_if
        dentemp=sin(phtemp)
        if dentemp>0 then
          zboxdist=ztemp/dentemp
        else
          zboxdist=10000.0
        end_if
        boxdist=min(xboxdist,min(yboxdist,zboxdist))
; Linear interpolation: P=A+u*(B)
        u=(dist)/(boxdist)
        if py<0 then
          gp_xpos(p_gp)=ax+u*(bx)
          gp_ypos(p_gp)=(-1)*(ay+u*(by))
          gp_zpos(p_gp)=az+u*(bz)
        else
          gp_xpos(p_gp)=ax+u*(bx)
          gp_ypos(p_gp)=ay+u*(by)
          gp_zpos(p_gp)=az+u*(bz)
        end_if
      end_if
    end_section
    p_gp=gp_next(p_gp)
  end_loop
end

def make_outersphere
; Loop over all GPs and remap their coordinates:
  p_gp=gp_head
  section
```

```
  loop while p_gp#null
; Get gp coordinate: P=(px,py,pz)
    px=gp_xpos(p_gp)
    py=gp_ypos(p_gp)
    pz=gp_zpos(p_gp)
; Get group name: grou
    grou=gp_group(p_gp,1)
; Origin shift depends on group
    if grou='rightb' then
      shift=16.0
    else
      if grou='leftb' then
        shift=-4.0
      else
         if grou='rwedge' then
           shift=px+pz*(5.46/30)
    else
      if grou='lwedge' then
        shift=px+pz*(5.46/30)
      else
        exit section
          end_if
        end_if
      end_if
    end_if
; New origin coordinates A=(ax,ay,az)
    ax=shift
    ay=0.0
    az=0.0
; new point coordinates relative to A, H=(hx,hy,hz)
; If py is negative, make hy positive
    if py<0 then
      hx=px-shift
      hy=-py
      hz=pz
    else
      hx=px-shift
      hy=py
      hz=pz
    end_if
; find radial distance from A to sphere shifted by -shift
; coordinates of this point (relative to A) are B=bx,by,bz
      dist=abs(sqrt(hx*hx+hy*hy+hz*hz))
      if dist>0 then
        th=atan2(hy,hx)
```

```
        ph=acos(hz/dist)
        atemp=(cos(th)*sin(ph))^2 + (sin(th)*sin(ph))^2 +(cos(ph))^2
        btemp=(2*shift*cos(th)*sin(ph))
        ctemp=shift^2-(rad)^2
        radtemp=(-btemp+sqrt(btemp^2-4*atemp*ctemp))/(2*atemp)
        k=radtemp/dist
        bx=hx*k
        by=hy*k
        bz=hz*k
; Find distance to point on cube radially above H
; could be xboxdist, yboxdist, or zboxdist
; point on outer box is C=cx,cy,cz
        xtemp=30-abs(shift)
        ytemp=30
        ztemp=30
        xotemp=len-abs(shift)
        yotemp=len
        zotemp=len
        if th>pi/2 then
          thtemp=pi-th
        else
          thtemp=th
        end_if
        phtemp=ph-(pi/2)
        dentemp=cos(phtemp)*cos(thtemp)
        if dentemp>0 then
          xboxdist=xtemp/dentemp
          xoboxdist=xotemp/dentemp
        else
          xboxdist=10000.0
          xoboxdist=10000.0
        end_if
        dentemp=cos(phtemp)*sin(thtemp)
        if dentemp>0 then
          yboxdist=ytemp/dentemp
          yoboxdist=yotemp/dentemp
        else
          yboxdist=10000.0
          yoboxdist=10000.0
        end_if
        dentemp=sin(phtemp)
        if dentemp>0 then
          zboxdist=ztemp/dentemp
          zoboxdist=zotemp/dentemp
        else
```

```
          zboxdist=10000.0
          zoboxdist=10000.0
        end_if
        boxdist=min(xboxdist,min(yboxdist,zboxdist))
        oboxdist=min(xoboxdist,min(yoboxdist,zoboxdist))
        kn=oboxdist/dist
        cx=hx*kn
        cy=hy*kn
        cz=hz*kn
; Linear interpolation: P=A+B+u*(C-B)
        u=(dist-boxdist)/(oboxdist-boxdist)
        if py<0 then
          gp_xpos(p_gp)=ax+bx+u*(cx-bx)
          gp_ypos(p_gp)=(-1)*(ay+by+u*(cy-by))
          gp_zpos(p_gp)=az+bz+u*(cz-bz)
        else
          gp_xpos(p_gp)=ax+bx+u*(cx-bx)
          gp_ypos(p_gp)=ay+by+u*(cy-by)
          gp_zpos(p_gp)=az+bz+u*(cz-bz)
        end_if
      end_if
    end_section
    p_gp=gp_next(p_gp)
  end_loop
end

make_innersphere
make_outersphere

;========================================
;= Generate lower and surrounding blocks =
;========================================

gen zone brick p0 (6,40,0) p1 (16,40,0) p2 (13.28,40,-40) &
  p3 (6,200,0) & size 10 16 20 &
  rat 1.0 1.0 1.15 group rwedge
gen zone brick p0 (-4,40,0) p1 (6,40,0) p2 (3.28,40,-40) &
  p3 (-4,200,0) size 10 16 20 &
  rat 1.0 1.0 1.15 group lwedge
gen zone brick p0 (16,40,0) p1 (40,40,0) p2 (23.28,40,-40) &
  p3 (16,200,0) p4 (40,40,-40) p5 (23.28,200,-40) p6 (40,200,0) &
  p7 (40,200,-40) size 14 16 20 &
  rat 1.0 1.0 1.15 group rightb
gen zone brick p0 (-40,40,0) p1 (-4,40,0) p2 (-40,40,-40) &
  p3 (-40,200,0) p4 (3.28,40,-40) p5 (-40,200,-40) p6 (-4,200,0) &
```

```
  p7 (3.28,200,-40) size 26 16 20 &
  rat 1.0 1.0 1.15 group leftb
gen zone brick p0 (40,0,0) p1 (150,0,0) p2 (40,0,-40) &
  p3 (40,40,0) size 18 16 16 &
  rat 1.15 1.0 1.0 group rightb
gen zone brick p0 (40,40,0) p1 (150,40,0) p2 (40,40,-40) &
  p3 (40,200,0) size 18 16 20 &
  rat 1.15 1.0 1.15 group rightb
gen zone brick p0 (-150,0,0) p1 (-40,0,0) p2 (-150,0,-40) &
  p3 (-150,40,0) size 18 16 16 &
  rat 0.869565 1.0 1.0 group leftb
gen zone brick p0 (-150,40,0) p1 (-40,40,0) p2 (-150,40,-40) &
  p3 (-150,200,0) size 18 16 20 &
  rat 0.869565 1.0 1.15 group leftb
;layer 20-35k, inner
gen zone brick p0 (13.28,0,-40) p1 (23.28,0,-40) p2 (18.74,0,-70) &
  p3 (13.28,40,-40) size 10 8 16 &
  rat 1.0 1.15 1.0 group rwedge
gen zone brick p0 (3.28,0,-40) p1 (13.28,0,-40) p2 (8.74,0,-70) &
  p3 (3.28,40,-40) size 10 8 16 &
  rat 1.0 1.15 1.0 group lwedge
gen zone brick p0 (23.28,0,-40) p1 (40,0,-40) p2 (28.74,0,-70) &
  p3 (23.28,40,-40) p4 (40,0,-70) p5 (28.74,40,-70) p6 (40,40,-40) &
  p7 (40,40,-70) size 14 8 16 &
  rat 1.0 1.15 1.0 group rightb
gen zone brick p0 (-40,0,-40) p1 (3.28,0,-40) p2 (-40,0,-70) &
  p3 (-40,40,-40) p4 (8.74,0,-70) p5 (-40,40,-70) p6 (3.28,40,-40) &
  p7 (8.74,40,-70) size 26 8 16 &
  rat 1.0 1.15 1.0 group leftb
;layer 20-40, outer
gen zone brick p0 (13.28,40,-40) p1 (23.28,40,-40) p2 (18.74,40,-70) &
  p3 (13.28,200,-40) size 10 8 20 &
  rat 1.0 1.15 1.15 group rwedge
gen zone brick p0 (3.28,40,-40) p1 (13.28,40,-40) p2 (8.74,40,-70) &
  p3 (3.28,200,-40) size 10 8 20 &
  rat 1.0 1.15 1.15 group lwedge
gen zone brick p0 (23.28,40,-40) p1 (40,40,-40) p2 (28.74,40,-70) &
  p3 (23.28,200,-40) p4 (40,40,-70) p5 (28.74,200,-70) &
  p6 (40,200,-40) p7 (40,200,-70) size 14 8 20 &
  rat 1.0 1.15 1.15 group rightb
gen zone brick p0 (-40,40,-40) p1 (3.28,40,-40) p2 (-40,40,-70) &
  p3 (-40,200,-40) p4 (8.74,40,-70) p5 (-40,200,-70) &
  p6 (3.28,200,-40) p7 (8.74,200,-70) size 26 8 20 &
  rat 1.0 1.15 1.15 group leftb
gen zone brick p0 (40,0,-40) p1 (150,0,-40) p2 (40,0,-70) &
```

```
  p3 (40,40,-40) size 18 8 16 &
  rat 1.15 1.15 1.0 group rightb
gen zone brick p0 (40,40,-40) p1 (150,40,-40) p2 (40,40,-70) &
  p3 (40,200,-40) size 18 8 20 &
  rat 1.15 1.15 1.15 group rightb
gen zone brick p0 (-150,0,-40) p1 (-40,0,-40) p2 (-150,0,-70) &
  p3 (-150,40,-40) size 18 8 16 &
  rat 0.869565 1.15 1.0 group leftb
gen zone brick p0 (-150,40,-40) p1 (-40,40,-40) p2 (-150,40,-70) &
  p3 (-150,200,-40) size 18 8 20 &
  rat 0.869565 1.15 1.15 group leftb
gen zone reflect nor 0 -1 0 ori 0 0 -50
model elastic

;================================================
;= Separate blocks and define interfaces (faults) =
;================================================

gen separate rwedge
gen separate lwedge
gen separate crwedge
gen separate clwedge
gen separate cright
gen separate cleft
gen separate rightb
gen separate leftb
interface 1 wrap lwedge leftb
interface 1 wrap clwedge cleft
interface 1 wrap lwedge cleft
interface 2 wrap rwedge rightb
interface 2 wrap crwedge cright
interface 2 wrap rwedge cright
interface 3 wrap rwedge lwedge
interface 3 wrap crwedge clwedge
interface 3 wrap rwedge clwedge
range name rightwedge group rwedge any group crwedge any
range name leftwedge group lwedge any group clwedge any
range name rightside group cright any group rightb any
range name leftside group cleft any group leftb any
gen merge 0.1 range rightwedge
gen merge 0.1 range leftwedge
gen merge 0.1 range rightside
gen merge 0.1 range leftside

;===========================================
```

```
;= Deform and expand grid to final dimensions =
;==============================================

call squish.fis
squish
call expand.fis
expand
range name crater group cleft any group cright any &
  group crwedge any group clwedge any
range name outside group leftb any group rightb any &
  group rwedge any group lwedge any
save 35depth.sav
```

C.3 Initial and boundary conditions

The following code sets up the material properties and boundary conditions of the model.

```
;============================================================
;= Set model parameters and initial and boundary conditions =
;============================================================

model elastic
config zextra 20
config gpextra 20

;=============================================
;= Set outer modulus (values vary with depth) =
;=============================================

prop bulk 25844 grad 0 0 -7.8106 dens 0.0027 &
shear 15548 grad 0 0 -9.2722 range outside z -1440 0
prop bulk 32616 grad 0 0 -3.1082 dens 0.0027 &
shear 27986 grad 0 0 -0.6346 range outside z -7440 -1440
prop bulk 45583 grad 0 0 -1.3653 dens 0.0027 &
shear 27986 grad 0 0 -0.6346 range outside z -19440 -7440
prop bulk 56254 grad 0 0 -0.8164 dens 0.0027 &
shear 27986 grad 0 0 -0.6346 range outside z -36000 -19440

;=============================================
;= Set crater modulus (Values vary with depth) =
```

```
;=============================================

prop bulk 6461 grad 0 0 -1.95265 dens 0.0027 &
shear 3887 grad 0 0 -2.31805 range crater z -1440 0
prop bulk 8154 grad 0 0 -0.77705 dens 0.0027 &
shear 6996.5 grad 0 0 -0.15865 &
range crater z -7440 -1440
prop bulk 11395.75 grad 0 0 -0.341325 dens 0.0027 &
shear 6996.5 grad 0 0 -0.15865 &
range crater z -19440 -7440

set gravity 9.81

;=================================================================
;= Set fault frictional strength parameters and initialize stress =
;=================================================================

interface 1 prop fric 5 kn 1000 ks 1000 co 0
interface 2 prop fric 5 kn 1000 ks 1000 co 0
interface 3 prop fric 5 kn 1000 ks 1000 co 0
ini sxx 0 grad 0 0 0.026487
ini syy 0 grad 0 0 0.026487
ini szz 0 grad 0 0 0.026487

;================================
;= Set up the boundary conditions =
;================================

range name boundcond x 150000 any x -150000 any y 200000 &
any y -200000 any
range name boundcondbott z -35000 any

def thetad
thetad=15 ;theta in degrees
end
thetad


def setbc
thetar=thetad*(pi/180) ;theta in radians
srat=-2.0e-7 ;selected strain rate (per time cycle)
xvelxgr=srat*(sin(thetar))^2
xvelygr=srat*(cos(thetar)*sin(thetar))
yvelxgr=srat*(cos(thetar)*sin(thetar))
yvelygr=srat*(cos(thetar))^2
```

```
command
apply xvel 0 grad xvelxgr xvelygr 0 range boundcond
apply yvel 0 grad yvelxgr yvelygr 0 range boundcond
apply zvel 0 range boundcondbott
endcommand
end
setbc
```

C.4 Subroutines

The following subroutines are used to monitor slip activity along the rift faults through time. The data exported from them was used to produce Figure 4.10. After running the model for an initial 100 time steps the subroutine sheardisp is used to calculate and store the accumulated relative shear displacement at each interface node. Sheardispprintout is then called to export the data to a text file for post-processing. The subroutine sheardispreset then resets the recorded shear displacement to zero before another 100 time steps are run and the process is completed.

```
;=======================================================
;= subroutine sheardisp loops through interface nodes =
;= and saves relative shear displacement to an array  =
;=======================================================
def sheardisp
array sdispout(nzone,7)
npos=1
p_i=i_head
loop while p_i#null
internum=i_id(p_i)
p_in=i_node_head(p_i)
loop while p_in#null
posi_x=in_pos(p_in,1)
posi_y=in_pos(p_in,2)
posi_z=in_pos(p_in,3)
ixsdisp=in_sdisp(p_in,1)
iysdisp=in_sdisp(p_in,2)
```

```
izsdisp=in_sdisp(p_in,3)
sdispout(npos,1)=internum
sdispout(npos,2)=posi_x
sdispout(npos,3)=posi_y
sdispout(npos,4)=posi_z
sdispout(npos,5)=ixsdisp
sdispout(npos,6)=iysdisp
sdispout(npos,7)=izsdisp
npos=npos+1
p_in=in_next(p_in)
end_loop
p_i=i_next(p_i)
end_loop
totalarraysize=npos
end

;=========================================================
;= Subroutine sheardispprintout exports shear           =
;= displacement data to a text file for post processing =
;=========================================================
def sheardispprintout
array sdispprintout(totalarraysize)
loop i (1,totalarraysize)
sdispprintout(i)=string(sdispout(i,1))+' '&
+string(sdispout(i,2))+' '+string(sdispout(i,3))+' '&
+string(sdispout(i,4))+' '+string(sdispout(i,5))+' '&
+string(sdispout(i,6))+' '+string(sdispout(i,7))
endloop
status = open('sdispreset-15a35d5-modagrad25-'+string(step)+'.dat',1,1)
status = write(sdispprintout,totalarraysize)
status = close
end

;=================================================
;= Subroutine sheardispreset loops through       =
;= interface nodes and resets their value to zero =
;=================================================
def sheardispreset
p_i=i_head
loop while p_i#null
p_in=i_node_head(p_i)
loop while p_in#null
in_sdisp(p_in,1)=0.0
in_sdisp(p_in,2)=0.0
in_sdisp(p_in,3)=0.0
```

```
p_in=in_next(p_in)
end_loop
p_i=i_next(p_i)
end_loop
end
```